AFOSR-TR- 85-0017

(13)

IN SITU CHARACTERIZATION OF SOILS FOR PREDICTION OF STRESS-STRAIN RELATIONSHIP (UNCLASSIFIED)

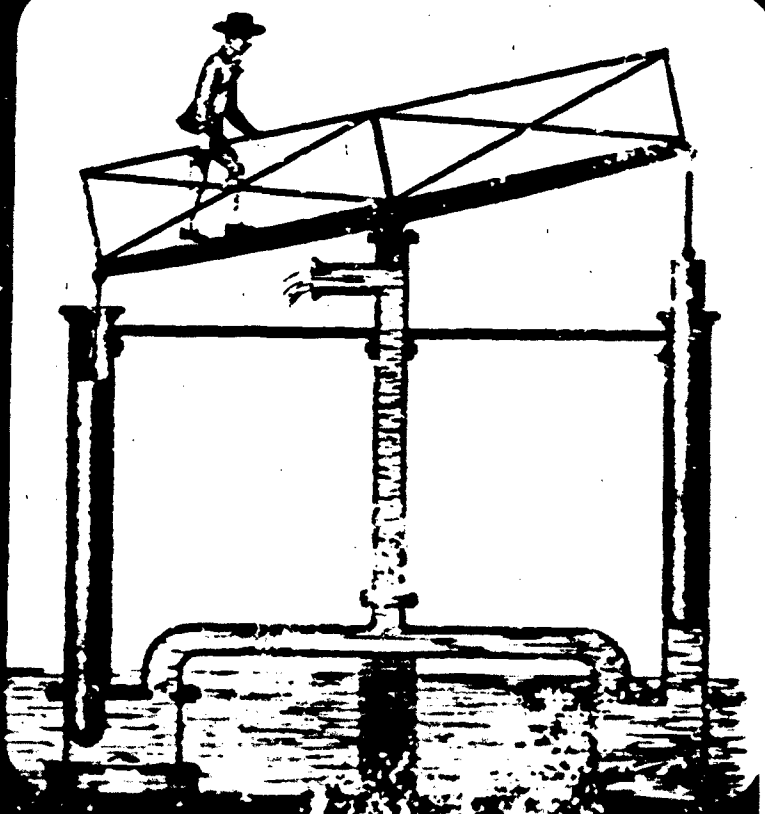

Department of Civil Engineering

University of California, Davis

"Qualified requestors may obtain addi-
-tional copies from the Defense Technical -
Information Service."

UNCLASSIFIED

SECURITY CLASSIFICATION OF THIS PAGE

REPORT DOCUMENTATION PAGE

1a. REPORT SECURITY CLASSIFICATION: Unclassified	1b. RESTRICTIVE MARKINGS
2a. SECURITY CLASSIFICATION AUTHORITY	3. DISTRIBUTION/AVAILABILITY OF REPORT: Approved for Public Release; Distribution Unlimited.
2b. DECLASSIFICATION/DOWNGRADING SCHEDULE	
4. PERFORMING ORGANIZATION REPORT NUMBER(S)	5. MONITORING ORGANIZATION REPORT NUMBER(S): AFOSR-TR- 85-0017
6a. NAME OF PERFORMING ORGANIZATION: UNIVERSITY OF CALIFORNIA, DAVIS; 6b. OFFICE SYMBOL (If applicable)	7a. NAME OF MONITORING ORGANIZATION
6c. ADDRESS (City, State and ZIP Code): DEPARTMENT OF CIVIL ENGINEERING, DAVIS, CA 95616	7b. ADDRESS (City, State and ZIP Code)
8a. NAME OF FUNDING/SPONSORING ORGANIZATION: AIR FORCE OFFICE OF SCIENTIFIC RESEARCH; 8b. OFFICE SYMBOL (If applicable): AFOSR/NA	9. PROCUREMENT INSTRUMENT IDENTIFICATION NUMBER: AFOSR-81-0216
8c. ADDRESS (City, State and ZIP Code): BOLLING AFB, DC 20332	10. SOURCE OF FUNDING NOS.

PROGRAM ELEMENT NO	PROJECT NO	TASK NO	WORK UNIT NO.
61102F	2307	C1	

11. TITLE (Include Security Classification): IN SITU CHARACTERIZATION OF SOILS FOR PREDICTION OF STRESS/STRAIN RELATIONSHIP (UNCLASSIFIED)

12. PERSONAL AUTHOR(S): K. ARULANANDAN, Y. DAFALIAS, L. HERRMANN, A. ANANDARAJAH, N. MEEGODA, ABDULLA ASSAAD

13a. TYPE OF REPORT	13b. TIME COVERED	14. DATE OF REPORT (Yr., Mo., Day)	15. PAGE COUNT
Final	FROM Nov. 1982 TO Nov. 1983	1983, November	118

16. SUPPLEMENTARY NOTATION

17 COSATI CODES			18. SUBJECT TERMS (Continue on reverse if necessary and identify by block number)
FIELD	GROUP	SUB GR	
			ELECTRICAL METHOD, BOUNDING SURFACE, IN SITU STRESS STATE AND STRESS STRAIN BEHAVIOR

19. ABSTRACT (Continue on reverse if necessary and identify by block number)

A non-destructive method of characterizing particulate systems using electrical properties is presented. The application of this methodology for the demarkation of cohesive and granular soils is demonstrated. The significance of this approach is that electrical properties of soils such as conductivity, σ, and dielectric constant, ϵ, as a function of frequency, can be measured in situ. These properties, when suitably interpreted, can be used to quantify the structure of particulate systems including the inter and intra cluster void ratios. These structural properties can then be correlated with mechanical properties such as k_o, λ, k and M. Incorporating these mechanical properties into a bounding surface plasticity model, the in situ stress state and in situ stress strain behavior could be predicted. Application of this method to mixed soils is demonstrated in this report. This approach therefore provides a non-destructive method of characterization soils for the prediction of mechanical behavior.

20. DISTRIBUTION/AVAILABILITY OF ABSTRACT	21. ABSTRACT SECURITY CLASSIFICATION
UNCLASSIFIED/UNLIMITED ☒ SAME AS RPT ☐ DTIC USERS ☐	Unclassified

22a. NAME OF RESPONSIBLE INDIVIDUAL	22b. TELEPHONE NUMBER (Include Area Code)	22c. OFFICE SYMBOL
LAWRENCE D. HOKANSON, Lt. Col., USAF	(202) 767-4935	AFOSR-NA

DD FORM 1473, 83 APR EDITION OF 1 JAN 73 IS OBSOLETE

UNCLASSIFIED

SECURITY CLASSIFICATION OF THIS PAGE

FINAL REPORT TO THE AIR FORCE
OFFICE OF SCIENTIFIC RESEARCH

Grant Number AFOSR-81-0216

IN SITU CHARACTERIZATION OF SOILS FOR PREDICTION OF STRESS-STRAIN RELATIONSHIP

by

K. Arulanandan
Y. Dafalias
L.R. Herrmann
A. Anandarajah
N. Meegoda
Abdulla Assaad

November 1983

IN SITU CHARACTERIZATION OF SOILS FOR PREDICTION OF STRESS-STRAIN RELATIONSHIP

1. Introduction

The solution of most geotechnical engineering problems requires a knowledge of engineering properties. One of the major difficulties in obtaining soil properties accurately is the disturbance during sampling or the use of penetration methods of in situ testing which alters the engineering properties. In situ testing techniques, however, have begun to play an increasingly important role in the determination of soil properties. This trend towards in situ testing techniques could be ascribed to several reasons as follows: (1) the soil is tested in its in situ environmental conditions which influence the engineering properties, (2) continuous data through the profile may be obtained, and (3) properties can be obtained in cases where obtaining undisturbed samples is very difficult, such as in the case of saturated sands.

Presently, several in situ testing techniques are employed for the evaluation of soil properties and for the establishment of empirical criteria for the prediction of potential behavior of soils. The standard penetration test (SPT) and the cone penetration test (CPT) are the most widely used in situ testing techniques. Other in situ testing techniques such as the pressure meter test (PMT), the Iowa Bore Hole Shear Test (BST) and the dilatometer are being used on a modest scale.

The reliability and usefulness of test results obtained from the in situ testing techniques described above are limited owing to various reasons. The drainage conditions in soils during the in situ testing may be unknown in some tests. The failure modes may not simulate those anticipated for the actual project and in some cases the exact failure mode is unknown. Due to these unknown drainage and failure conditions, and the specific nature of testing

procedures and the failure mode simulated in different techniques, interpretation of the test results is highly empirical at the present time. The generalization of the test results, obtained from the current in situ testing techniques in order to analyze soil behavior under general loading conditions and various drainage and boundary conditions, is very difficult.

A nondestructive method of characterizing particulate systems is presented by considering the electrical properties of soils which can be determined in situ without causing disturbance to the soils. The objectives of this report are:

1) characterization of soil by electrical methods
2) quantification of the compositional and aggregate properties of soils in terms of electrical parameters
3) quantification of the inter- and intra-cluster void ratios
4) establishment of correlations between electrical parameters and compression index, λ, swell index K, and the slope of the critical state line, M for soils
5) methodology to predict stress strain relationship of soils in situ
6) establish correlation between K_o and the electrical parameters.

2. Characterization of Soils by Electrical Methods

When an alternating electrical field is applied to a clay-water-electrolyte system, a response is produced which can be measured in terms of a resistance, R, and a capacitance, C. The measured value of the capacitance can be converted into a quantity known as the dielectric constant. This value is defined as $C/_{Co}$, in which Co is the capacitance of a condenser with only a vacuum between the electrodes. The dielectric constant is actually a measure of the ability of the clay to store electrical potential energy under the influence of an electric field. From a knowledge of the dimensions of the sample the

dielectric constant and conductivity can be calculated from values of R and C using the following relationships.

$$\varepsilon' \varepsilon_a = \frac{Cd}{A} \tag{1}$$

$$\sigma = \frac{d}{RA} \tag{2}$$

in which d = length of a specimen; A = cross-sectional area; and ε_a = the dielectric constant of vacuum (8.85×10^{-14} farad/cm).

The dielectric constant of a dry silicate material is about 4.5, and that of water is about 79. A mixture of soil and water should, therefore, have a dielectric constant weighted between 4.5 and 79. However, when the dielectric constant of a clay-water-electrolyte system is measured with an alternating current in the radio-frequency range, it is found to be in excess of the sum of the weighted dielectric constant of the components. This measured value, ε', referred to as the "apparent dielectric constant," reflects the heterogeneous nature of the path of the current and the electrical properties of the pore fluid and the clay mineral as shown by Arulanandan and Smith (1973).

When the conductivity, σ, and apparent dielectric constant, ε', of a cohesive system are measured as a function of frequency, in the radio frequency range, it is found that ε' and σ vary as shown in Figure 2. This variation of σ and ε' is referred to as electrical dispersion. However, for a granular system it has been observed that σ and ε' are independent of frequency (see Figure 1). It is thus possible to classify all particulate systems into two groups. All cohesive systems are characterized by electrical dispersion behavior and granular systems by nondispersive electrical behavior.

This method of classification is non-destructive, quantitative and fundamental in nature as opposed to the present qualitative, arbitrary methods of classifying soils based on grain size and plasticity indices.

The factors that influence the magnitude of dielectric dispersion $\Delta\varepsilon_o$ (see Figure 2) were investigated in detail by Arulanandan et al. (1973). It was shown that $\Delta\varepsilon_o$ depend predominately on the type and amount of clay mineral and the fabric having a second order effect. Thus the composition of cohesive soils can be characterized nondestructively and quantified in terms of the parameters $\Delta\varepsilon_o$. The significance of this parameter to the classification of soils, Arulanandan et al. (1973), to the prediction of cation exchange capacity Fernando et al. (1975), swell potential Basu and Arulanandan (1973), lime reactivity Castle and Arulanandan (1979), erosion potential Heinzen and Arulanandan (1977) and compression index Scharlin (1974), has been demonstrated.

2.1 Electrical Models to Predict Electrical Dispersive Behavior

Arulanandan and Mitra (1970), Arulanandan and Smith (1973) have shown it is possible to describe the electrical dispersion behavior of soils in terms of an electrical network model.

The current through the sample is considered to have three paths (Figure 3): (1) through the intercluster solution and clusters, (2) through clusters in contact with each other, and (3) through the intercluster solution. The corresponding three element model representation of the impedances of individual components is shown in Figure 4c.

Referring to Figure 4c, k_r = conductivity of the solution, ε_r = dielectric constant of the cluster, ε_s = dielectric constant of the solution, a = area of cluster-solution path, b = area of the particle contact path and c = area of the solution path. In the case of soils saturated in water, ε_s is approximately 79 and k_s is approximately equal to the conductivity of the pore fluid.

The expressions for the apparent dielectric constant, ε', and the apparent conductivity, σ', have been found utilizing the electrical network theory as follows:

$$\varepsilon' = \frac{a}{d(1-d)S}\left\{\frac{\varepsilon_r k_s^2}{1-d} + \frac{\varepsilon_s k_r^2}{d} + \omega^2\alpha^2\left(\frac{\varepsilon_r \varepsilon_s^2}{1-d} + \frac{\varepsilon_r^2 \varepsilon_s}{d}\right)\right\} + b\varepsilon_r + c\varepsilon_s \qquad (3)$$

$$\sigma' = \frac{a}{d(1-d)S}\left\{\frac{k_r k_s^2}{1-d} + \frac{k_r^2 k_s}{d} + \omega\alpha^2\left(\frac{\varepsilon_s^2 k_r}{1-d} + \frac{\varepsilon_r^2 k_s}{d}\right)\right\} + bk_r + ck_s \qquad (4)$$

where

$\omega = 2\Pi f$

$S = \left(\frac{k_s}{1-d} + \frac{k_r}{d}\right)^2 + \omega^2\alpha^2\left(\frac{\varepsilon_s}{1-d} + \frac{\varepsilon_r}{d}\right)^2$

f = current frequency

α = capacitance of a unit capacitor in vacuum (8.85×10^{-4} farad/cm)

k_r = conductivity of the cluster

ε_r = dielectric constant of the cluster

k_s = conductivity of the solution

ε_s = dielectric constant of the solution

a = x-sectional area of cluster-solution path

b = x-sectional area of particle contact path

c = x-sectional area of solution path

d = length of path in the solids in the solid-solution phase.

2.2 Quantification of Inter- and Intra-cluster Void Ratios

Anandarajah (1982), Arulanandan et al. (1983) equated the three element electrical model, Figure 4a, described in the previous pages to the model shown in Figure 4b in order to obtain the volume properties such as porosity.

Defining:

cluster tortuosity, $$t_1 = \frac{L_{2e}}{L} = \frac{L_{11e}}{L_{11}} \quad (5)$$

solution tortuosity, $$t_2 = \frac{L_{3e}}{L} = \frac{L_{12e}}{L_{12}} \quad (6)$$

$$a = \frac{A_1}{At_1t_2} \quad (7)$$

$$b = \frac{A_2}{At_1^2} \quad (8)$$

$$c = \frac{A_3}{At_2^2} \quad (9)$$

but $A = A_1 + A_2 + A_3$, i.e. $at_1t_2 + bt_1^2 + ct_2^2 = 1$ (10)

$$d = \frac{L_{11e}}{L \cdot t_1} \quad , \quad 1 - d = \frac{L_{12e}}{L \cdot t_2} \quad (11)$$

Therefore

$$L_{11} = L \cdot d \quad \text{and} \quad L_{12} = (1-d)L \quad (12)$$

and assuming electrical volumes equal to true volumes.

Then

$$A_{2e} \cdot L_{2e} = L \cdot A_2 \qquad A_{2e}/A_2 = 1/t_1 \quad (13)$$

$$A_{3e} \cdot L_{3e} = L \cdot A_3 \qquad A_{3e}/A_3 = 1/t_2 \quad (14)$$

$$A_{11e} \cdot L_{11e} = L_{11} \cdot A_1 \qquad A_{11e}/A_1 = 1/t_1 \quad (15)$$

$$A_{12e} \cdot L_{12e} = L_{12} \cdot A_1 \qquad A_{12e}/A_1 = 1/t_2 \quad (16)$$

Considering the three element model and the above mentioned definitions, and assumptions, one can show that:

$$\sigma' = \frac{a}{d(1-d)s}\left[\left\{\frac{k_r k_s^2}{(1-d)}\left(\frac{t_1}{t_2}\right) + \frac{k_s k_r^2}{d}\left(\frac{t_2}{t_1}\right)\right\} + \omega^2\alpha^2\left\{\frac{\varepsilon_r k_s^2}{(1-d)}\left(\frac{t_1}{t_2}\right) + \frac{\varepsilon_s k_r^2}{d}\left(\frac{t_2}{t_1}\right)\right\}\right] + bk_r + ck_s \qquad (17)$$

and

$$\varepsilon' = \frac{a}{d(1-d)s}\left[\left\{\frac{k_r \varepsilon_s^2}{(1-d)}\left(\frac{t_1}{t_2}\right) + \frac{k_s \varepsilon_r^2}{d}\left(\frac{t_2}{t_1}\right)\right\} + \omega^2\alpha^2\left\{\frac{\varepsilon_r \varepsilon_s^2}{(1-d)}\left(\frac{t_1}{t_2}\right) + \frac{\varepsilon_s \varepsilon_r^2}{d}\left(\frac{t_2}{t_1}\right)\right\}\right] + b\varepsilon_r + c\varepsilon_s \qquad (18)$$

where

$$s = \left[\frac{k_s}{(1-d)}\left(\frac{t_1}{t_2}\right) + \frac{k_r}{d}\left(\frac{t_2}{t_1}\right)\right]^2 + \omega^2\alpha^2\left[\frac{\varepsilon_s}{(1-d)}\left(\frac{t_1}{t_2}\right) + \frac{\varepsilon_r}{d}\left(\frac{t_2}{t_1}\right)\right]^2 \qquad (19)$$

The cluster dielectric constant depends on amount of water in the clusters and solids. Therefore, using the simple mixing rule proposed by Arulanandan (1980)

$$\varepsilon_r = n_I\,\varepsilon_s + \varepsilon_{prt}\,(1-n_I) \qquad (20)$$

where:

ε_s = dielectric constant of water

ε_{prt} = dielectric constant of dry clay particles

n_I = cluster porosity

but ε_{prt} is measured and found to be in the range 4 - 5

and ε_s is measured and found to be in the range 78 - 80.

Therefore, assuming $\varepsilon_s = 79$ and $\varepsilon_{prt} = 4.5$

$$n_I = \frac{\varepsilon_r - 4.5}{74.5} \tag{21}$$

but

$$e_I = \frac{n_I}{1-n_I} \tag{22}$$

Hence,

$$e_I = \frac{\varepsilon_r - 4.5}{79 - \varepsilon_r} \tag{23}$$

and

$$n_p = \frac{Vp}{Vp+Vc} = \frac{e_p}{1+e_p+e_I} \tag{24}$$

$$e_p = \frac{n_p}{1-n_p}(1+e_I) \tag{25}$$

but

$$n_p = \frac{A_1 L_{12} + LA_3}{LA} \tag{26}$$

$$\therefore \quad n_p = a(1-d)t_1 t_2 + ct_2^2 \tag{27}$$

A digital computer optimization program utilizing the simplex method was employed to analyze the dielectric constant and conductivity dispersion curves. The optimization program determines the values of the geometrical (a, b, c, d), compositional (ε_r, k_r, k_s, ε_s) and tortuosity (t_1, t_2) parameters of the model shown in Figure 4c such that the frequency dispersion curves of the apparent

dielectric constant and conductivity calculated from the theoretical Equations 17 and 18 fit the the experimental results within acceptable error limits. ε_s, the dielectric constant of water, was kept constant at 79 during all computer runs.

There are, in fact, eight random parameters b, c, d, ε_r, k_r, k_s, t_1, t_2 involved in the curve fitting procedure by optimization technique. At first sight, it might seem that the choice of eight seemingly random parameters would be enough to fit almost any set of curves and that the physical meaning of the result is doubtful. It is important to realize, however, that only the three independent geometrical parameters are genuine unknowns (b, c, d) and as $b \approx 0$, there are only two independent unknown parameters, "c" and "d". The respective conductivities, k_r and k_s, of the cluster and the interstitial solution and the dielectric constant of the solid particles must have values that are reasonable from the point of view of physical science. One would expect the conductivity of the interstitial solution to be of the same order as the conductivity of the pore fluid extract; the conductivity of the solid should be of the same order as the isoconductivity value (Arulanandan et al., 1973); the dielectric constant of the clusters should be between 4.5 (the dielectric constant of dry silicate mineral) and 79 (the dielectric constant of pure water), depending on the water content. Although these limitations were not written into the computer program, the numerous results obtained in earlier investigations show that the requirements were indeed met. However, a large number of computer runs is necessary to select the best set of parameters that fit the experimental curves and are reasonable from a physical science point of view. Thus the three-element electrical model can be used to quantify the inter- and intra-cluster void ratios.

The quantification of the inter- and intra-cluster void ratios by the above approach is time-consuming, as several computer runs are needed to be made to obtain the model parameters, combined with a certain amount of judgement

needed to choose the right parameters. This is due to the fact that Equations 17 and 18 are highly non-linear. In order to make the optimization technique more efficient and to choose the suitable model parameters, it was thought necessary to impose an additional constraint in the optimization. This would be achieved utilizing the measured water content of the soil. Once the dielectric constant and conductivity of the sample in the radio frequency range is available, to get the model parameters and hence the inter- and intra-cluster void ratios one needs to optimize the results due to the nonlinearity of the problem.

For this purpose optimization program called "Simplex" is used with modification to suit the problem.

Subroutine Simplex is called from main program "Opti" and cost function "Funct" is called by Simplex.

In the cost function "Funct" using the predicted model parameters dielectric constant and conductivity are calculated in the frequency range and compared with measured to obtain the minimum percentage error. To this cost function another term is added to take into account the difference between calculated and measured water contents.

There are several constraints imposed on model parameters to obtain a realistic picture. (All model parameters should be positive.) Eight parameters are considered as variables namely b, c, d, ϵ_r, k_r, k_s, t_1 and t_2. Model parameter a is obtained from the following condition

$$at_1t_2 + bt_1^2 + c_2^2 = 1 \qquad (10)$$

Following constraints are imposed for the model

$0 \leq b \leq 0.3$

$0 \leq c \leq C_{max}$

$0.5 \leq d \leq 1.0$

$$\epsilon_{r_{min}} \leq \epsilon_r \leq 74.5$$

$$k_{s_{min}} \leq k_s \leq k_{s_{max}}$$

$$k_{r_{min}} \leq k_r \leq k_{r_{max}}$$

$$0 \leq t_1 \leq 1.7$$

$$0 \leq t_2 \leq 1.5$$

C_{max} and $\epsilon_{r_{min}}$ are normally set at 0.5 and 8.0 respectively but could be changed in using input data. $k_{s_{min}}$, $k_{r_{min}}$, $k_{s_{max}}$, and $k_{r_{max}}$ are given as data for the problem. Successful optimization with least amount of computer time involves selecting a narrow range for k_s and k_r while keeping it within the expected range.

As the problem is highly nonlinear, mostly it hits a local minima, instead of true global minimum. To avoid this situation the computer program should be run several times with different initial values. Program "Opti" allows to change the starting points and number of runs required. It changes the starting value of c, d, ϵ_r, t_1 and t_2 between the specified values given as input data.

Even with several runs of different starting points it is extremely hard to hit the local minima. Therefore one should select a local minima which gives close values of inter- and intra-cluster void ratios for vertical and horizontal measurements.

This constraint for selecting local minima as the optimum point is quite justifiable as irrespective of the direction of electrical measurement, one should get the same cluster void ratio even in highly nonlinear problems like this.

2.3 Formation Factor and Shape Factor

From the low frequency (1 KHZ) conductivity measurements, the formation factor F is defined as the ratio of the pore fluid conductivity, σ_s, to the soil sample conductivity, σ, as follows:

$$F = \sigma_s/\sigma \tag{28}$$

The formation factor has been shown to relate to the porosity and anisotropy of soil particles, Arulanandan et al. (1979).

The formation factor was shown to be a tensorial parameter with tensorial components related to the microstructural features in soils, Dafalias et al. (1979). The average formation factor $\bar{F}$ and the anisotropy index, A, are defined, for a transversely isotropic soil, as follows:

$$\bar{F} = (F_v + 2F_H)/3 \tag{29}$$

$$A^2 = F_v/F_H \tag{30}$$

where:

F_v = formation factor in the vertical direction

F_H = formation factor in the norizontal direction

An integration technique proposed by Bruggeman (1935) was used by Dafalias and Arulanandan (1978) to derive an expression for average formation factor, $\bar{F}$, as a function of porosity, n, and average shape factor, $\bar{f}$, as

$$\bar{F} = n^{-\bar{f}} \tag{31}$$

The average shape factor, $\bar{f}$, is the negative slope of the log $\bar{F}$ - log n plot. It is the first invariant of the second order shape factor tensor f and it relates the electric fields inside and outside the soil particles. It has been shown both theoretically and experimentally that the shape factor is direction dependent and depends on porosity, gradation and particles' shape and orientation, Kutter (1978), Arulanandan et al. (1979), Dafalias et al. (1979), and Arulmoli (1980). Since the average formation factor is independent of orientation of

particles, the average shape factor, for a given soil, is expected to be a function of porosity and the shape of particles.

The electrical parameters $\bar{F}$, A, $\bar{f}$ of soil deposits are governed by the grain and aggregate characteristics of the particles.

3. Experimental Procedure and Results

A detailed experimental study was conducted to investigate the variation of stress state with the electrical parameters for several soils. For this purpose, it was necessary to develope a series of identical cells to measure the stress state and electrical parameters simultaneously.

Four identical circular cells of internal diameter 2" and height 5" (Figures 5 and 6) were fabricated out of teflon tubes of ½" thickness. Two of the cells were used to measure electrical parameters in the vertical and horizontal directions and the other two to measure total lateral pressure and pore water pressure.

The cell used for the determination of electrical properties in the vertical direction consists of two perforated brass electrodes placed at top and bottom of the sample. The other cell, used for the determination of electrical properties in the horizontal direction consists of two curved brass electrodes of radius of curvature 1", length 2" and height 1⅝". These electrodes were embedded in the teflon walls on diametrically opposite ends. The electrodes in the cells were connected to the impedance analyzer by a 6" long coaxial transmission cable.

Since the impedance of the transmission line and cell was very significant in the radio frequency range, its effect had to be elminiated by calibration. The calibration procedure used by Anandarajah (1982) was adopted using water of known conductivity and dielectric constant of 79. Hewlett-Packard impedance analyzer (Figure 7), which is designed for precise impedance measurements in

the frequency range of 1 MHZ - 1000 MHZ, was used for the measurements in the radio frequency range. A low frequency impedance comparator (Figure 8) was used for the determination of sample conductivity and consequently the formation factor - at a frequency of 100 KHZ. The cell was calibrated to obtain the cell constant using the low frequency impedance comparator along with water of known conductivity.

Water conductivity and pore fluid extract conductivity were measured using Beckmann conductivity meter (Figure 9).

Pressure transducer model PG-003-5C was fitted to one of the cells for the purpose of measuring the total lateral stress and it was in turn connected to a Daytronic digital strain indicator (Figure 10). As the surface of the transducer was not curved, a curved pad was made using silicon glue, and the transducer was calibrated by applying hydraulic pressure to the cell. This calibration accounts for the effects of the pad and the strains induced by fixing the transducer to the cell.

Pore pressure transducer model GT-300 was fitted for the purpose of measuring the pore pressure variation during consolidation. A small porous stone was inserted between the cell and the transducer for the measurement of pore water pressure. The transducer was connected to the Budd strain indicator (Figure 11). The transducer was calibrated - before fixing - using air pressure in the working pressure range.

The soils used were:

1. Snow Cal (60%) + Illite (40%)
2. Snow Cal (95%) + Bentonite (5%)
3. Yolo Loam
4. Marysville Red Soil
5. Na - Illite

6. Kaoline - M.P.

7. Snow Cal (70%) + Bentonite (30%)

and

Mixed soils, detailed proportions are given in Table 1.

Each soil except mixed soils was sieved through a #200 mesh sieve. Sufficient amount of water was added to the fines to bring the water content to about 3-4 times the liquid limit of the soil. This procedure ensures that the sample would behave very similar to a sample sedimented from a dilute suspension Olson (1962). The slurry was mixed for 6 hours in a mechanical mixer and kept inside a vibrator under a vacuum pressure for 24 hours to ensure complete saturation. Then the sample was kept for 2-4 weeks for it to attain equilibrium with its pore fluid. The samples of Yolo Loam, Marysville Red and Kaoline - M.P. were prepared with 0.05N salt solution.

The mixed six soils were prepared by mixing certain proportions of sand, silt and clay. Soil samples were mixed with a 0.05N solution (2.925 gm of NaCl in 1000 cc of distilled water), and left for about twenty hours to achieve a state of equilibrium.

The electrical properties - R and x (resistance and reactance) - both in horizontal and vertical directions, lateral stress and excess pore water pressure were measured at each stage of consolidation.

The electrical dispersion data were obtained by reducing the impedance analyzer data to take account of line impedance.

The dispersion data were plotted and joined by a smooth curve to eliminate any calibration and measuring errors. Subsequently data points extracted from those curves were used for the optimization program to get the three element model parameters and the intra- and inter-cluster void ratios.

The electrical dispersion curves for mixed soils at different water contents are presented in Figures 12-35 for loading and unloading condition in both vertical and horizontal directions. The optimized model parameters using the experimental dispersion results corresponding to different water contents are presented in Tables 2-13. The formation factor, F, was plotted against the total porosity, n, and is presented in Figures 36-48.

4. Electrical Properties in Relation to Mechanical Properties

It has been shown that the principal factors influencing the dielectric dispersion of fine grained soils in the radio frequency range (10^6 - 10^8 HZ) are the compositional properties of the different phases and the heterogeneous nature of the system. The engineering properties of fine grained soils are also controlled by these factors. This mutual dependency is used as a basis to correlate the electrical properties to mechanical properties.

The purpose of this research is to establish possible correlations between those parameters which are needed for the prediction of stress-strain behavior of fine grained soils and the appropriate electrical parameters. It will then be possible to determine the stress-strain behavior of fine grained soils by estimating these mechanical properties from the above correlation and using them in a suitable constitutive model. This approach facilitates the determination of the stress-strain behavior of soils by nondestructive in situ measurements since the electrical properties can be determined in situ without disturbing the structure of the soil.

Any constitutive model for the prediction of stress-strain behavior of fine grained soils would require the knowledge of the slope of the consolidation line, λ, the slope of the swelling line, κ, the slope of the critical state line, M, the initial void ratio, e_o, and the overconsolidation ratio (along with other model parameters appropriate for the model under consideration). These parameters

are defined in Figure 51. The water content of the fine grained soils can be determined by conventional procedures and the initial void ratio, e_o, could be evaluated. The correlations between the electrical properties and the mechanical properties λ, κ and M for normally consolidated soils would be established in the following sections.

4.1 Slope of Isotropic Consolidation Line, λ

Bolt (1956) attempted to predict the compressibility characteristics of clays based on the concept of osmotic pressure using Gouy-Chapman diffuse double layer theory and Van't Hoff's theories of parallel platy particles. Experimental compression characterics of Na-montmorillonite and Na-illite were found to be close to the predicted relationships. The theory, however, was found to be valid only for clays exhibiting very strong colloidal properties such as montmorillonite. Derivations from Bolt's findings have been reported by Mitchell (1960) and Olson and Mitronovas (1962) and are ascribed mainly to particle orientation. Quigley and Thompson (1966) have observed fabric changes in natural Leda clay during consolidation using X-ray diffraction methods. It has been shown by Rosenquist (1958) that the compressibility of clay is dependent on the type as well as the valence and concentration of ions adsorbed on the surface of the clay particles. Further, Olson and Mesri (1970) have concluded that both mechanical and physico-chemical factors influence the compressibility of soils in general, although one or the other may dominate depending on the soil type.

The factors influencing the magnitude of dielectric dispersion, $\Delta\varepsilon_o$, were investigated in detail by Arulanandan et al. (1973). It has been found that $\Delta\varepsilon_o$ is significantly influenced by type and amount of clay mineral. The values of $\Delta\varepsilon_o$ were shown to increase in the sequence kaolinte < illite < montmorillonite. The compression index of these soil also increases in this sequence. The

magnitude of dispersion decreases with an increase in percentage of sand in sand-clay mixtures Arulanandan et al. (1973); so does the compression index as it is widely known. Olson et al. (1970) have shown that the compression index of kaolinite is decreased when the electrolyte concentration is increased from 0.0001 N sodium to 1.0 N sodium and Arulanandan et al. (1973) have shown that $\Delta\varepsilon_o$ also decreased with increasing electrolyte concentration.

The preceding discussion suggests that the factors influencing the mechanisms controlling the compression of clays and magnitude of dielectric dispersion are the same. Based on this mutual dependency, $\Delta\varepsilon_o$ has been correlated with λ. Sharling, J.R. (1972) has shown that there is a linear relationship between $\Delta\varepsilon_o$ and λ for natural clays as shown in Fig. 52. Further results confirm the general validity of this relationship between $\Delta\varepsilon_o$ and λ.

4.2 Slope of Isotropic Swelling Line, κ

The swelling characteristic of saturated clays due to the removal of external load has been investigated by many, either by mechanical models such as the one used by Terzaghi (1929) where swelling is assumed to result from elastic rebound of bent particles or by physico-chemical models such as the one used by Bolt (1956) where osmotic repulsive forces are assumed to be responsible for swelling. Although it has been possible to explain the mechanism controlling swelling characteristics by the above concepts it was not very successful owing to the complicated structural arrangements of particles in clays.

The concept of clusters in fine grained soils (Michael et al. 1954 and Quirk, 1959) has been utilized by Olsen (1961) in his study of hydraulic flow through saturated clays and he concluded that the discrepancy between the measured permeability and the one predicted by Kozeny-Carman equation in clays is mainly due to unequal pore sizes due to grouping of clay particles in

clusters. The existence of primary particles aggregation has been observed by many using electron microscope, Quigley et al. (1966).

Fig. 53 shows variation of intra- (e_I) and inter-cluster (e_p) void ratios with total void ratio evaluated using electrical dispersion data for Snow Cal (95%) + Montmorillonite (5%). The results corresponding to measurements made in the vertical and horizontal directions are identical and are very similar to those predicted by Olsen (1961).

Fig. 54 shows for mixed soils and Fig. 55 for clays the variation of intra- (e_I) and inter-cluster (e_p) void ratios with total void ratio evaluated using electrical dispersion data.

It has been shown that the swelling of fine grained soils is caused by swelling of clusters Smith and Arulanandan (1981) and the decrease in inter-cluster pores during compression is irreversible Meegoda (1983).

If the ratio of intra-cluster to total void ratio is large for a given soil, the elastic compression due to an increase in the external load would be high and consequently swelling would also be high when the load is removed. Assuming this mechanism of swelling, the ratio, e_I/e is corrected with κ as shown in Fig. 56.

4.3 Slope of Critical State Line M of the Bounding Surface Theory

When a soil element is sheared under drained or undrained conditions, experimental results indicate that the soil element fails when the stress path reaches the critical state line independent of the initial stress state of the soil element (Schofield et al., 1968). At failure, the void ratio, e, and the effective mean normal pressure, p, lie on a unique line, referred to as a critical state line on the e-p space. This concept is widely known as the critical state concept (Roscoe et al., 1968). The slope of the critical state line, on the p-q space, therefore represents the ultimate shear strength of soils.

Lambe (1960) has discussed the factors controlling ultimate shear resistance of fine grained soil which is considered to be due to friction and interference between particles. These components of ultimate shear resistance and hence M would depend on many factors such as particle size, shape, surface texture and the structure of the soils resulting from the attractive and repulsive forces between the adjacent clay particles. In fine grained soils, the shape factor would reflect in addition to shape of the particles the physico-chemical interaction between particles. In other words, the shape factor, $\bar{f}$, is a function of the shape, composition and arrangement of particles.

Soils which exhibit higher anisotropy were found to have lower strength when measurements are made in the direction of the major prinicipal axis. Based on these considerations, an attempt is made here to correlate M with an electrical index defined as a function of A and $\bar{f}$.

The values of M are obtained from the normally consolidated undrained test results. A computer program developed by Herrmann et al. (1980) for the calibration of bounding surface theory (i.e. evaluation of model parameters by matching theoretical and experimental stress-strain relationships) was used to obtain the values of M. A direct assessment from the failure value of q/p could only be approximate on account of the inaccuracies in measurement of the stress parameters at large strain and would underestimate M because failure intervenes before the critical state line.

The correlation between M and $A^2/\bar{f}$ based on results corresponding to four different clays and mixed soils tested is shown in Fig. 57. A reasonable nonlinear correlation between M and $A^2/\bar{f}$ is evident.

4.4 Correlation of Earth Pressure at Rest, K_o, with Electrical Parameters

If the material to be tested is purely elastic, K_o will depend on elastic properties (Poisson's ratio v) as given by equation (28). On the other hand, if

the material is purely plastic with no strength - such as viscous fluid - it will be equal to one.

$$K_o = \nu/1-\nu \tag{28}$$

For plastic materials with strength, K_o depends on the slope of the critical state line (i.e. friction angle) and using Bounding Surface Model Dafalias et al. (1982) K_o can be given as

$$3/2 = \frac{\mu^2 (pR-p_o)}{qR (R-1)^2} \tag{29}$$

where p and q are hydrostatic and deviation stresses respectively and are given by $p = \sigma_v' (1+2 K_o)/3$ and $q = \sigma_v' (1-K_o)$. R is a material constant depending on the shape of the yield surface and is usually assumed as 2 or 2.72 and

$$(p/p_o)^2 + \frac{(R-1)^2}{\mu^2} (q/p_o)^2 - \frac{2}{R} (p/p_o) = \frac{R-2}{R}$$

In reality, soils are elasto-plastic materials with viscous effects. As this study is not concerned with viscous effects, we can assume soil to be an elasto-plastic material. For elasto-plastic materials K_o depends on the slope of the critical state line, compression index λ and swelling index (K) as given below

$$3/2 = \frac{\mu^2 (pR-p_o)}{Rq (R-1)^2} (1 + \frac{K}{\lambda-K} Y) \tag{30}$$

where

$$Y = (\frac{po}{p})^2 \frac{p/po-(2-R)}{R-po/p + \frac{R(R-1)^2 q^2}{\mu^2 p^2}} \text{ and } (p/po)^2 + \frac{(R-1)^2}{\mu 2} (\frac{q}{po})^2 - \frac{2}{R} (p/po) = \frac{R-2}{R}$$

Only isotropic materials could be modelled by the above function. Real soils under K_o - loading are anisotropic due to the presence of platy type of particles. As the degree of anisotropy increases lateral stresses under zero lateral strains decreases since low lateral stresses are associated with parallel arrangement of particles. Therefore mechanical anisotropy has a marked effect on K_o in addition to friction angle or the strength of the material.

Mechanical anisotropy could be quantified by the electrical anisotropy parameter A. Particle friction could be quantified by the average shape factor f as the shape factor depends on the particle roughness Arulanandan et al. (1979).

The variation of K_o with consolidation pressure is given in Figure 58. This shows that after a pressure of around 10 psi K_o value approaches a constant value and remains around that value on further consolidation.

These constant values of K_o for each soil tested are used to correlate with electrical index A^4f and are given in Figure 59 (Meegoda (1983)). When there is no friction or anisotropy, K_o is assumed as 1 and the lower limit of K_o for fine grained soils is assumed as 0.38 in deriving the correlation between K_o and electrical index A^4f.

Figure 60 shows how K_o varies with the electrical index A^4f for different consolidation pressures for Snow Cal and 5% Montmorillonite. This result shows that the proposed correlation is justifiable for consolidation pressures greater than 10 psi.

5. In Situ Prediction of Stress-Strain Behavior of Cohesive Soils

Application of the theory of plasticity has gained wide popularity over the past few years for the analytical prediction of stress-strain relationship of soils. The most notable and earliest of the constitutive models developed using the theory of plasticity is the Cam-clay theory developed by the Cambridge

group (Schofield et al., 1968). The Cam-clay model can represent the strain hardening behavior depending on the state of the soil with respect to the critical state line. The verification of the Cam-clay model under simple shear and triaxial stress states has been carried out satisfactorily on soils that are "wet" of critical state (Roscoe et al., 1968). However, this model has not been demonstrated to be representative of the strain softening behavior of the soils. Yield surface, along with the normality rule, gives rise to prediction of unrealistic behaviors of isotropic loading. This is due to the fact that the yield surface derived as the result of assumptions made in Cam-clay theory does not intersect the p-axis at the right angle.

Roscoe et al. (1968) modified the theory by introducing an ellipse for the yield surface and using normality condition. The size of this elliptic yield surface is completely defined by the initial isotropic consolidation pressure, p_o, and the slope of the critical state line, M. The value of R, which is defined as the ratio of the mean normal pressure, p_o, at which the yield surface intersects the p-axis and the mean normal pressure, p_1, at which the yield surface intersects the critical state line (refer to Figure 61), is assumed to be 2.0, a constant value. It is, however, desirable to be able to use different values of R in the theory in order to be able to predict the stress-strain behavior of a broad range of soil types.

Numerous theories have since been developed to describe the stress-strain behavior of soils under a general loading condition. Bounding surface plasticity model (Dafalias et al., 1980), cap model (Di Maggio et al., 1971), endochronic theory (Valanis et al., 1971), and model developed by Prevost (1978) are some of them.

The bounding surface plasticity model has been developed to describe a generalized stress-strain behavior of fine grained soils under a variety of

conditions such as normally consolidated and over-consolidated, strain hardening and strain softening, monotonic and cyclic, compression and extension, loading paths in the tension zone (i.e., the effective mean normal stress is tension), etc. The verification of this theory under some of the above conditions has been carried out satisfactorily. The value of R can be varied as required to predict a given experimental stress-strain relationship, unlike in the case of critical state theory developed by Roscoe et al. (1968). When R = 2, these two theories predict identical stress-strain behavior in the case of normally consolidated soils.

5.1 Bounding Surface Plasticity Model

The theory of plasticity, along with the bounding surface concept and the critical state concept, was used to develop a bounding surface plasticity model for the description of the stress-strain behavior of fine grained soils.

The bounding surface concept is that the plastic modulus of the material at a given stress state can be determined knowing the stress state, a distance from a point on the bounding surface (defined by means of a suitable mapping rule) to the point representing the current stress state, a plastic internal variable to account for the effect of past loading history and the plastic modulus corresponding to the projected point on the bounding surface. The bounding surface and a radial mapping rule are illustrated schematically in Figure 62 where the bounding surface is shown in the space of I_1 (first effective stress invariant) and J_2 (second stress invariant).

The plastic modulus at point B can be found by the consistency condition knowing the functional form of the bounding surface. The plastic internal variable chosen in developing the theory for soils is the integral of the plastic void ratio, e^p. The plastic modulus at the current state, A, can be expressed as follows:

$$K = K_b + H(\sigma_{ij}, e^P) \frac{\delta}{\delta_o(\sigma_{ij}, e^P) - \delta} \tag{31}$$

where K plastic modulus at A, K_b = plastic modulus at B, σ_{ij} = stress tensor, e^P = plastic void ratio, δ_o = reference stress, H = positive "shape" hardening function of the state of stress.

Knowing the plastic modulus, the plastic strain increment due to a given stress increment can be determined through the plastic constitutive relation using a suitable flow rule as follows:

$$\dot{\epsilon}_{ij} = \langle L \rangle n_{ij} \tag{32}$$

$$L = \frac{1}{K} \dot{\sigma}_{kl} n_{kl} \tag{33}$$

where ϵ_{ij} = plastic strain increment tensor, L = loading function, σ_{ij} = stress increment tensor and n_{ij} = direction of the plastic strain increment vector. Assuming normality rule, n_{ij} is the unit normal to bounding surface at the projection point B (Figure 62). The behavior of the material is elastic in unloading and elasto-plastic in loading.

One of the desirable features of this approach is that the plastic deformation takes place within the bounding surface unlike in the classical plasticity theory where the behavior is fully elastic within the yield surface. This feature of the model yields realistic predictions for overconsolidated soils and under cyclic loading conditions. The loading function L (Equation 33) includes K to account for loading during the unstable behavior since $\dot{q}_{kl} n_{kl} < 0$ when $K < 0$ and consequently $L > 0$.

The detail description of the theory could be found in many references (e.g., Dafalias et al. 1980). The bounding surface used for soils is shown in the triaxial space as in Figure 63.

The undrained stress path of a normally consolidated soil can be expressed by a closed form equation as follows:

$$\frac{q}{p_o} = \frac{M}{R-1}\left[\frac{2}{R}\left(\frac{p}{p_o}\right)^{\frac{\lambda-2\kappa}{\lambda-\kappa}} + \left(1-\frac{2}{R}\right)\left(\frac{p}{p_o}\right)^{\frac{-2\kappa}{\lambda-\kappa}} - \left(\frac{p}{p_o}\right)^2\right]^{1/2} \qquad (34)$$

where p_o = isotropic preconsolidation pressure, p_i = mean normal at peak value of q on the yield line, R = material constant = p_o/p_i.

Since $q_u = Mp_u$ at failure, the undrained strength of a normally consolidated soil can be expressed as follows:

$$q_u = M\, p_o\, R^{-\frac{\lambda-\kappa}{\lambda}} \qquad (35)$$

The information required for the prediction of the stress-strain behavior of normally consolidated soils is λ, κ, M, R, e_o and p_o.

5.2 Application to In Situ Prediction of Stress-Strain Behavior

The model parameters defining the bounding surface plasticity model can be obtained using a set of triaxial test data by a trial and error procedure, i.e., the model parameters should be chosen so that the predicted and measured stress-strain relationships are close to each other. A computer program was developed Herrmann et al. (1982) as described in the earlier section incorporating the bounding surface theory in order to predict the stresses and strains. This program was used to obtain the value of M which predicts the relationships of q vs. ε_1 and q vs. p (ε_1 = axial strain) as close to the corresponding experimental relationships as possible. The values of "M" obtained in this manner are correlated with the electrical index, A^2/f as shown in Figure 57.

A reasonably good agreement between the experimental and theoretical predictions of stress-strain behavior of soils is seen from the results presented in Figures 64-76. It is therefore possible to predict the stress-strain behavior of normally consolidated fine grained soils using bounding surface plasticity model

if model parameters can be determined by in situ tests. In situ model parameters could be predicted from in situ electrical measurements. Therefore it can be concluded that if in situ electrical measurements (i.e., apparent dielectric constants and conductivity in the radio frequency range along with conductivity of the solution extract) are made in situ, stress-strain behavior and in situ stress state of normally consolidated fine grained soils could be predicted.

6. Future Work

It is proposed to investigate the possibility of the prediction of initial in situ stress state using the electrical method. The prediction of in situ stress-strain behavior of overconsolidated soils requires a knowledge of O.C.R. or preconsolidation pressure (P_c) and the value of K_o. It is proposed to establish correlations between the mechanical parameters K_o, P_c and $\bar{K}$ and electrical parameters in order to enable the prediction of K_o, P_c and $\bar{K}$ in situ where $\bar{K} = K_o$, O.C.R.$^{\alpha}$ ($\alpha \approx .45$-$.55$).

In this study, correlations between electrical and mechanical properties have been established to enable the prediction of stress-strain relationship of normally consolidated soils. It is proposed now to verify these predictions. Electrical properties will be used to predict λ, k and M of normal consolidated soils. These predicted mechanical properties will be used in the bounding surface plasticity model to predict the stress-strain relationships. These relationships will be compared with the measured values. Sufficient number of soils will be tested to establish the sensitivity of the predicted parameters λ, k and M to the variations between the measured and predicted stress-strain relationships. It is also proposed to develop a relationship between mechanical and electrical anisotropy.

7. References

Anandarajah, A., (1982), "In Situ Prediction of Stress-Strain Relationships of Clays Using A Bounding Surface Plasticity Model and Electrical Methods." Dissertation presented to the University of California, Davis, California, in 1982, in partial fulfillment of the requirements for the degree of Doctor of Philosophy.

Arulanandan, K. and Mitra, S.K., (1970), "Soil Characterization by Use of Electrical Network," Proceedings of the 4th Asilomar Conference on Circuits and Systems, Nov. 1970, pp. 480-485.

Arulanandan, K. and Smith, S.S., (1973), "Electrical Dispersion in Relation to Soil Structure," Journal of the Soil Mechanics and Foundation Division, ASCE, Vol. 99, No. SM12, Proc. Paper 10235, Dec. 1973.

Arulanandan, K., Basu, R., and Scharlin, R. J., "Significance of the Magnitude of Dielectric Dispersion in Soil Technology," Highway Research Record, Number 426, pp. 23-32, 1973.

Arulanandan, K. and Kutter, B., (1978), "A Directional Structural Index Related to Sand Liquefaction," Proceedings on the Specialty Conference on Earthquake Engineering and Soil Dynamics, ASCE, Pasadena, California, June 1978, pp. 213-229.

Arulanandan, K. and Dafalias, Y.F., (1979), "Significance of Formation Factor in Sand Structure Characterization," Letters in Applied and Engineering Sciences, Vol. 17, 1979, pp. 109-112.

Arulanandan, K., (1980), CE 283 Class Notes, Dept. of Civil Engineering, University of California, Davis.

Arulanandan, K., Anandarajah, A., and Meegoda, N.J., (1983), "Quantification of Inter and Intra-Cluster Void Ratios Using Three Element Electrical Model," UCD Report to be published.

Arulmoli, K., (1980), "Sand Structure Characterization for In Situ Testing," Thesis submitted in partial satisfaction of the requirement for the Degree of Master of Science in Engineering, University of California, Davis, June 1980.

Basu, R. and Arulanandan, K., (1974), "A New Approach for the Identification of Swell Potential of Soils," Proceedings of the Third International Conference on Expansive Soils, Techion - Israel Institute of Technology, July 1973. Also in Bulletin of the Association of Engineering Geologist Vol. XI, No. 4, 1974.

Bolt, G.H., (1956), "Physico-Chemical Analysis of the Compressibility of Pure Clay," Geotechnique, Vol. 6, pp. 86-93.

Bruggeman, D.A.G., (1935), "Berechung Verschiuedenez Physikalischev Konstanten Von Heterogenen Substanzen," Ann. Phys. Lpz., 5, Vol. 24, p. 636.

Castle, A.K. and Arulanandan K., (1979), "New Approach to Predict Lime Reactivity of Soils," Journal of the Geotechnical Engineering Division, Proceedings of the American Society of Civil Engineers, Vol. 105, No. GT4, April 1979.

Dafalias, Y.F. and Arulanandan, K., (1979), "The Formation Factor Tensor in Relation to Structural Characteristics of Anisotropic Granular Soils," Proceedings, Colloque International du C.N.R.S., Euromech Colloquium 115, Villard-de-Law, France, June 1979.

Dafalias, Y.F. and Herrmann, L.R., (1980), "A Bounding Surface Soil Plasticity Model," Int. Symp. on Soils Under Cyclic and Transient Loading, Swansea, U.K., 1980, pp. 335-345.

Dafalias, Y.F. and Herrmann, L.R., (1982), "Bounding Surface Formulation of Soil Plasticity," Chapter 10 in Soil Mechanics - Transient and Cyclic Loading, O.E. Zienkiewicz and G.N. Pande, eds., J. Wiley and Sons publs., 1982.

Di Maggio, F.L. and Sandler, I.S., (1979), "Material Model for Granular Soils," J. Eng. Mech. Div., ASCE, 97, 1971, pp. 935-950.

Fernando, J., Smith, R. and Arulanandan, K., (1979), "New Approach to Determination of Expansion Index," Journal of the Geotechnical Engineering Division, Proceedings of the ASCE, Vol. 101, No. GT9, September 1979.

Heinzen, R.T. and Arulanandan, K., (1977), "Factors Influencing Erosion, Dispersive Clays and Methods of Identification," Proceedings of the Paris Symposium on Erosion and Solid Matter Transport on Inland Waters, International Association of Hydrological Sciences - Association Internationale des Sciences Hydrologiques, No. 122, pp. 75-81, 1977.

Herrmann, L.R., Dafalias, Y.F., and DeNatale, J.S., (1980), "Bounding Surface Plasticity for Soil Modeling," October 1980, Final Report to Civil Engineering Laboratory, Naval Construction Battalion Center, Port Hueneme, CA, 93043.

Herrmann, L.R., Dafalias, Y.F. and DeNatale, J.S., "Numerical Implementation of Bounding Surface Soil Plasticity Model," Proceedings of the International Symposium on Numerical Models in Geomechanics, 1982.

Lambe, T.W., (1960), "A Mechanism Picture of Shear Strength in Clay," Proceedings, Research Conference on Shear Strength of Cohesive Soils," Soil Mechanics and Foundation Division, ASCE, Univ. of Colorado, Boulder, Colorado, June 1960.

Meegoda, N.J., (1983), "Prediction of In Situ Stress State Using Electrical Method," Thesis submitted in partial satisfaction of the requirements for the degree of Master of Science in Engineering, University of California, Davis, March 1983.

Michaels, A.S. and Lin, C.S., (1954), "The Permeability of Kaolinite," Ind. and Eng. Chem., Vol. 46, pp. 1239-1246.

Mitchell, J.K., (1960), "The Application of Colloidal Theory to the Compressibility of Clays," Proceedings, Seminar on Interparticle Forces in Clay-Water-Electrolyte System, Commonwealth Scientific and Industrial Research Organization, Melbourne, Australia, pp. 2.92-2.97.

Olsen, H.W., (1961), "Hydraulic Flow Through Saturated Clays," submitted in partial fulfillment of the requirements for the degree of Doctor of Science in Civil Engineering, M.I.T.

Olson, R.E., (1962), "The Shear Strength Properties of Calcium Illite," Geotechnique Vol. XII, pp. 23-43.

Olson, R.E. and Mitronovas, F., (1962), "Shear Strength and Consolidation Characteristics of Calcium and Magnesium Illite," Proc. 9th Nat. Conf. Clays and Clay Minerals, pp. 185-209.

Olson, R.E. and Mesri, G. (1970), "Mechanics Controlling Compressibility of Clays," ASCE, J. of Soil Mechanics and Foundation Division, SM6, Nov. 1970.

Prevost, J.H., (1978), "Plasticity Theory for Soil Stress-Strain Behavior," J. Eng. Mech. Division, ASCE, 1978, 104, pp. 1177-1196.

Quigley, R.M. and Thompson, C.D., (1966), "The Fabric of Anisotropically Consolidated Sensitive Marine Clay," Canadian Geotechnical Journal 3, Vol. 2, pp. 61-73.

Quirk, J.P., (1959), "Permeability of Porous Media," Natron, Vol. 183, pp. 387-388.

Roscoe, K.H. and Burland, J.B., (1968), "On the Generalized Stress-Strain Behavior of Wet Clay," Engineering Plasticity, ed. J. Heyman and F.A. Leckie, Cambridge University Press, pp. 535-609.

Rosenquist, I. Th., (1958), "Physico-Chemical Properties of Soils: Soil Water System," Journal of Soil Mech. and Foundations Div., ASCE, Vol. 85, No. SM2, Proc. Paper 2000, April 1958, pp. 31-53.

Schofield A.N. and Wroth, C.P., (1968), "Critical State Soil Mechanics," McGraw-Hill, London, 1968.

Sharlin, J.R., (1972), "A New Approach to Soil Classification," M.S. Thesis, University of California, Davis, 1972.

Smith, S.S. and Arulanandan, K., (1981), "Relationship of Electrical Dispersion to Soil Properties," J. of Geotechnical Engineering Division, ASCE, Vol. 107, No. GT5, May 1981.

Terzaghi, K., (1929), "Tecnisch - Geologische Beschreibung der Bodenbeschaffenheit fur bautechnische Zwecke," Chapter IX, Part A, Ingenieurgeologie, by K.A. Redlich, K. Terzaghi, and R. Kampe, Julis Springer, Wien and Berlin.

Valanis, K.C., "A Theory of Viscoplasticity without a Yield Surface, Part I: General Theory, Part II: Application to Mechanical Behaviour of Metals," Arch. of Mech. 1971, 23, 517-551.

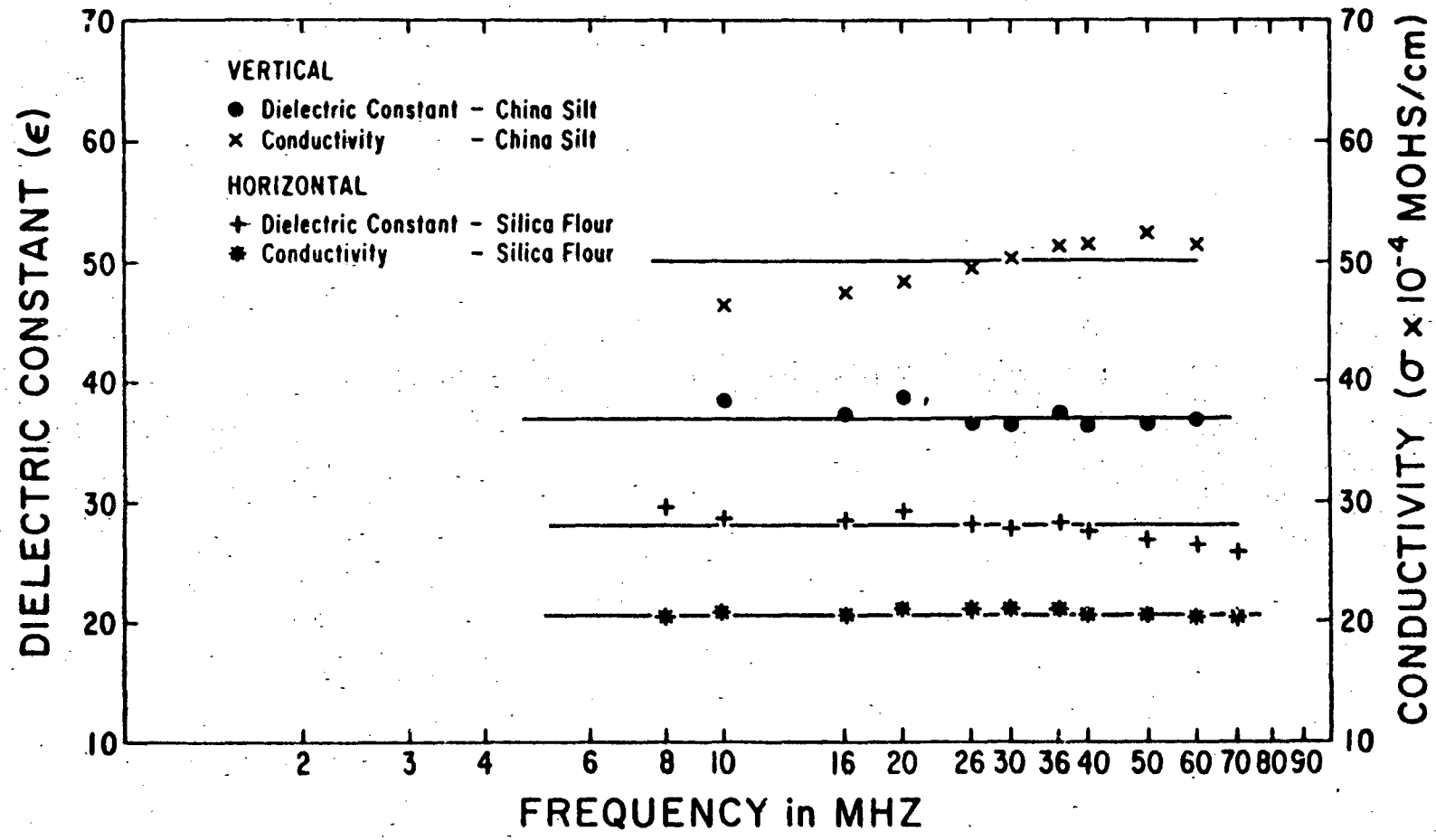

FIG. 1 Variation of Dielectric Constant and Conductivity as a Function of Frequency for Sands and Silts

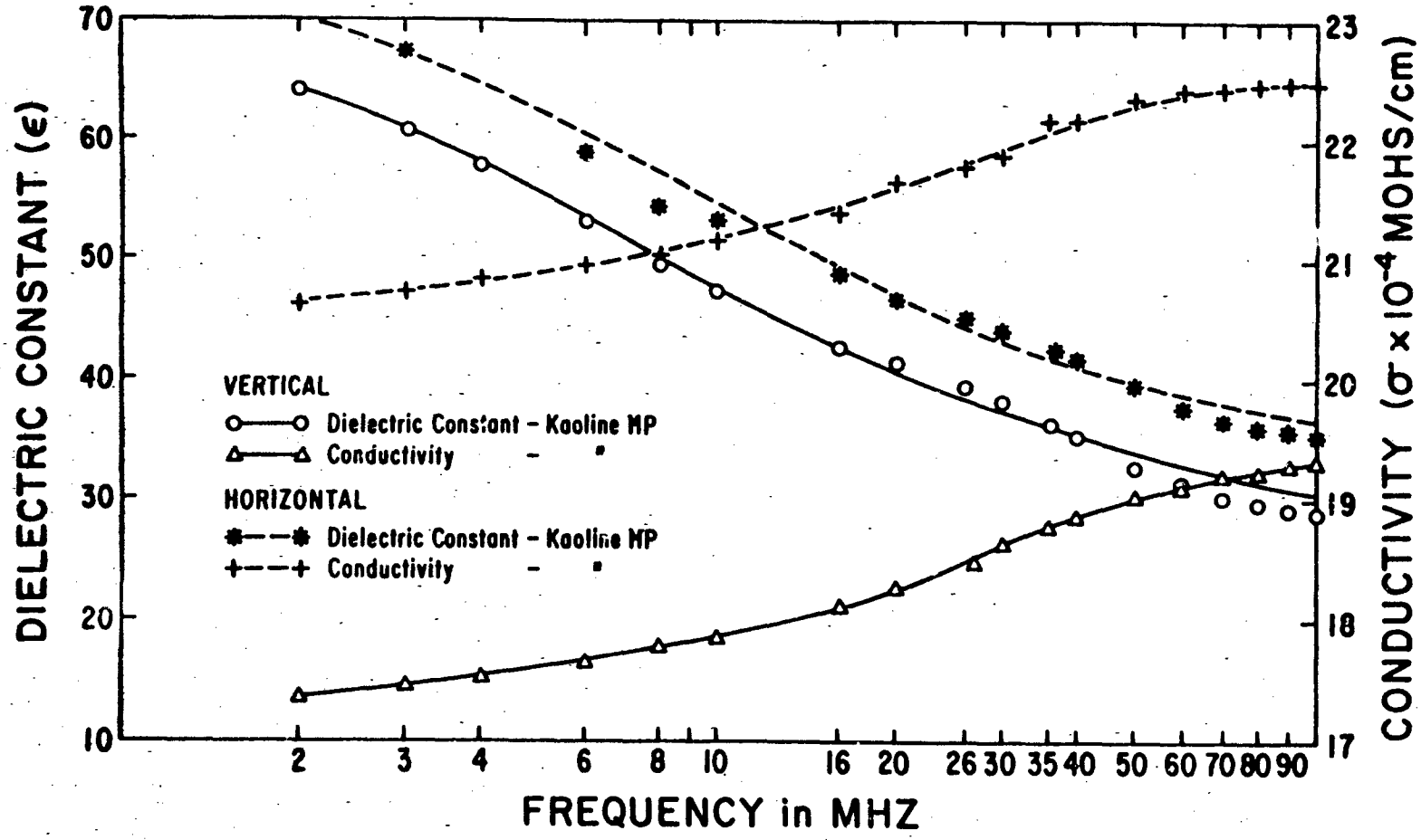

FIG. 2 Variation of Dielectric Constant and Conductivity as a Function of Frequency for Cohesive Soils

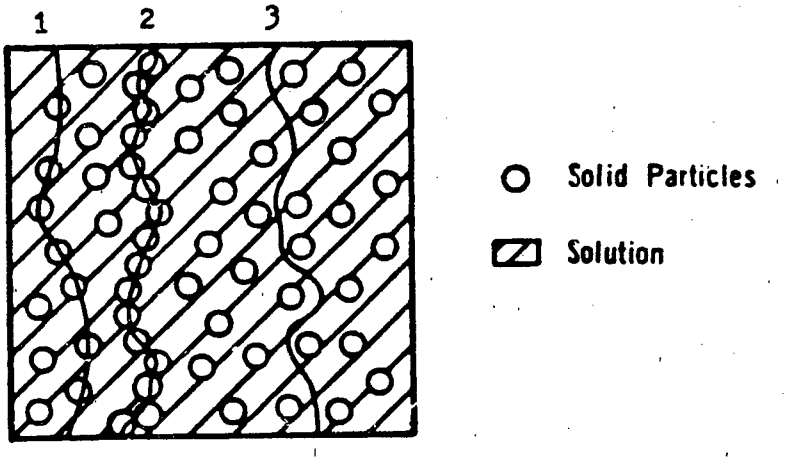

Fig. 3 Three components of the current paths through the soil sample.

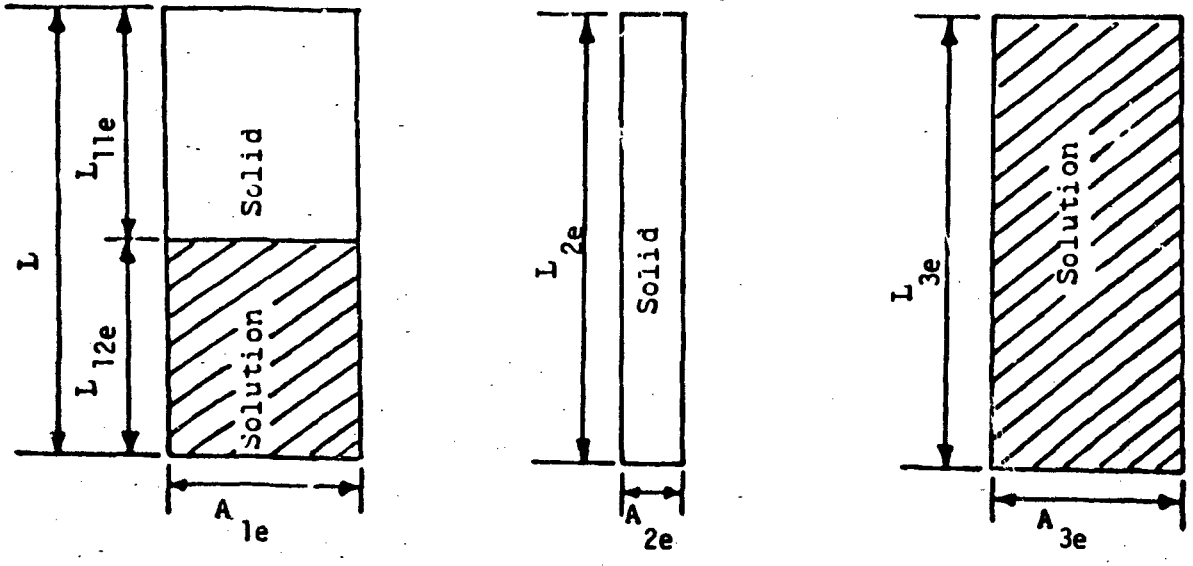

Fig. 4a : Three Element Electrical Model

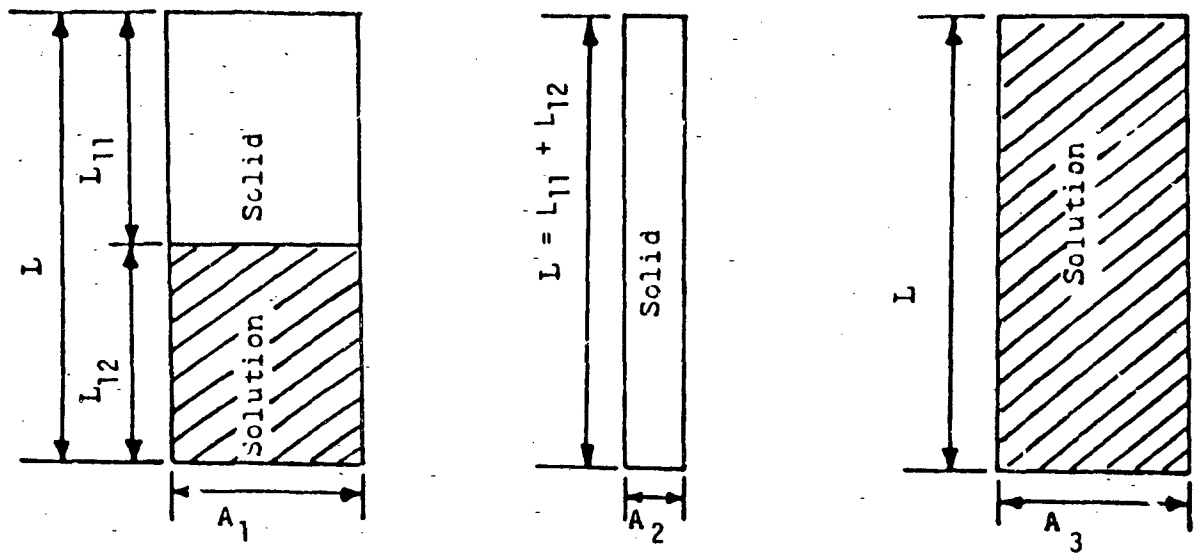

Fig. 4b : Three Element Model Representing The True Volumes

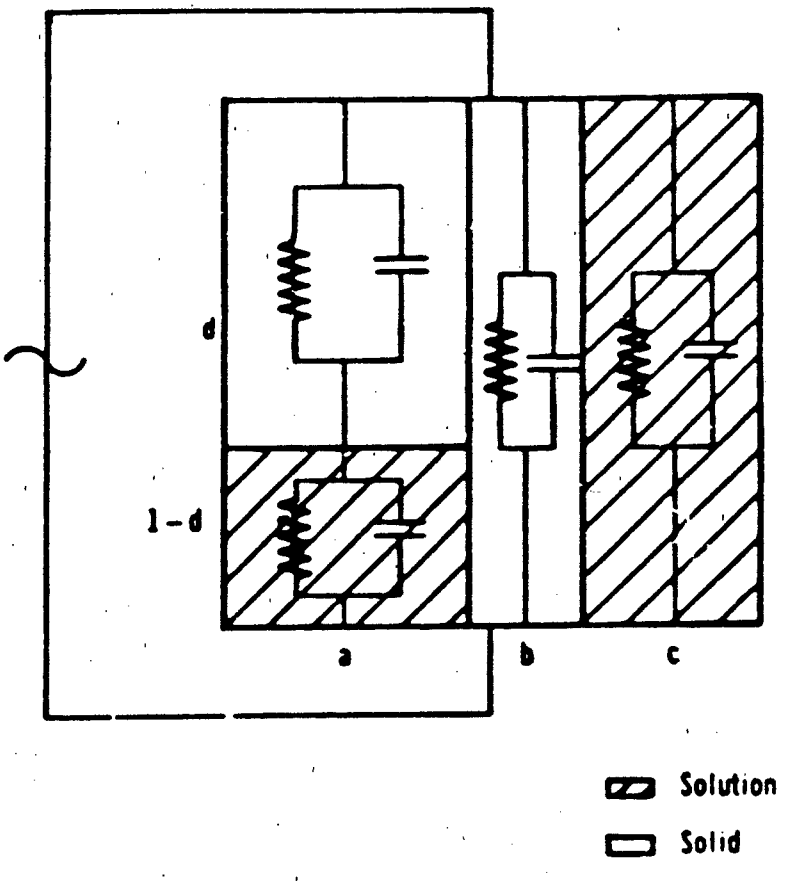

Figure 4c Three Element Electrical Model
Each Zone is Represented by a Parallel Circuit of Resistor and Capacitor. Impedance of Each Zone is Determined by its Dimension (a, b, c, d) and Specific Conductivity and Dielectric Constant of Material Forming the Zone (k_s, k_f, e_s, e_f).

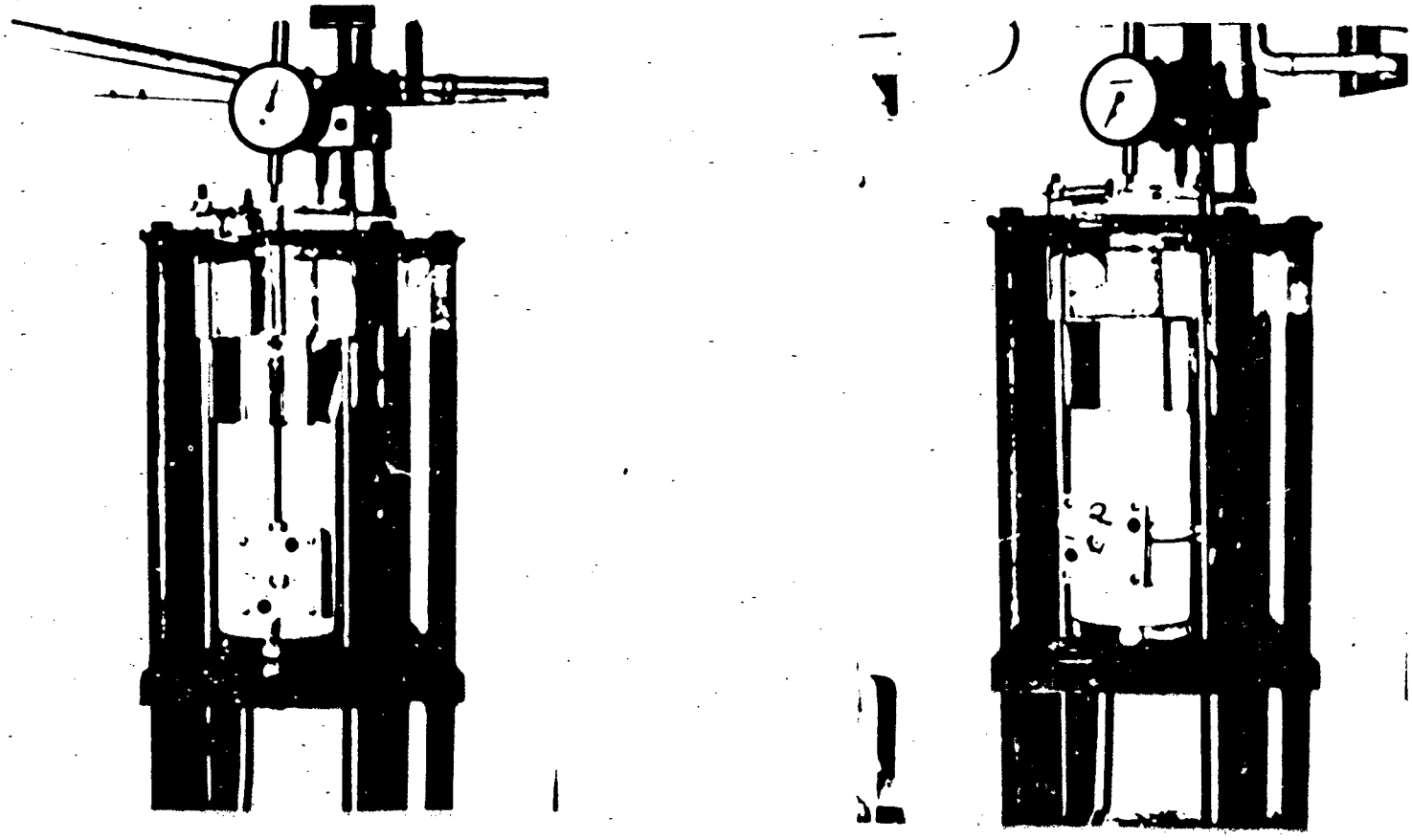

Vertical Cell

Horizontal Cell

Figure 5 - Electrical measuring cells and consolidation frames for the determination of electrical properties in horizontal and vertical directions at different water contents

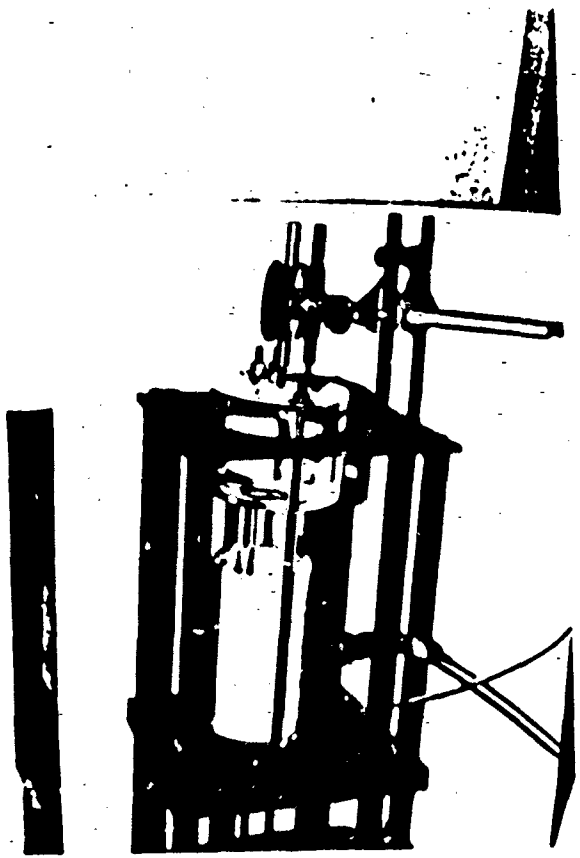

K_o - Cell

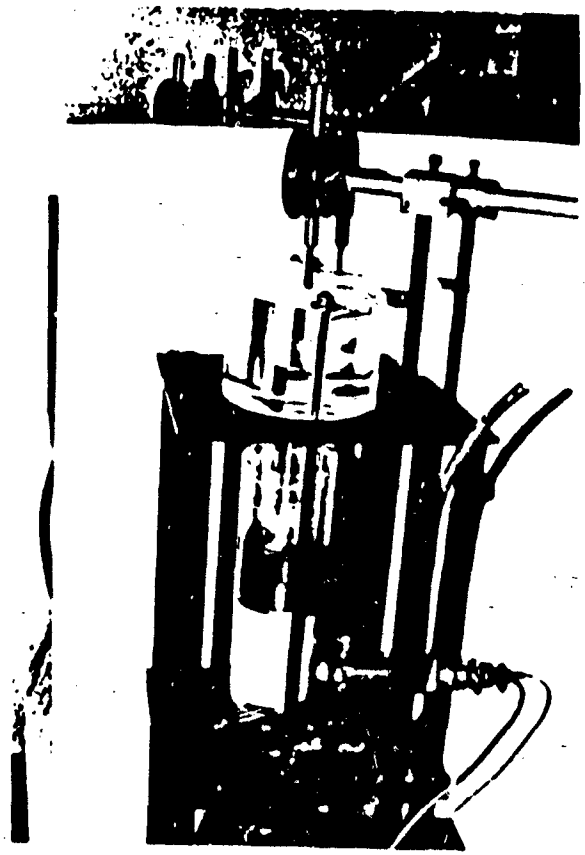

Pore Pressure Cell

Figure 6 - Cells and consolidation frames for the determination of pore water pressure and lateral stress at different water content

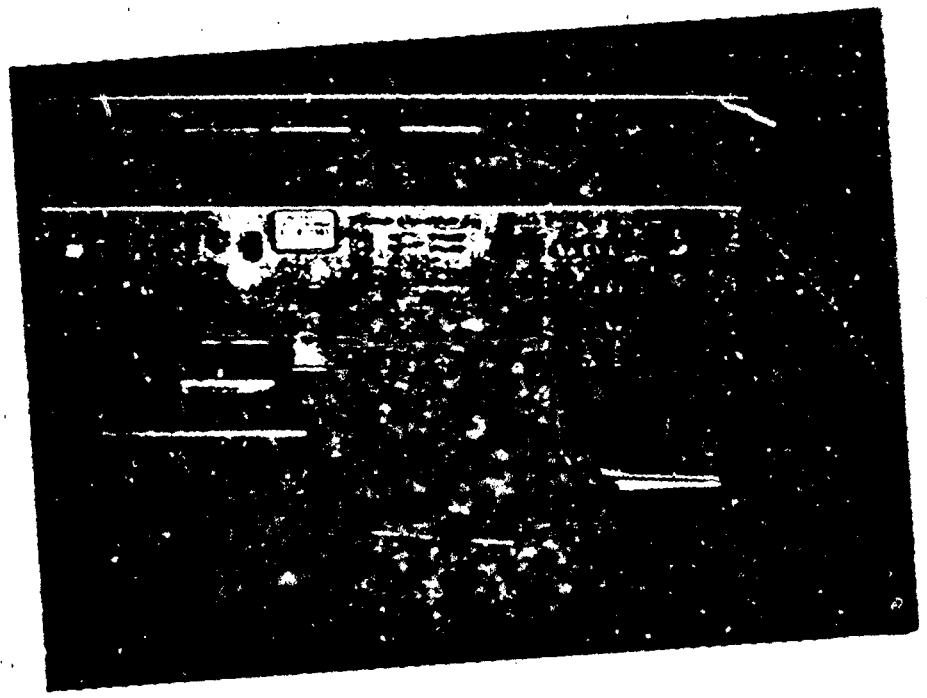

Fig. 7 . Hewlett-Packard Impedance Analyzer for the Measurement of Electrical Properties in the Radio Frequency Range

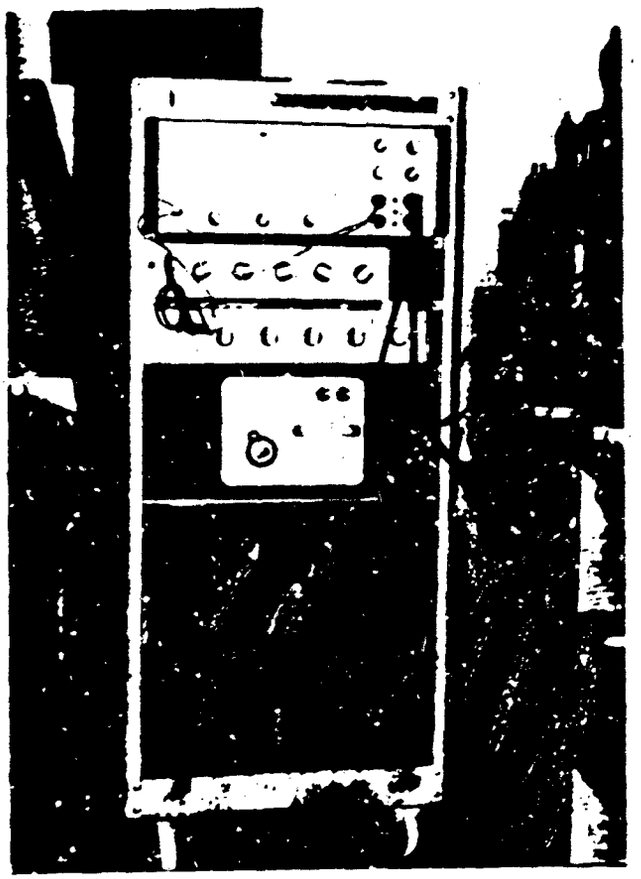

Fig. 8 : The Impedance Comparator for the Measurment of Electrical Properties at Low Frequency (1 KHZ)

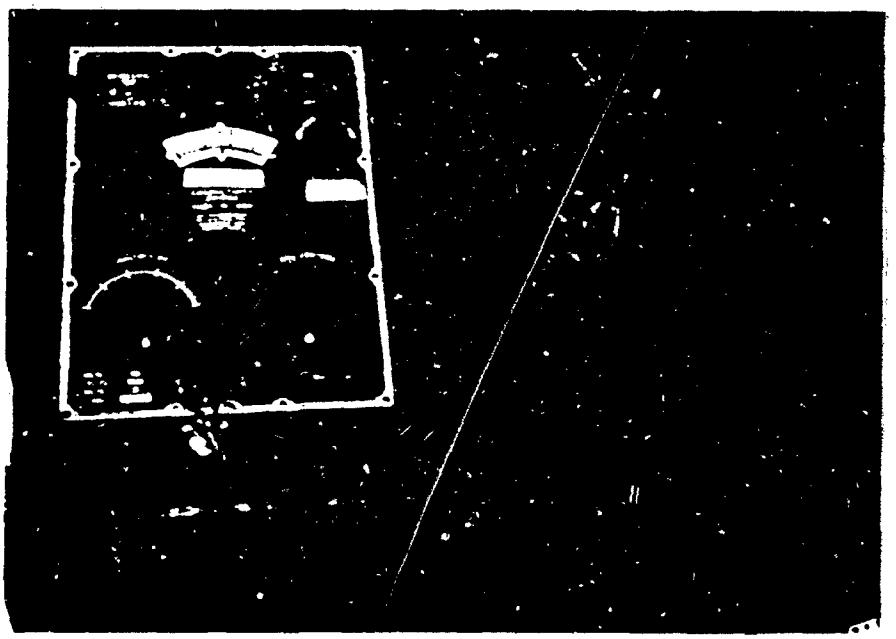

Fig. 9 . The "Beckmann" Conductivity Meter for the Measurement of Electrical Conductivity of Pore Fluid Extract

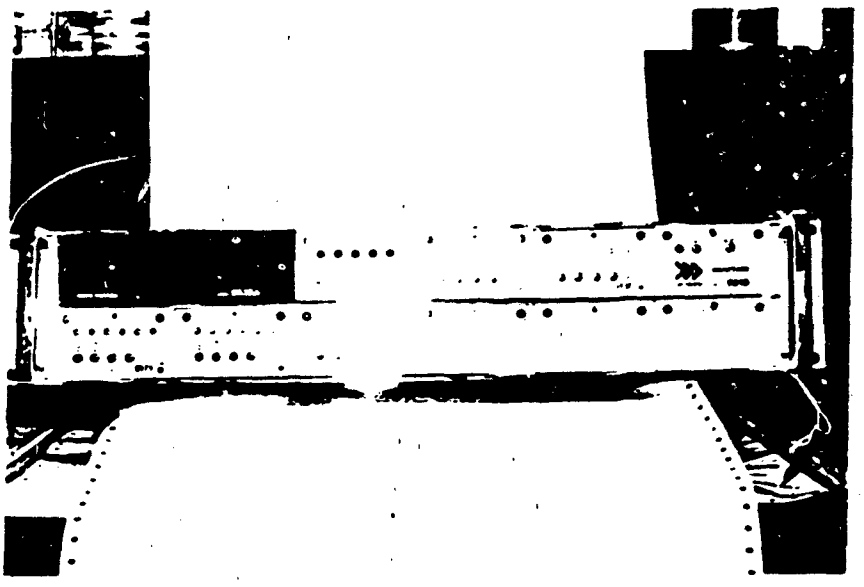

Figure 10 - The Digital "Daytronic" strain indicator for the measurement of lateral stress at different water contents during consolidation

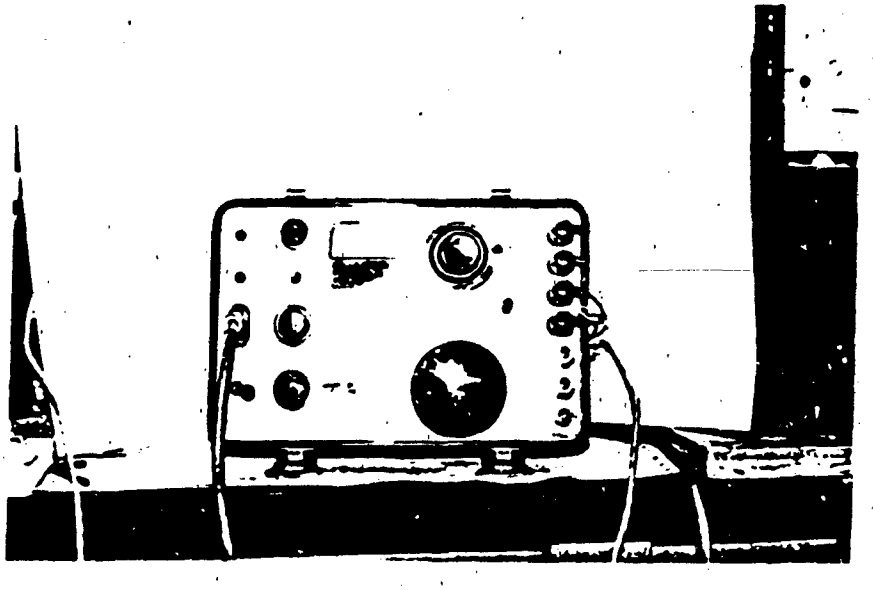

Figure 11 - The "Budd" strain indicator for the measurement of pore water pressure at different water contents during consolidation

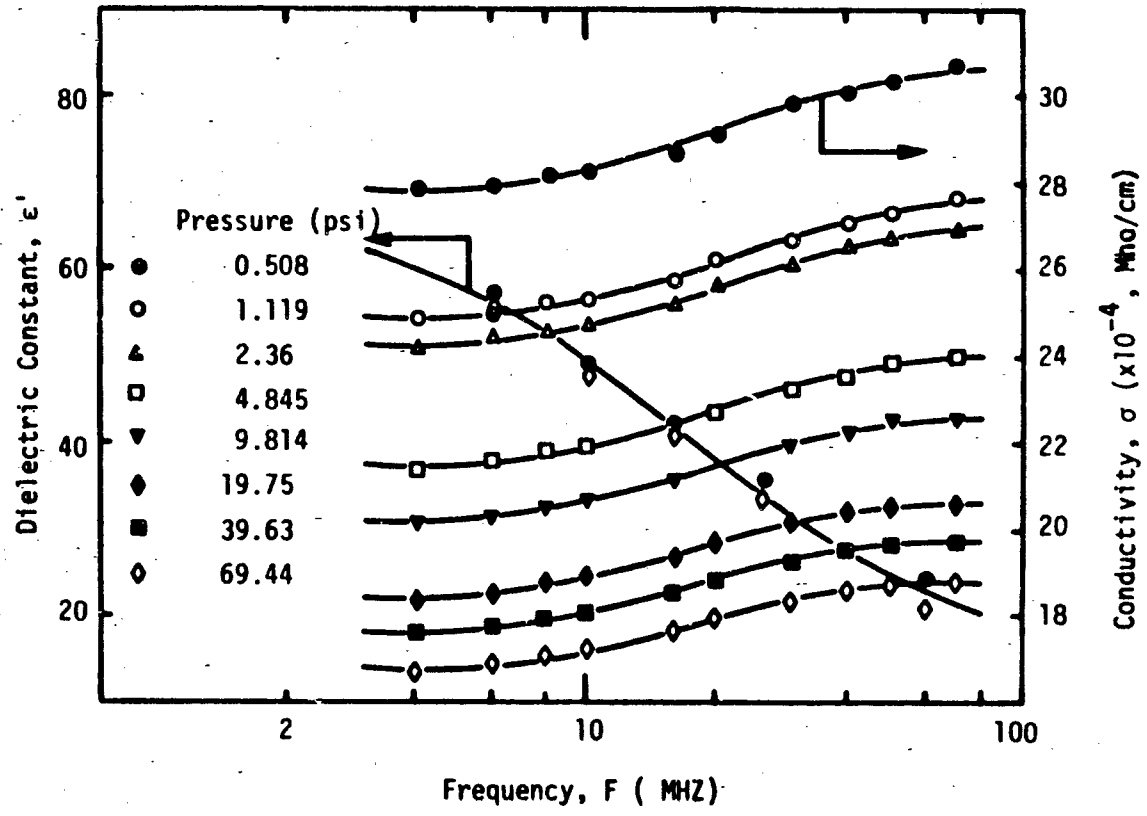

Fig. 12 : Variation Of Conductivity And Dielectric Constant As A Function Of Frequency (Soil #1, Vertical Measurement, Loading)

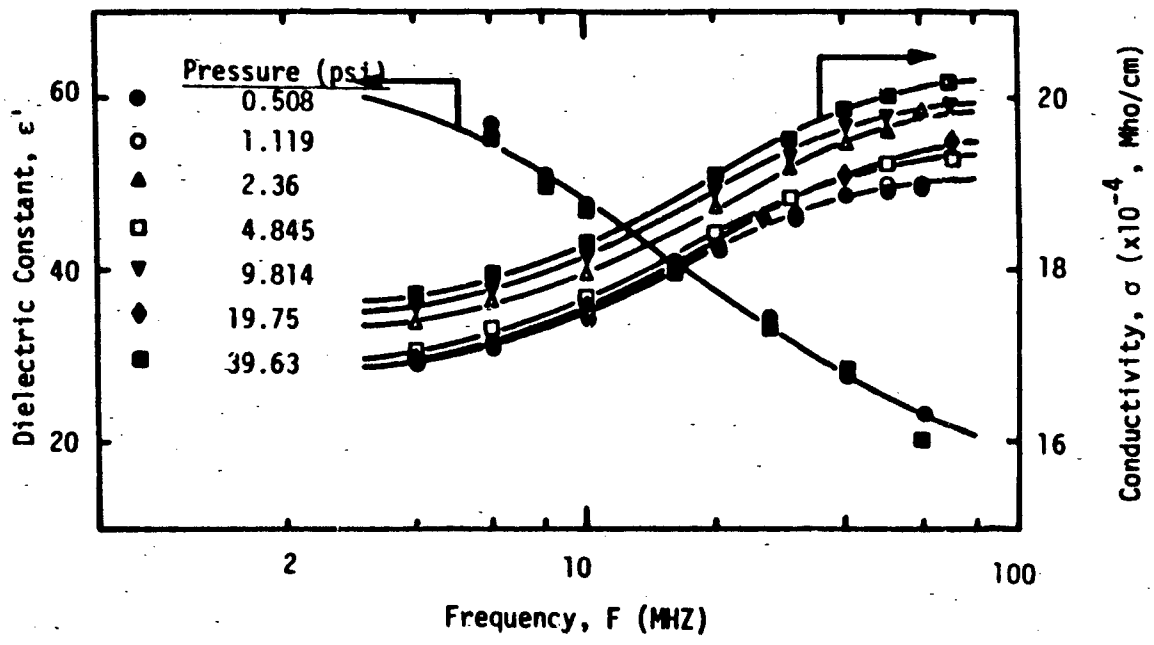

Fig. 13. : Variation Of Conductivity And Dielectric Constant As A Function of Frequency (Soil #1, Vertical Measurement, Unloading)

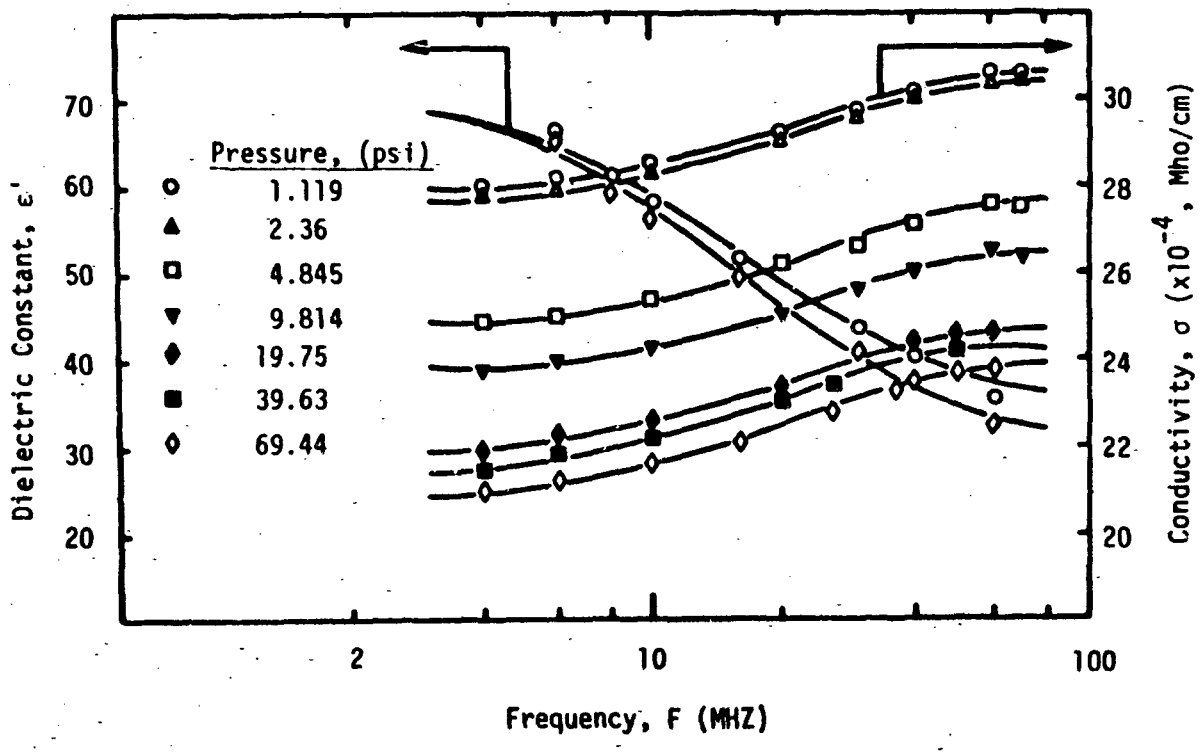

Fig. 14: Variation Of Conductivity And Dielectric Constant As A Function of Frequency (Soil #1, Horizontal Measurement, Loading)

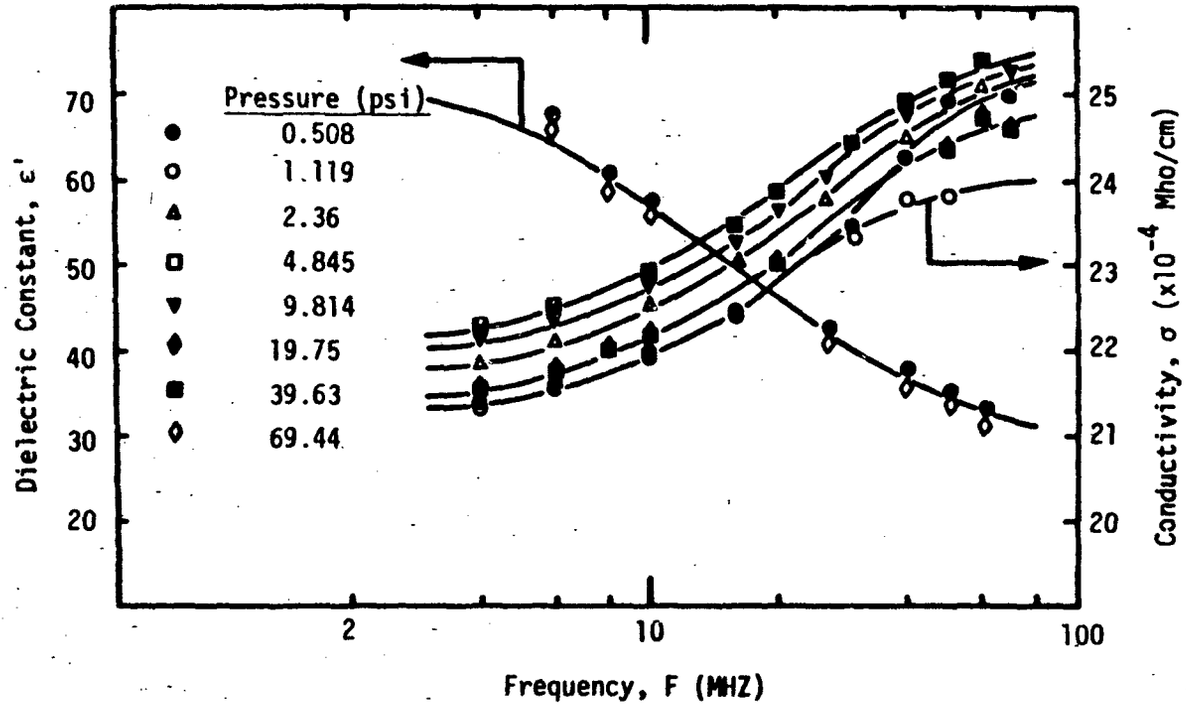

Fig. 15 . Variation Of Conductivity And Dielectric Constant As A Function Of Frequency (Soil #1, Horizontal Measurement, Unloading)

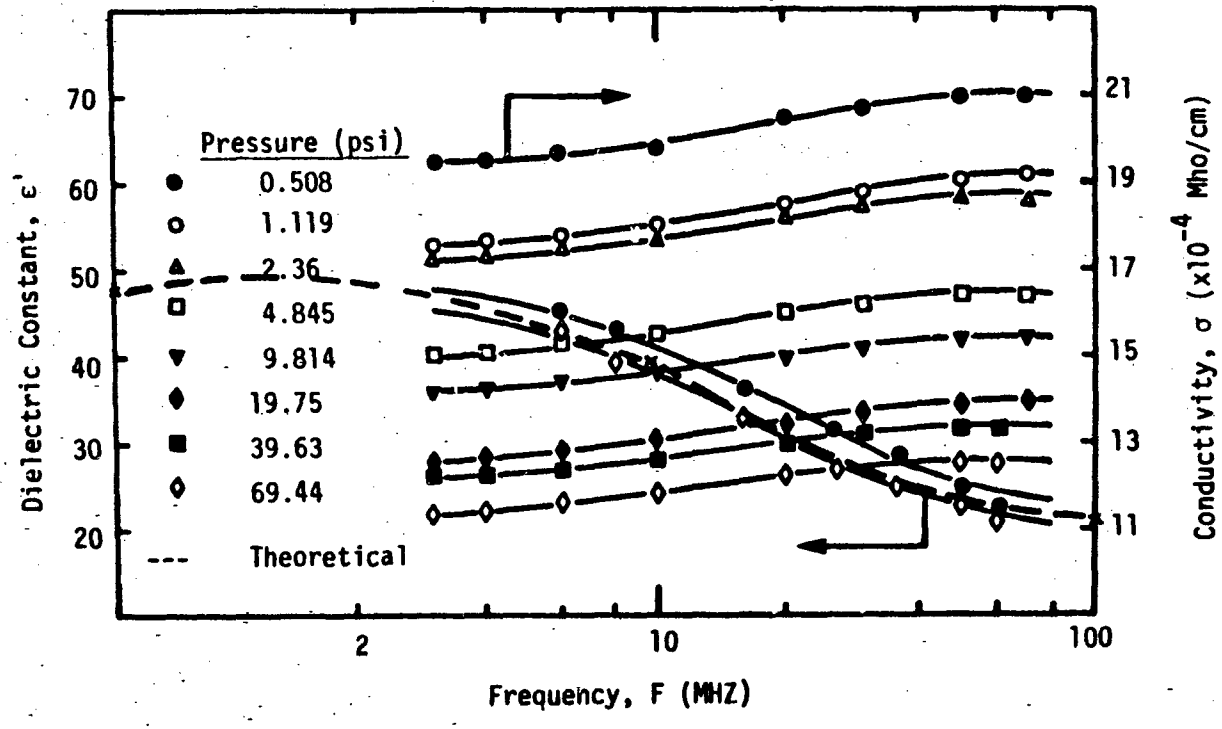

Fig. 16 : Variation Of Conductivity And Dielectric Constant As A Function Of Frequency (Soil #2, Vertical Measurement, Loading)

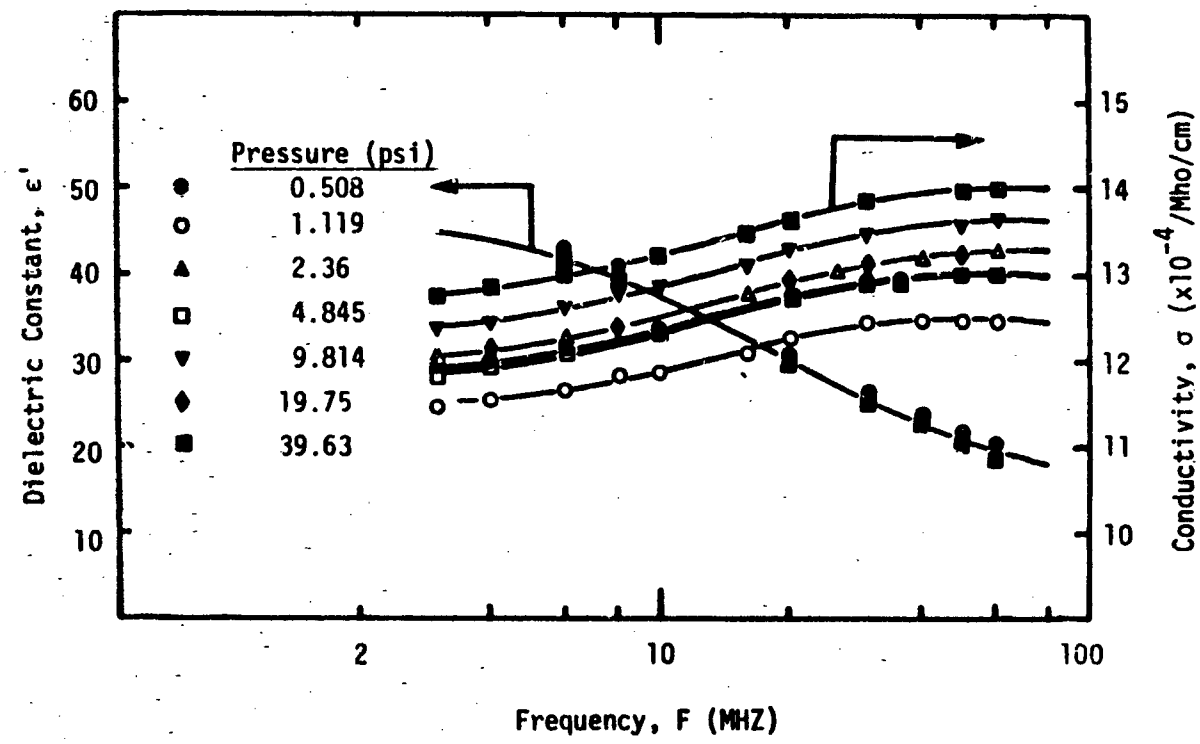

Fig. 17 · Variation Of Conductivity And Dielectric Constant As A Function Of Frequency (Soil #2, Vertical Measurement, Unloading)

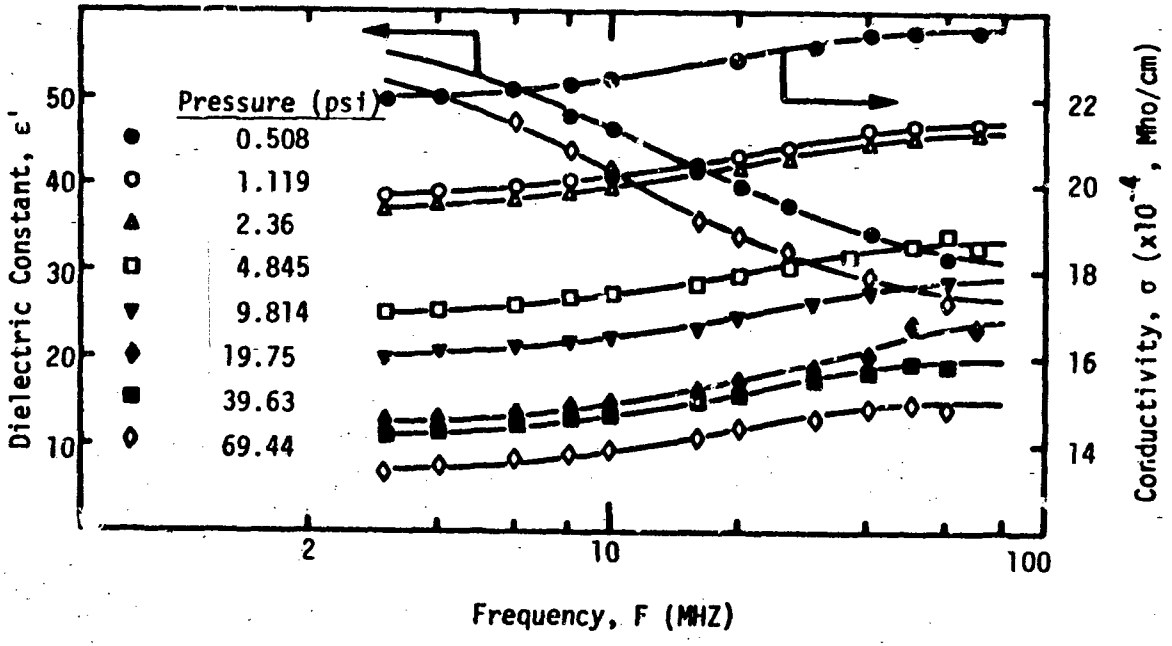

Fig. 18 Variation Of Conductivity And Dielectric Constant As A Function Of Frequency (Soil #2, Horizontal Measurement, Loading)

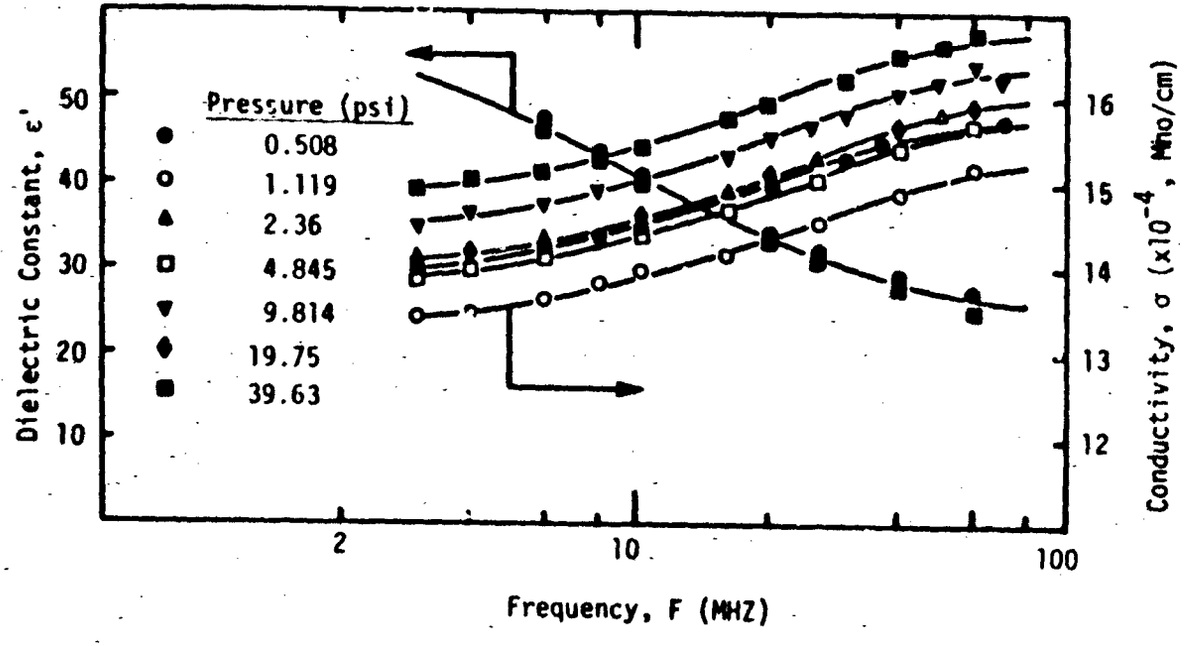

Fig. 19 Variation Of Conductivity And Dielectric Constant As A Function Of Frequency (Soil #2, Horizontal Measurement, Unloading)

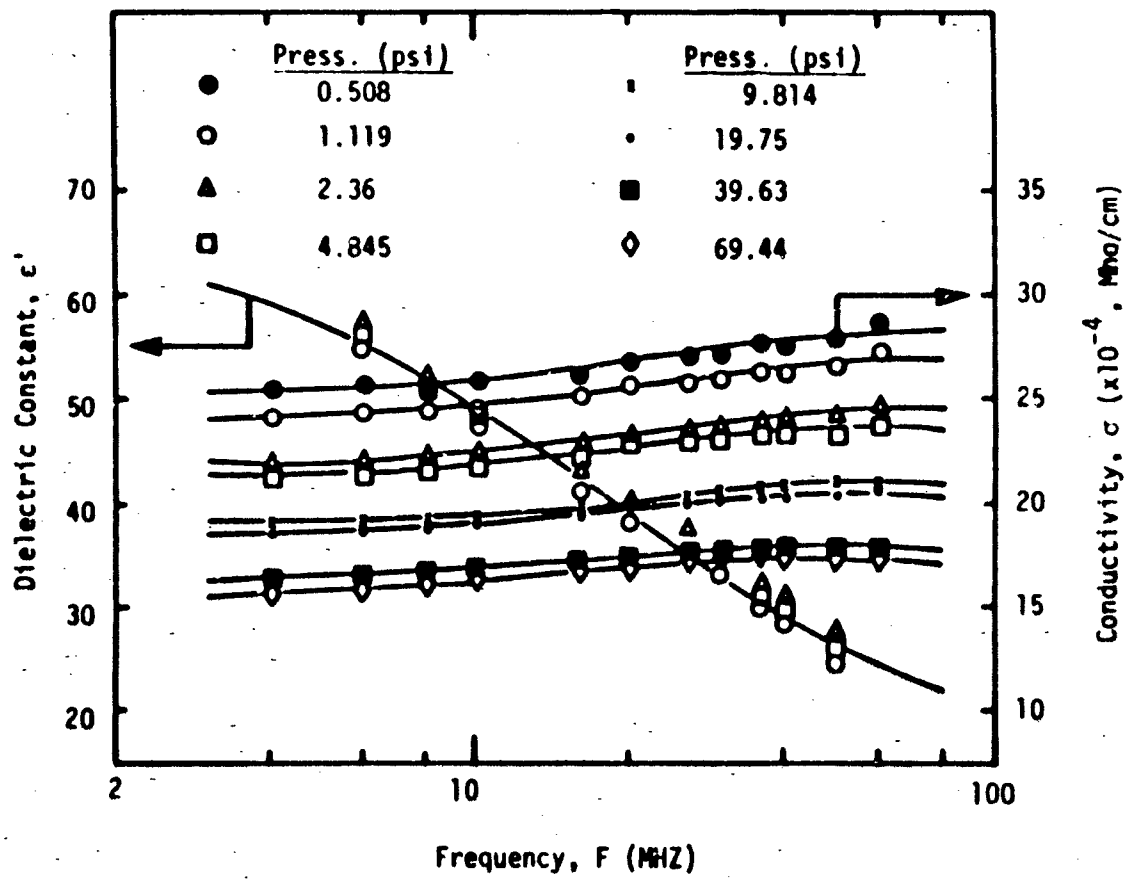

Fig. 20 : Variation Of Conductivity And Dielectric Constant As A Function Of Frequency (Soil #3, Vertical Measurement, Loading)

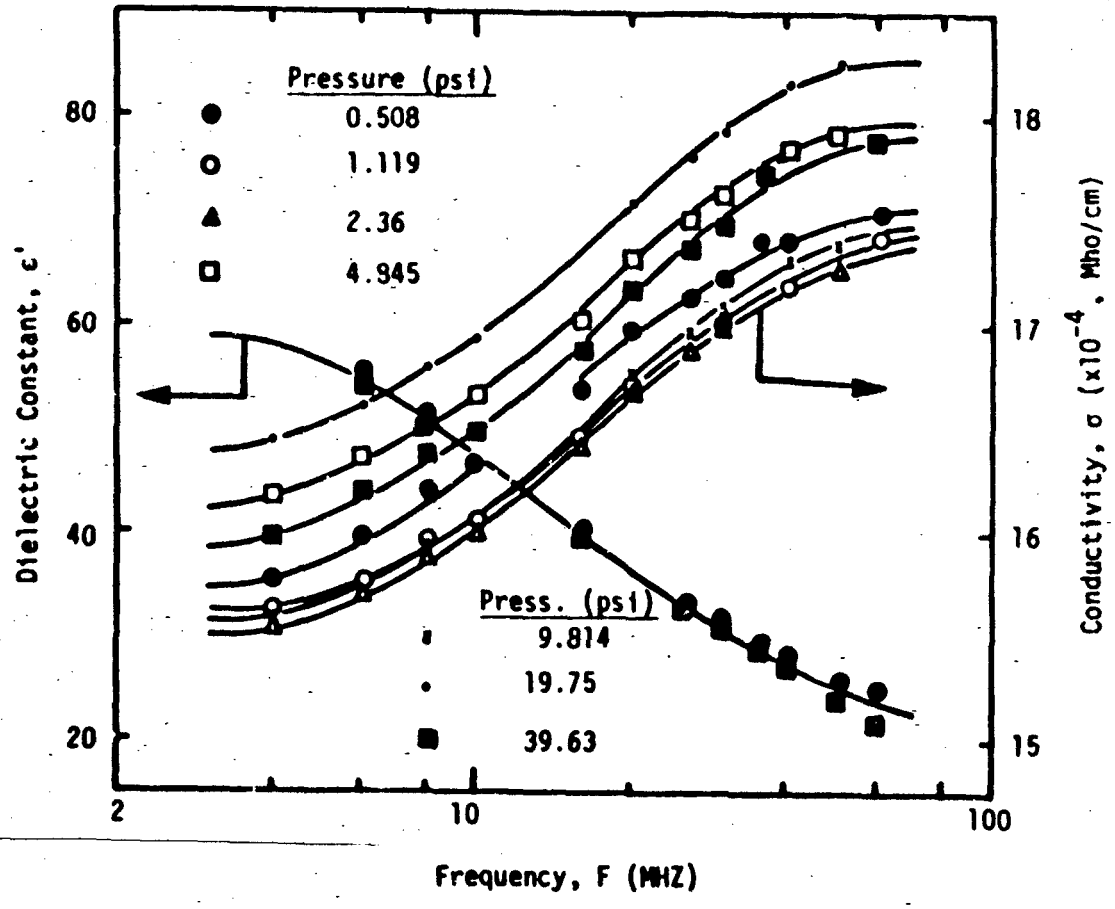

Fig. 21 · Variation Of Conductivity And Dielectric Constant As A Function Of Frequency (Soil #3, Vertical Measurement, Unloading)

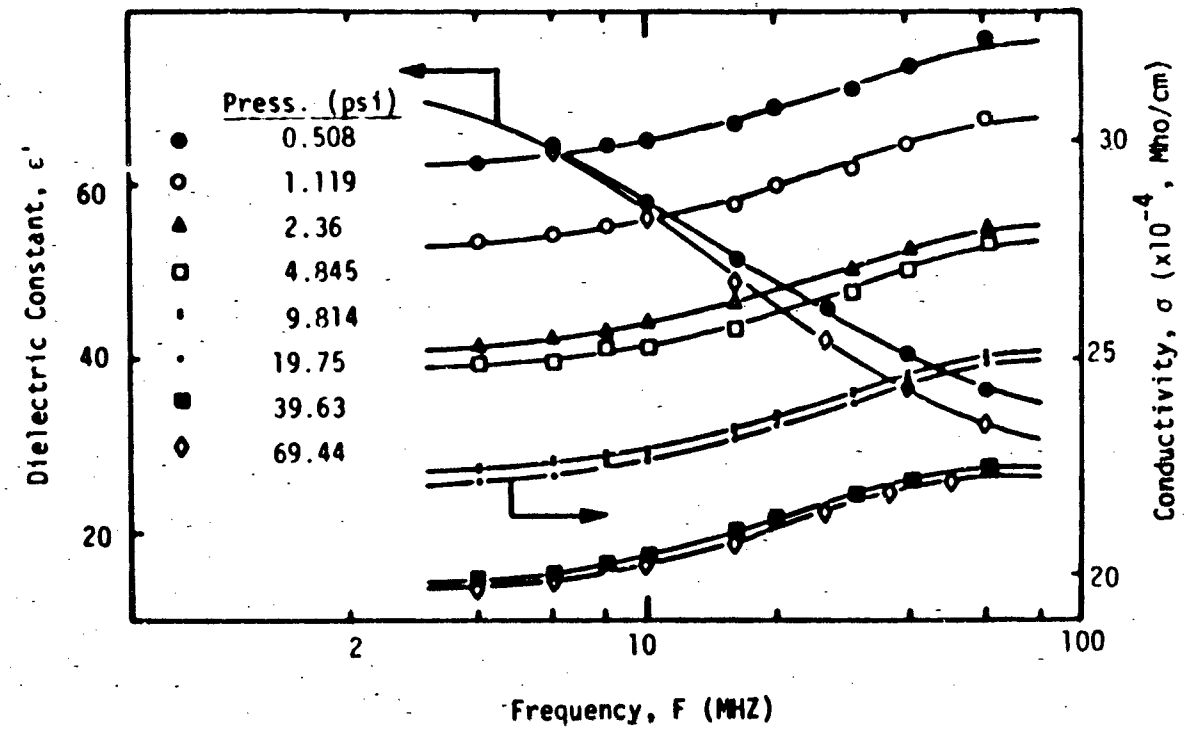

Fig. 22 Variation Of Conductivity And Dielectric Constant As A Function Of Frequency (Soil #3, Horizontal Measurement, Loading)

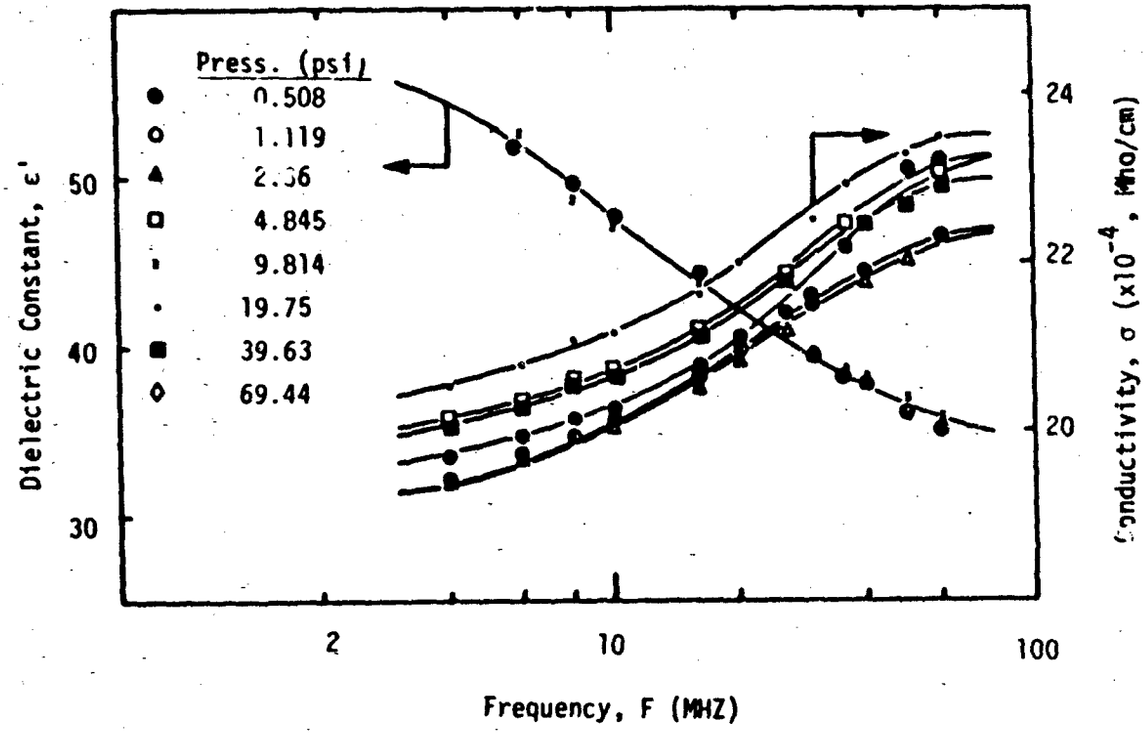

Fig. 23 : Variation Of Conductivity And Dielectric Constant As A Function Of Frequency (Soil #3, Horizontal Measurement, Unloading)

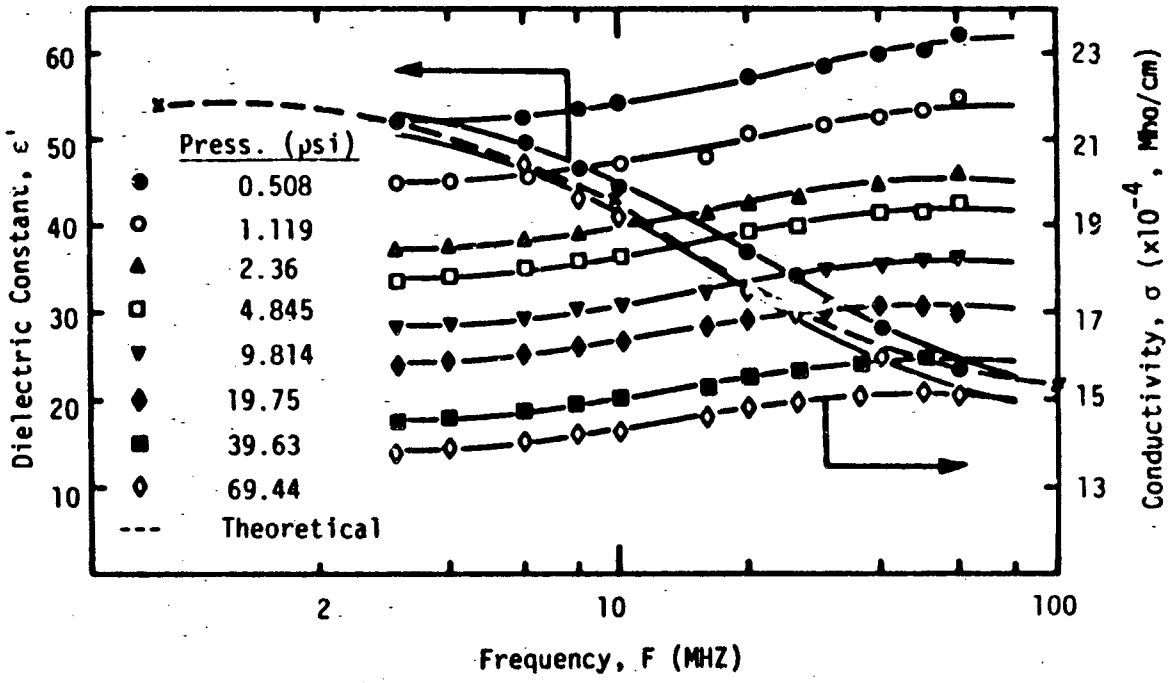

Fig. 24 Variation Of Conductivity And Dielectric Constant As A Function Of Frequency (Soil #4, Vertical Measurement, Loading)

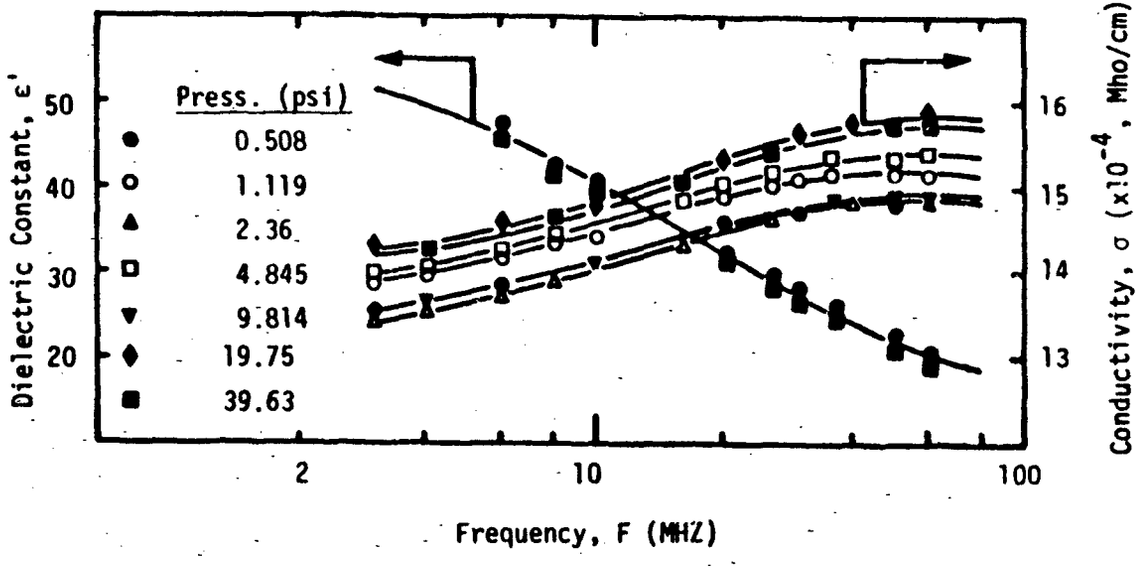

Fig. 25 : Variation Of Conductivity And Dielectric Constant As A Function Of Frequency (Soil #4, Vertical Measurement, Unloading)

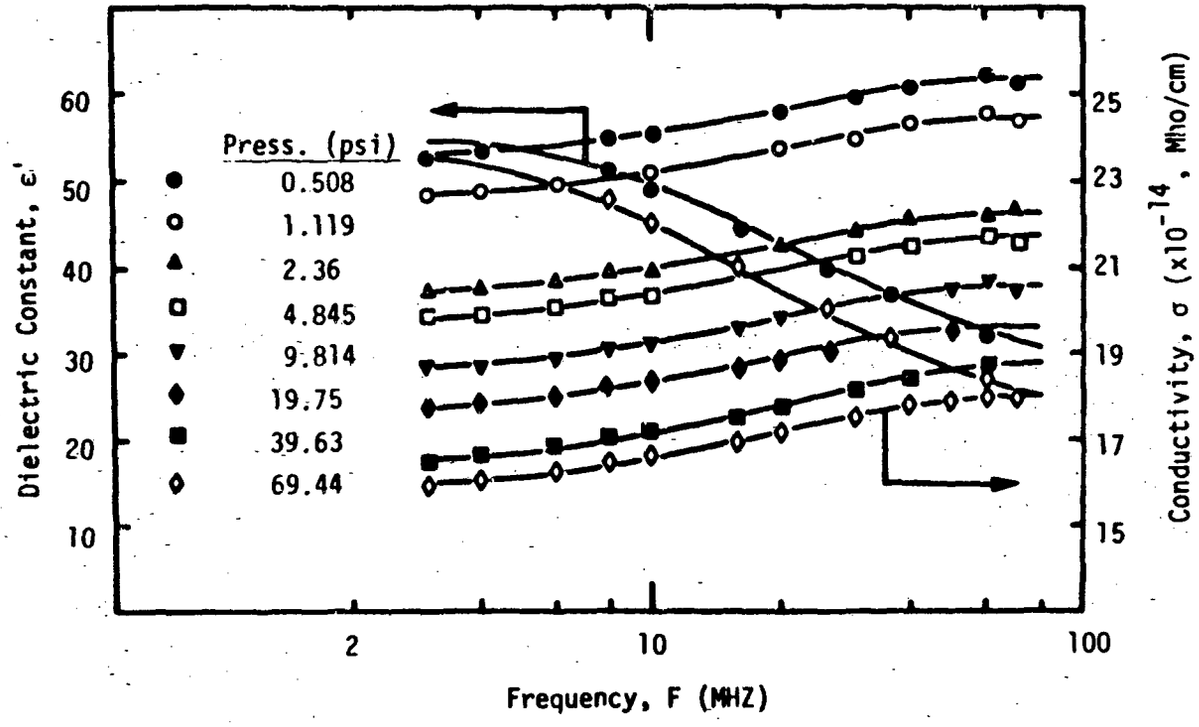

Fig. 26 Variation Of Conductivity And Dielectric Constant As A Function Of Frequency (Soil #4, Horizontal Measurement, Loading)

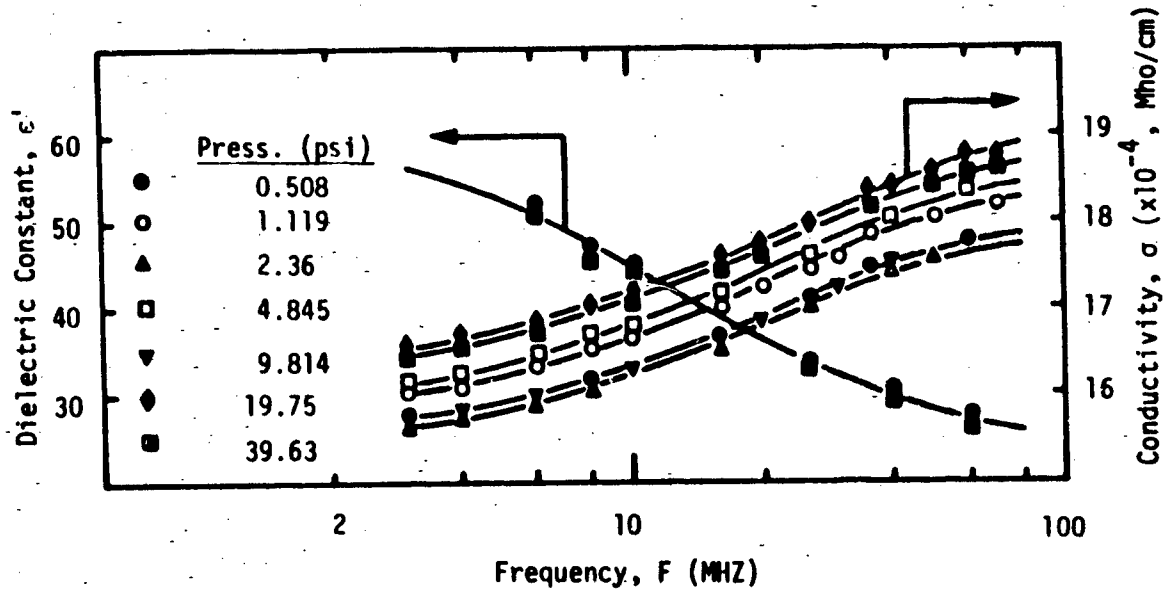

Fig. 27 : Variation Of Conductivity And Dielectric Constant As A Function of Frequency (Soil #4, Horizontal Measurement, Unloading)

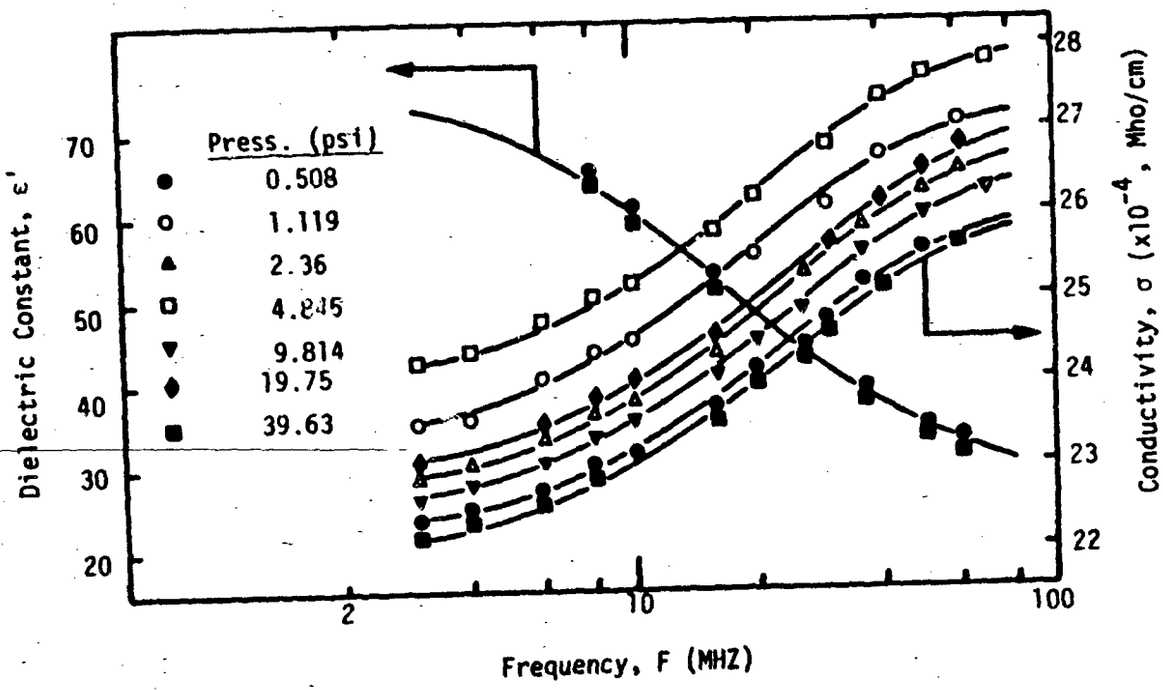

Fig. 28 : Variation Of Conductivity And Dielectric Constant As A Function Of Frequency (Soil #5, Horizontal Measurement, Unloading)

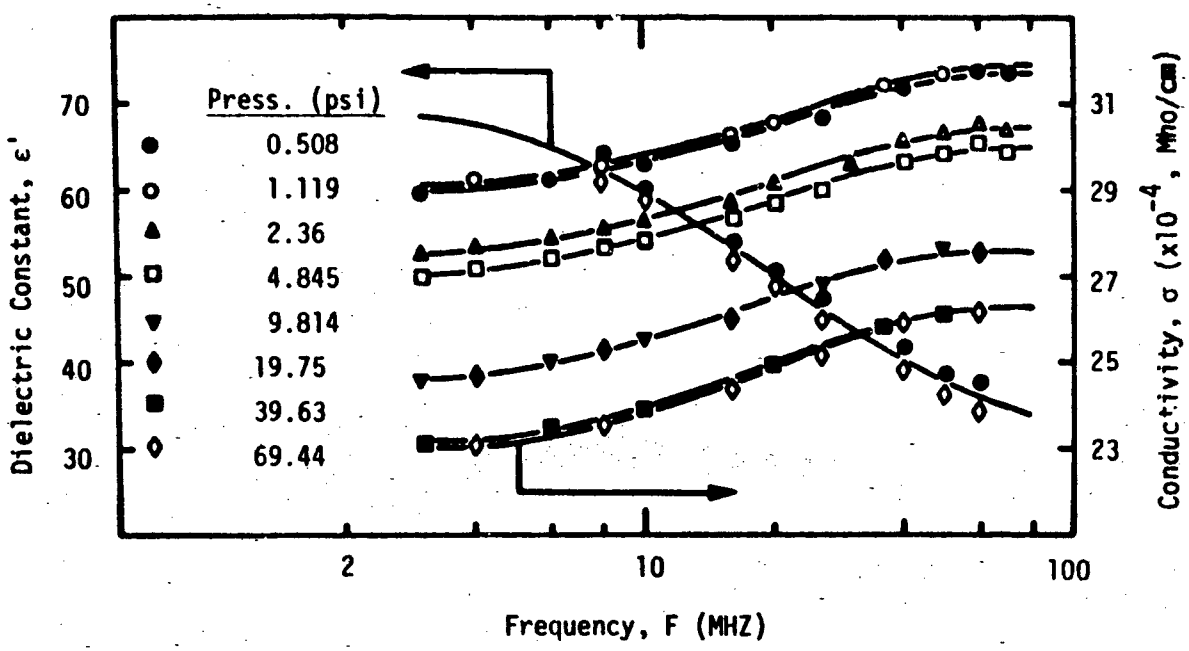

Fig. 29 : Variation Of Conductivity And Dielectric Constant As A Function Of Frequency (Soil #5, Horizontal Measurement, Loading)

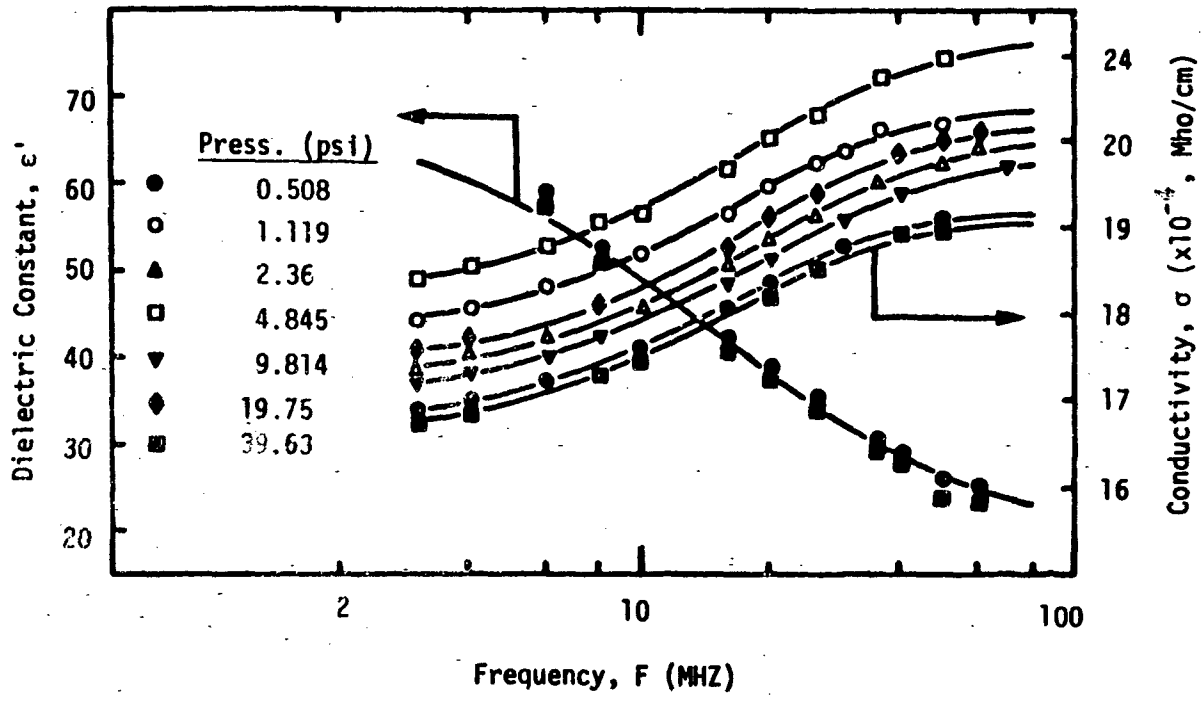

Fig. 30 : Variation Of Conductivity And Dielectric Constant As A Function Of Frequency (Soil #5, Vertical Measurement, Unloading)

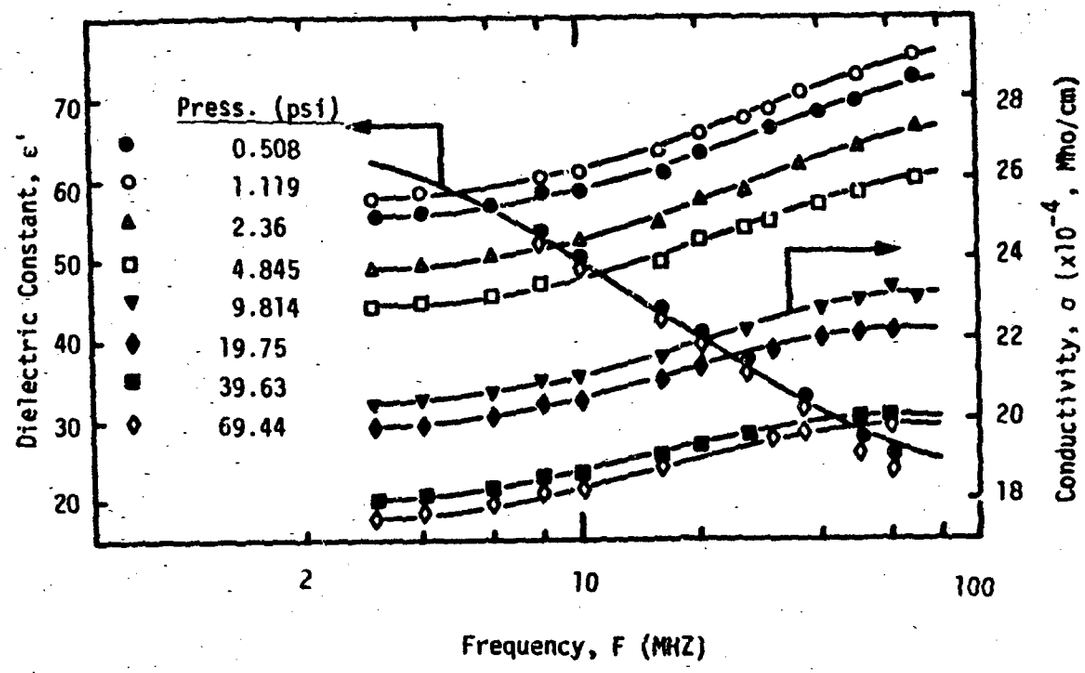

Fig. 31 : Variation Of Conductivity And Dielectric Constant As A Function Of Frequency (Soil #5, Vertical Measurement, Loading)

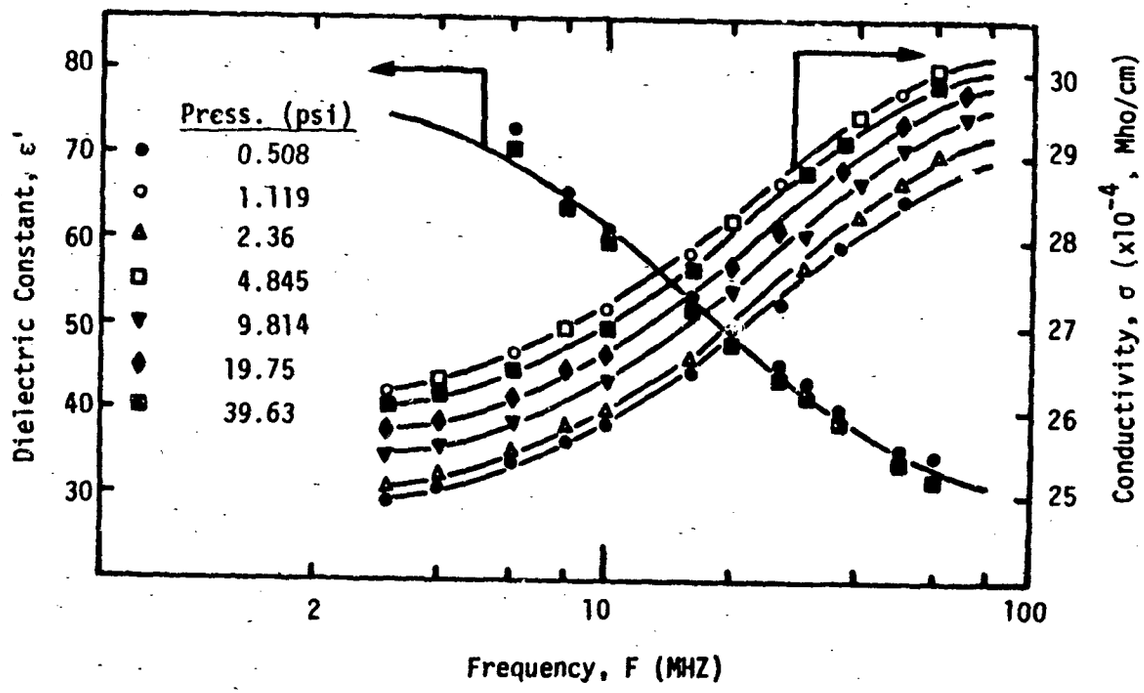

Fig. 32 : Variation Of Conductivity And Dielectric Constant As A Function Of Frequency (Soil #6, Horizontal Measurement, Unloading)

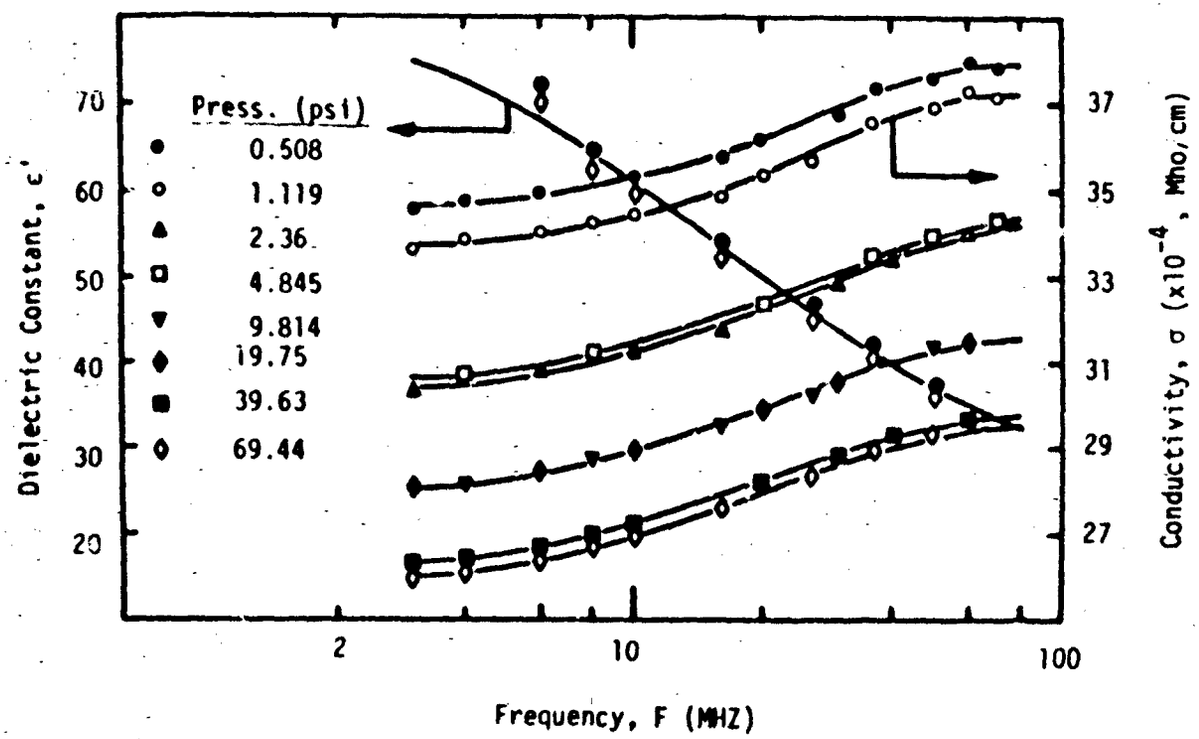

Fig. 33 : Variation Of Conductivity And Dielectric Constant As A Function Of Frequency (Soil #6, Horizontal Measurement, Loading)

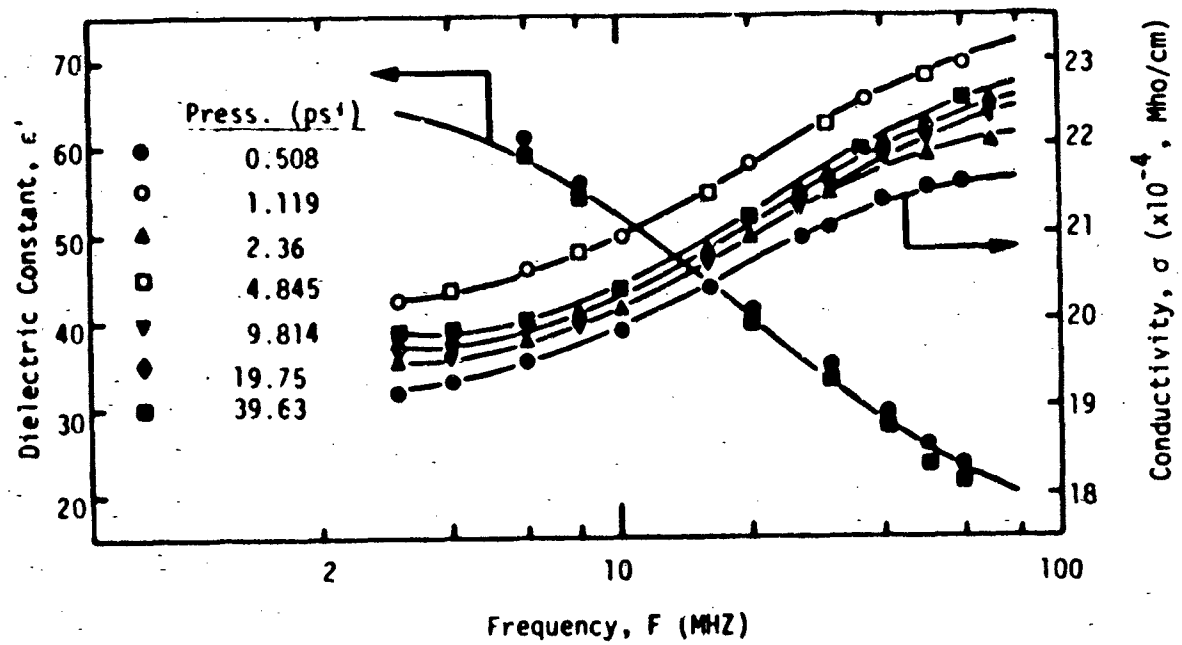

Fig. 34 : Variation Of Conductivity And Dielectric Constant As A Function Of Frequency (Soil #6, Vertical Measurement, Unloading)

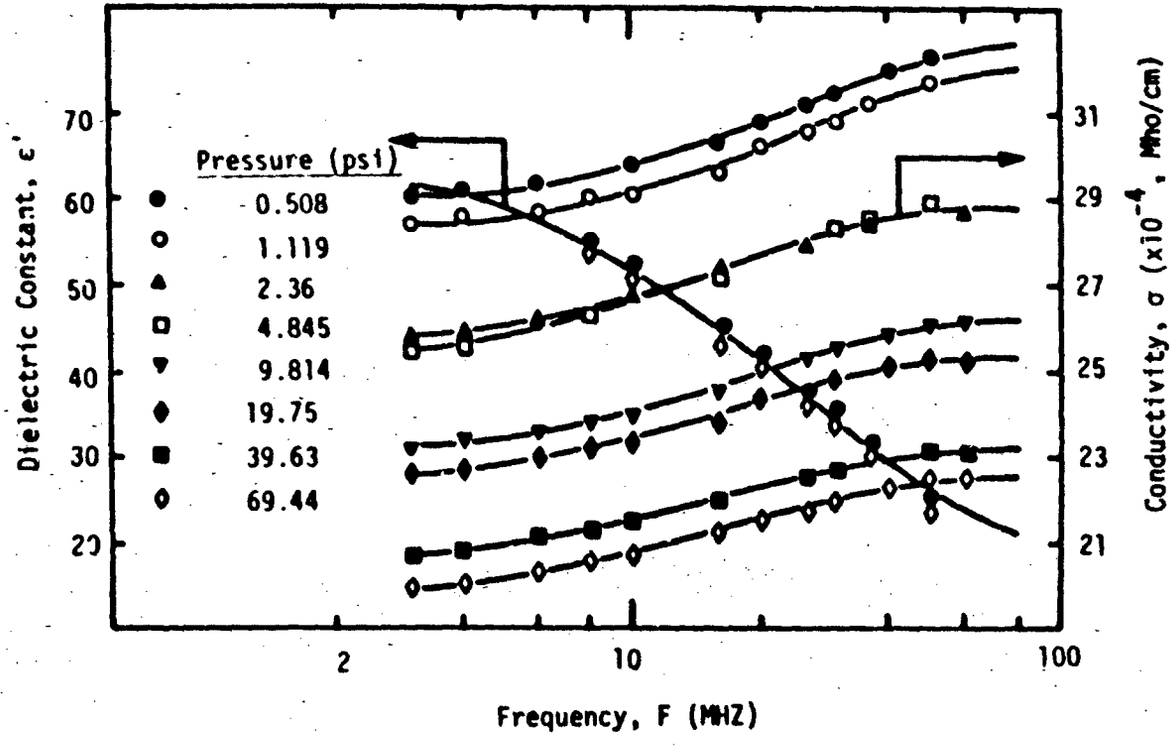

Fig. 35 · Variation Of Conductivity And Dielectric Constant As A Function Of Frequency (Soil #6, Vertical Measurement, Loading)

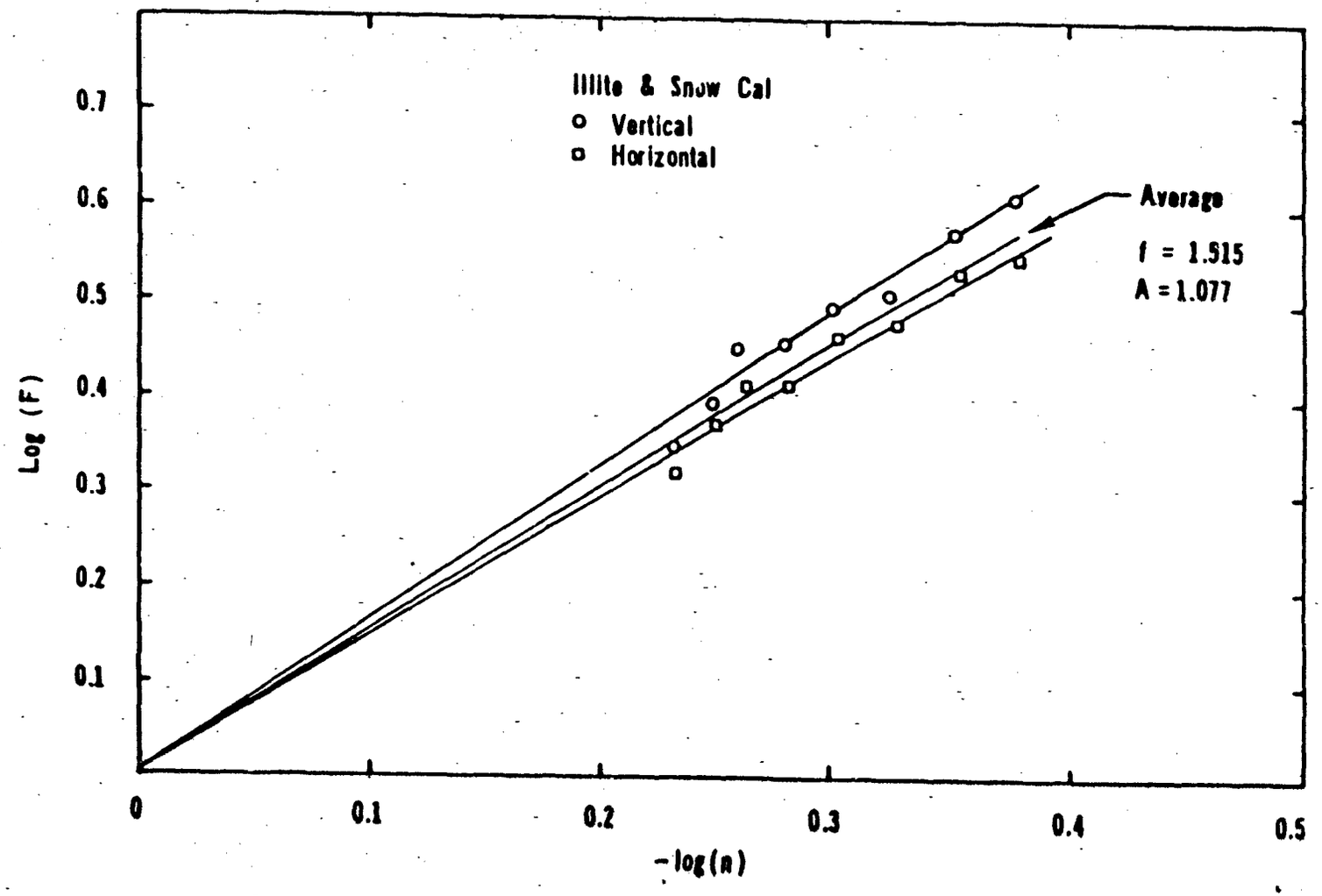

Figure 36 - The relationship between the horizontal and vertical formation factors and the total porosity, n for Snow Cal + Illite

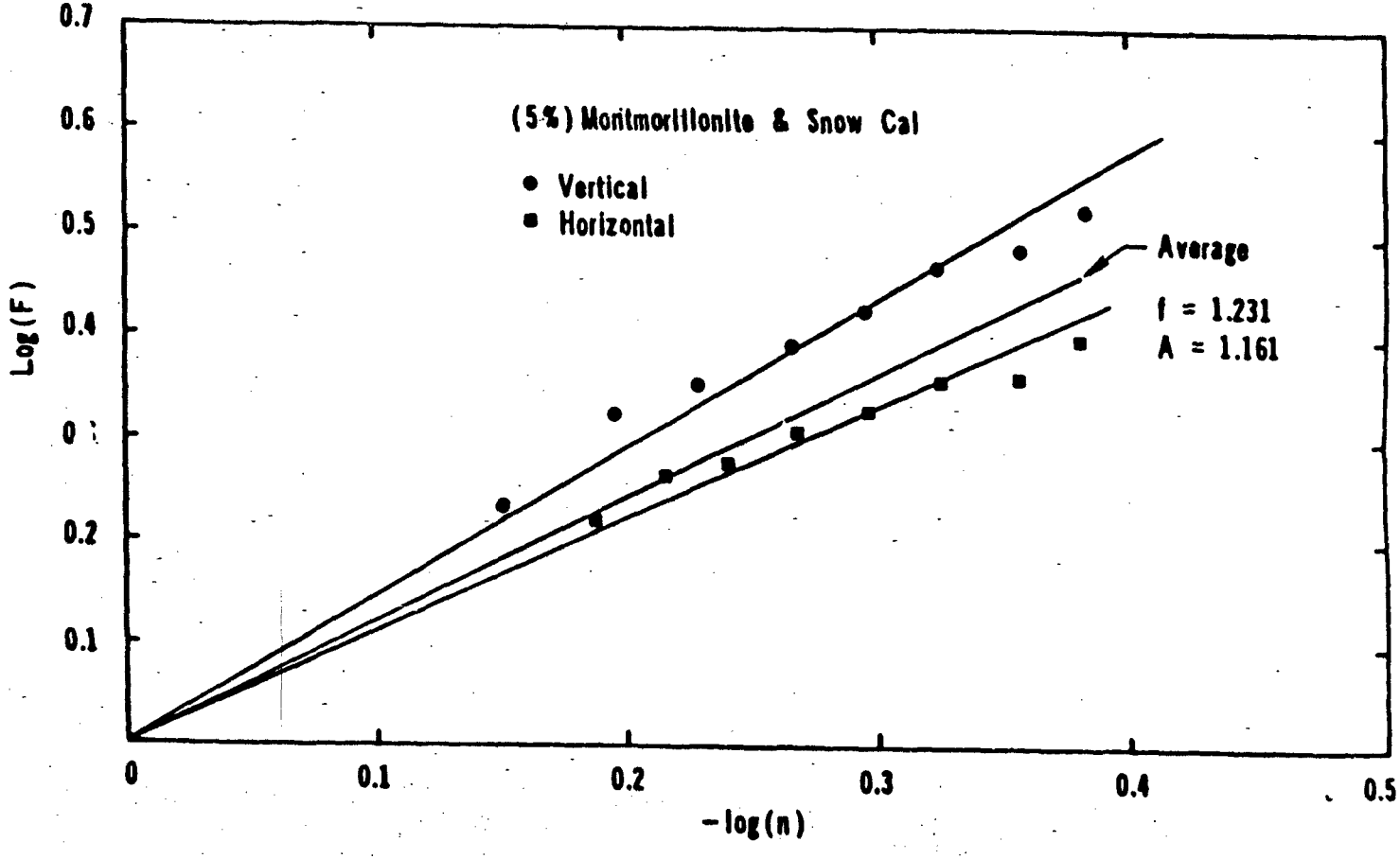

Figure 37 - The relationship between the horizontal and vertical formation factors and the total porosity, n for Snow Cal + (5%) Montmorillonite

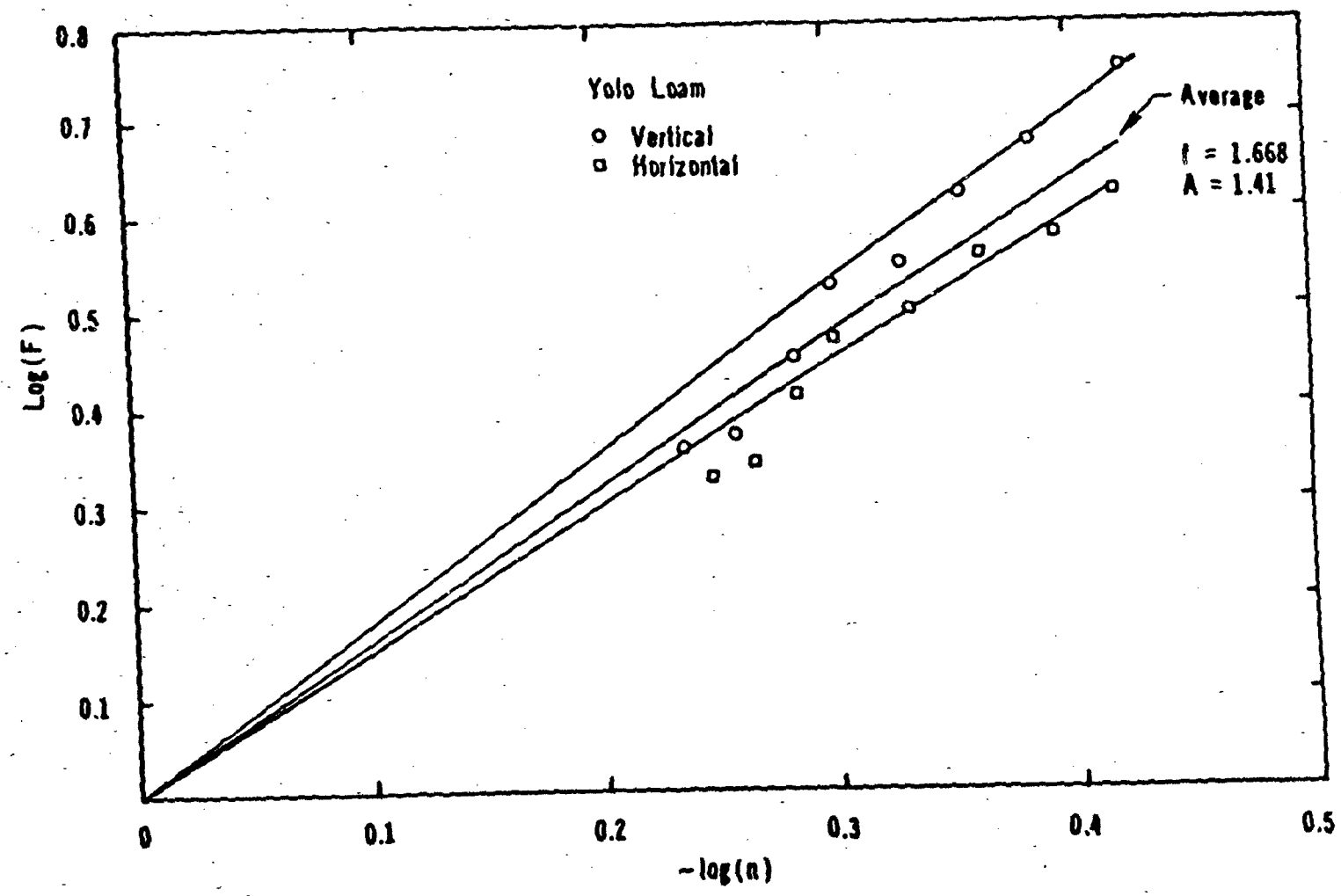

Figure 38 - The relationship between the horizontal and vertical formation factors and the total porosity, n for Yolo Loam

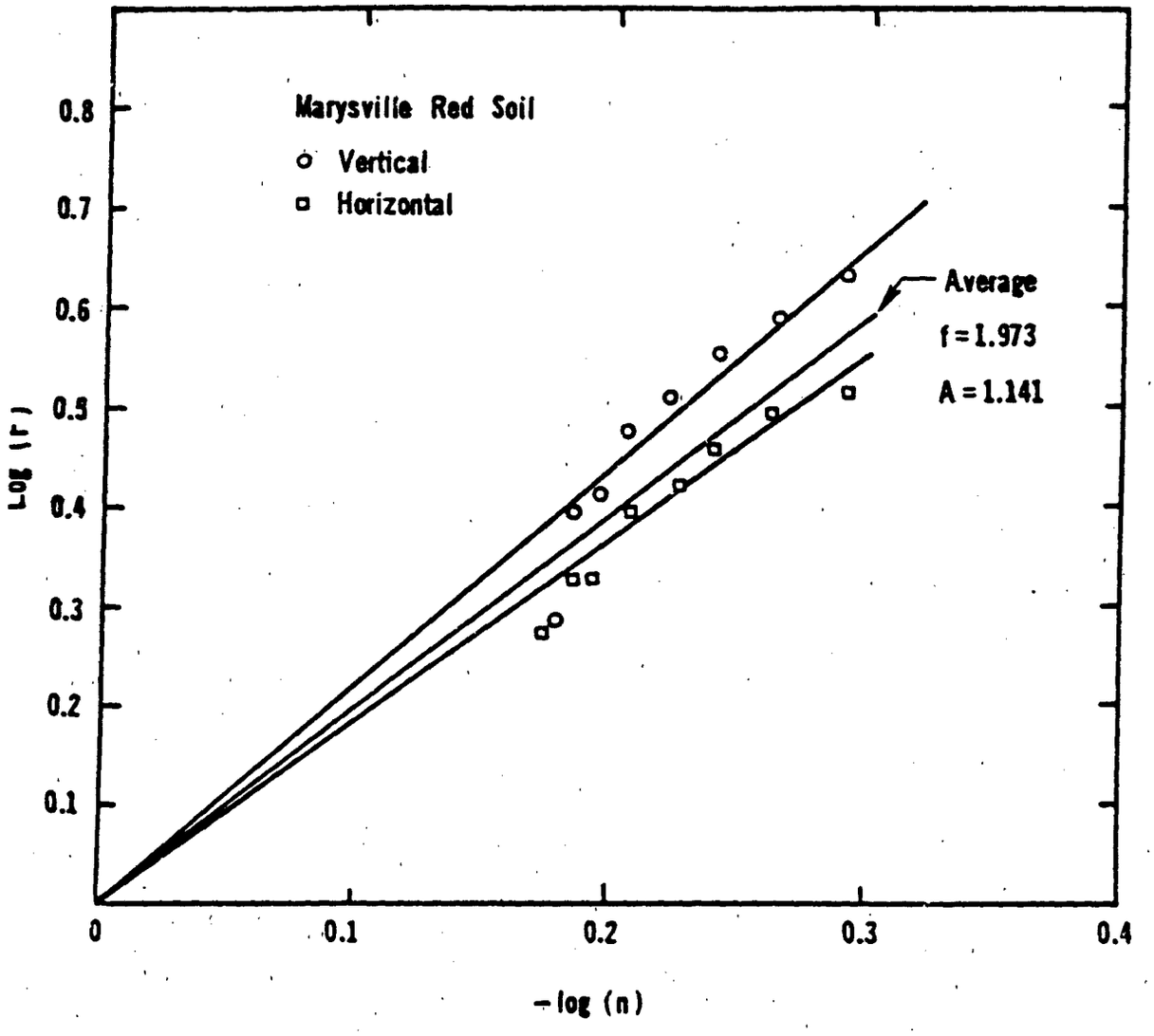

Figure 39 - The relationship between the horizontal and vertical formation factors and the total porosity, n for Marysville red soil

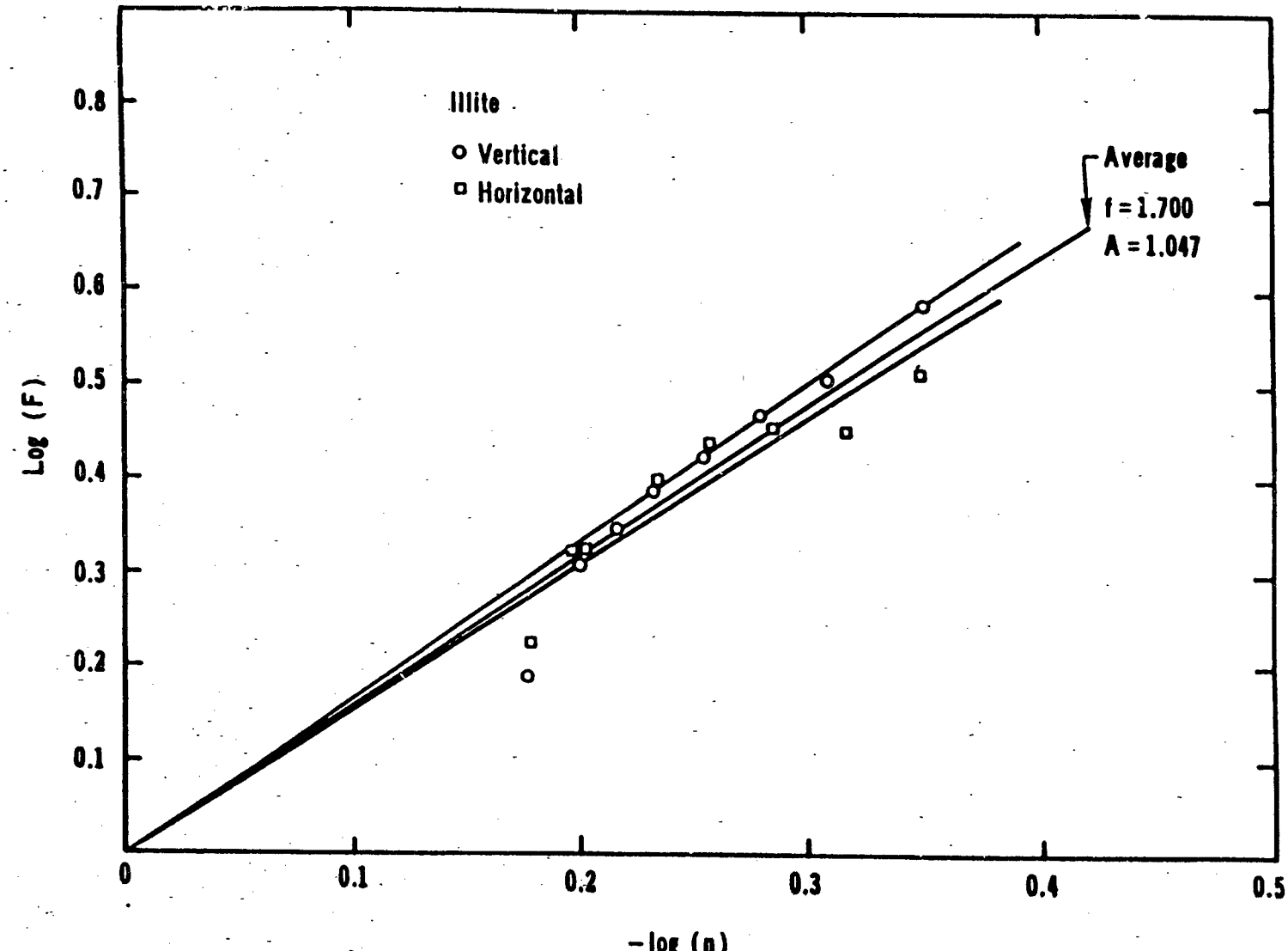

Figure 40 - The relationship between the horizontal and vertical formation factors and the total porosity, n for Illite

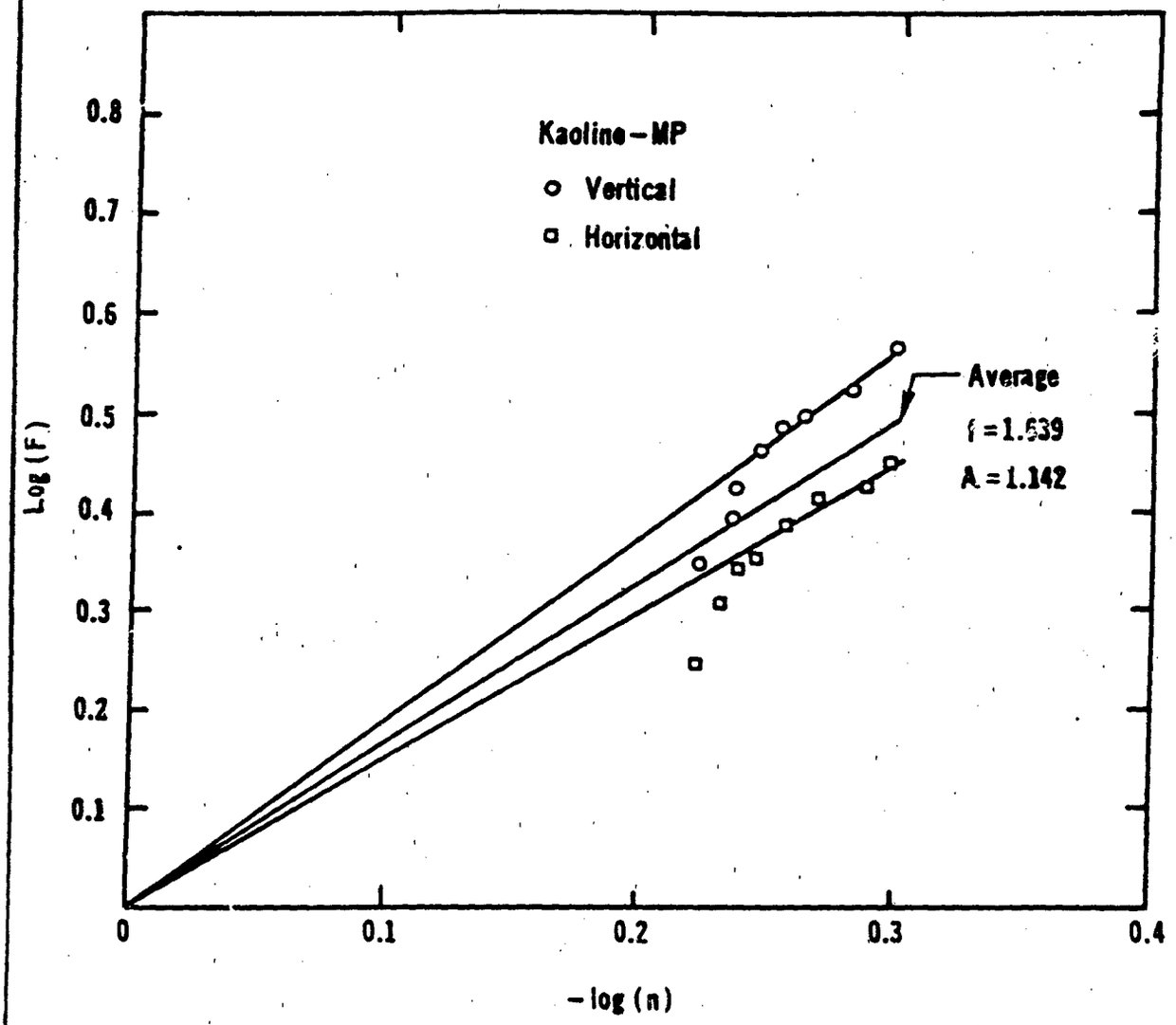

Figure 41 - The relationship between the horizontal and vertical formation factors and the total porosity, n for Kaoline - MP

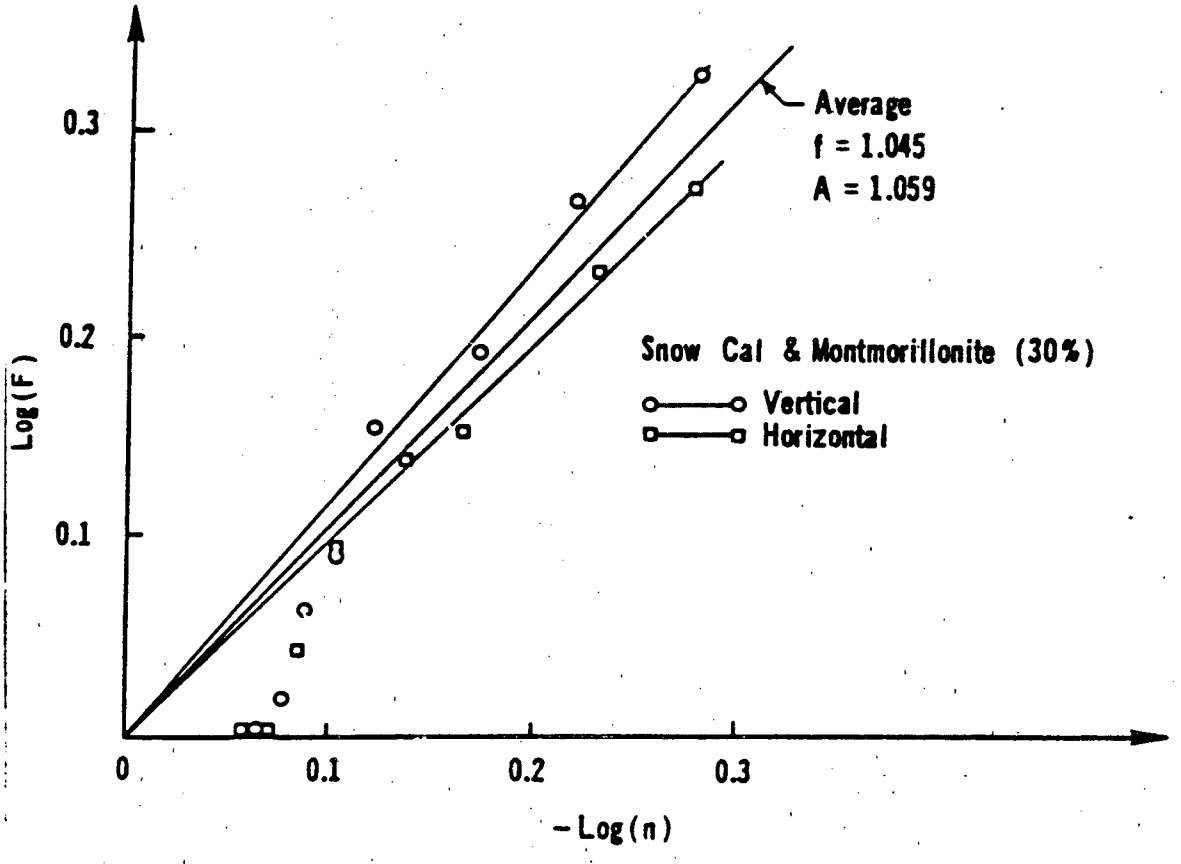

Figure 42 - The relationship between the horizontal and vertical formation factors and the total porosity, n for Snow Cal + (30%) Montmorillonite

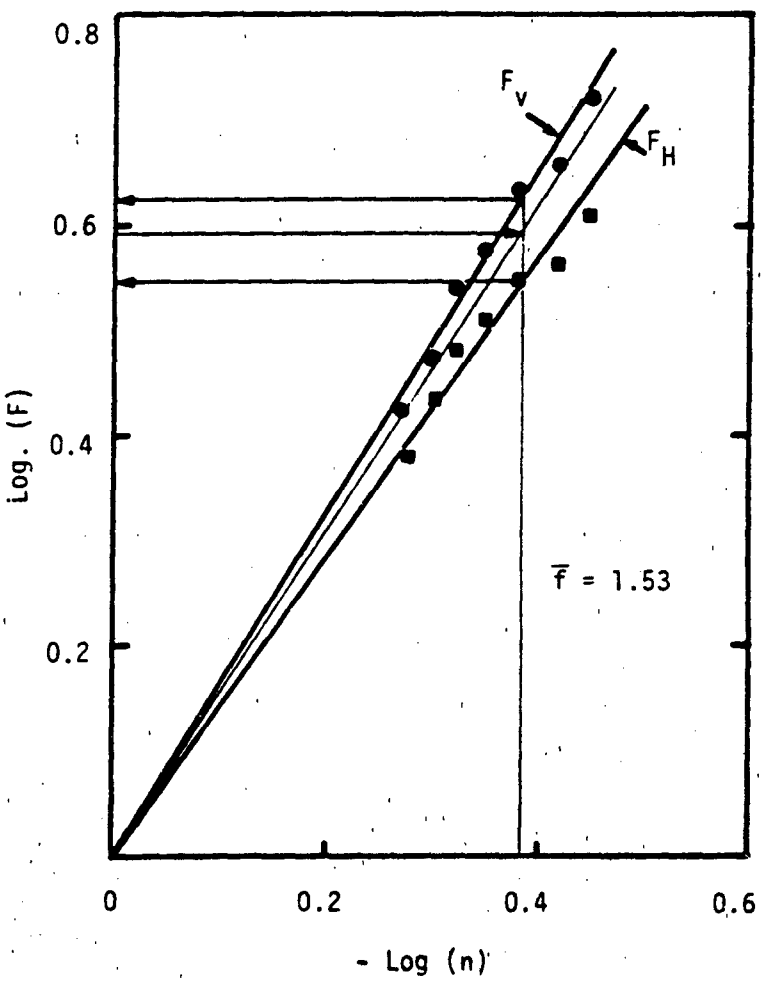

Fig. 43 Log. Formation Factor vs Negative Log. Porosity Relationship (Soil #1)

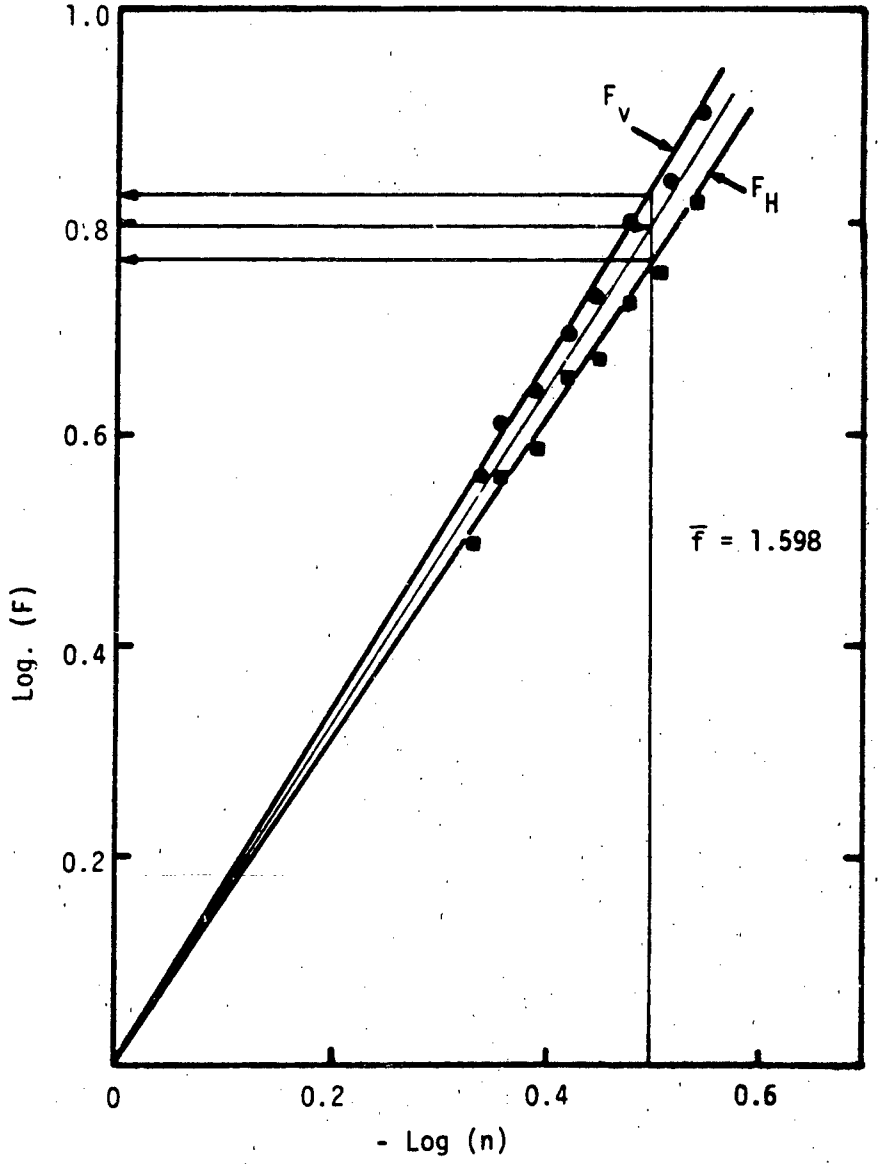

Fig. 44 : Log. Formation Factor vs Negative Log. Porosity Relationship (Soil #2)

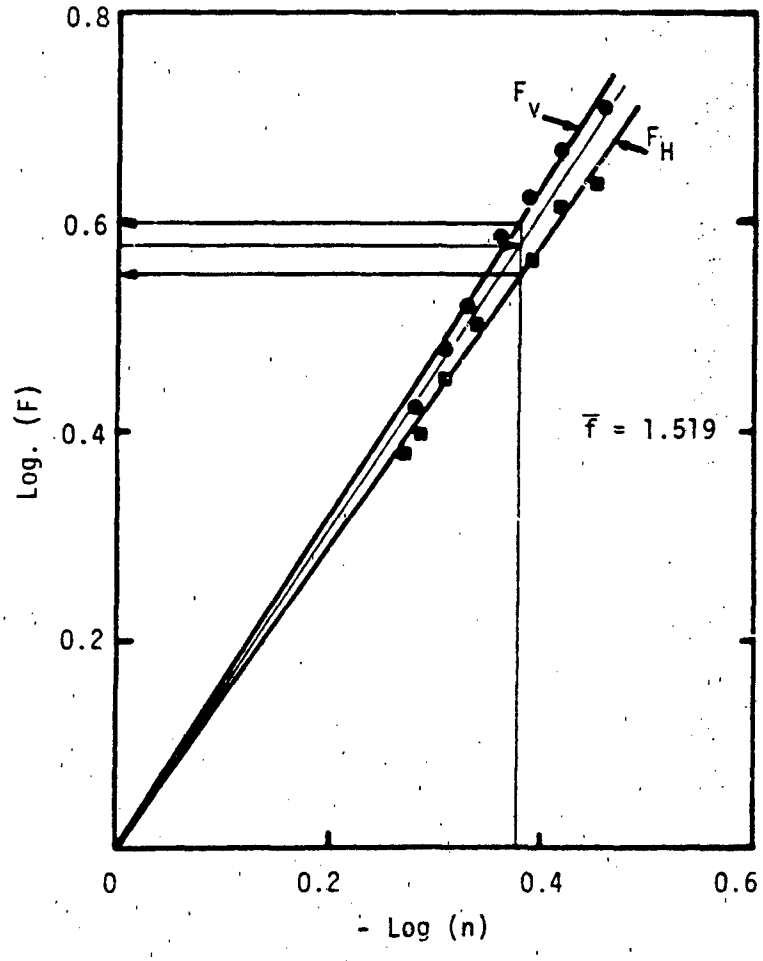

Fig. 45 : Log. Formation Factor vs Negative Log. Porosity Relationship (Soil #3)

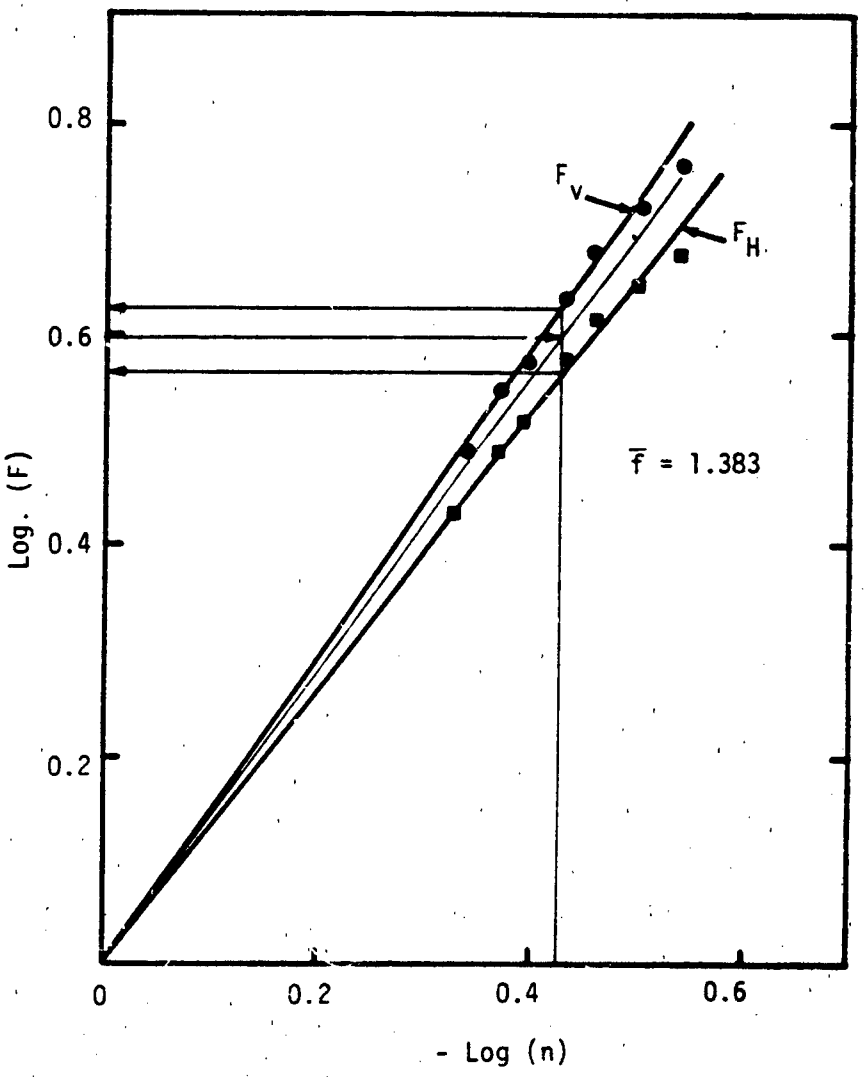

Fig. 46 : Log. Formation Factor vs Negative Log. Porosity Relationship (Soil #4)

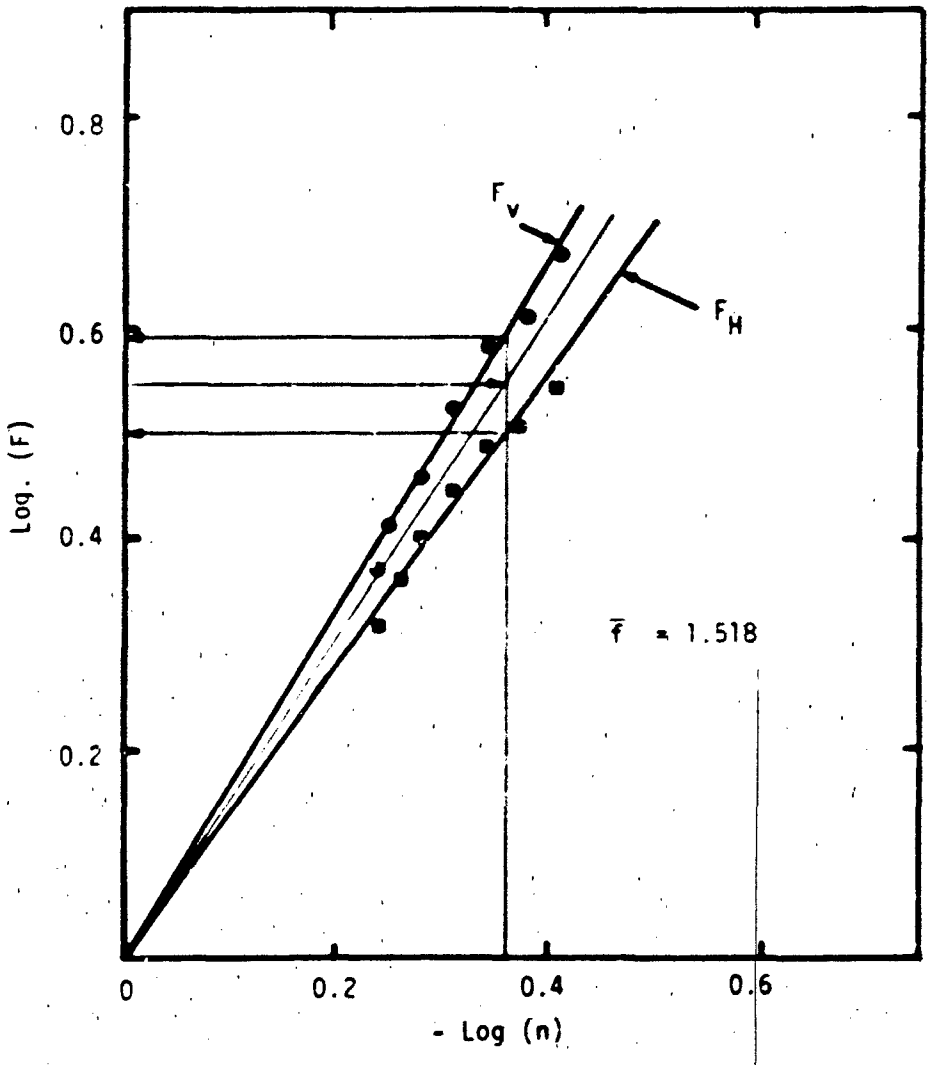

Fig. 47 : Log. Formation Factor vs Negative Log. Porosity Relationship (Soil #5)

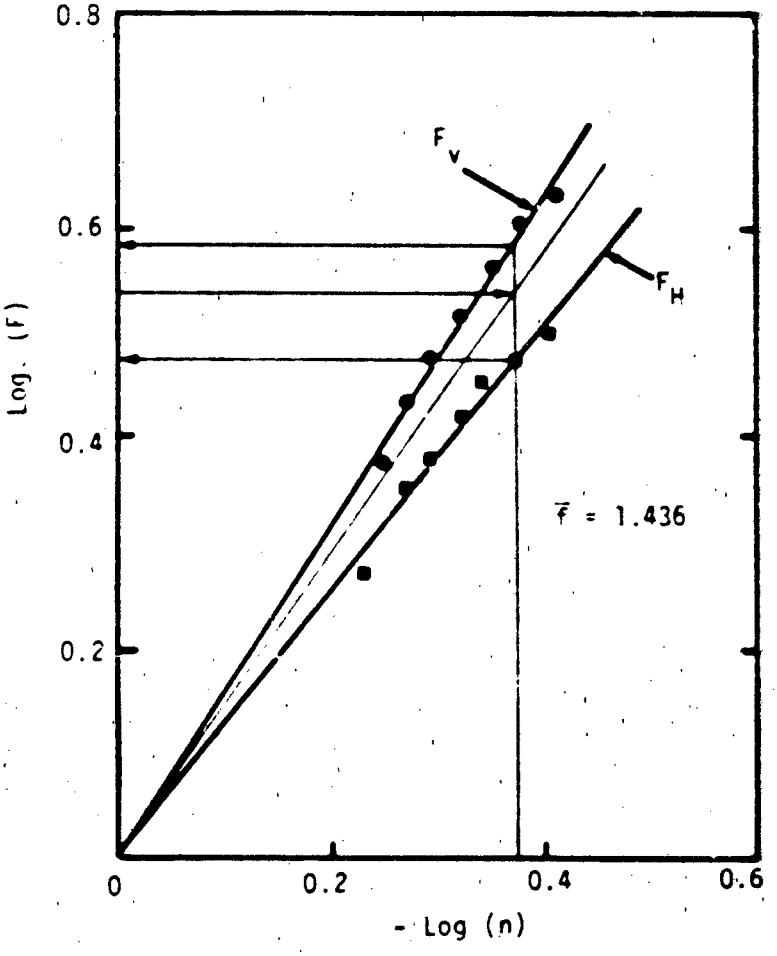

Fig. 48 : Log. Formation Factor vs Negative Log. Porosity Relationship (Soil #6)

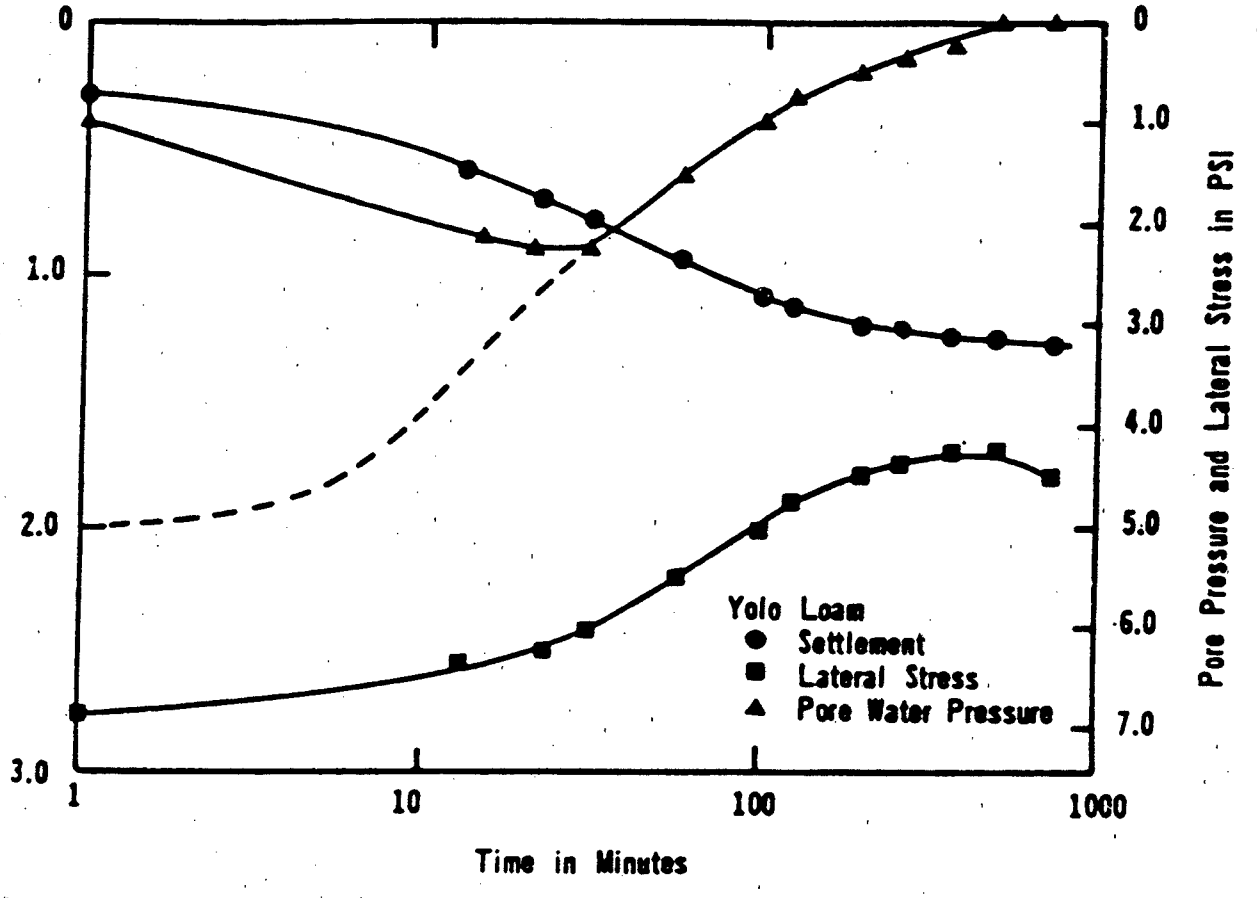

Figure 49 - Variation of settlement, lateral stress and pore pressure with time for Yolo Loam 4.85 - 9.85 psi

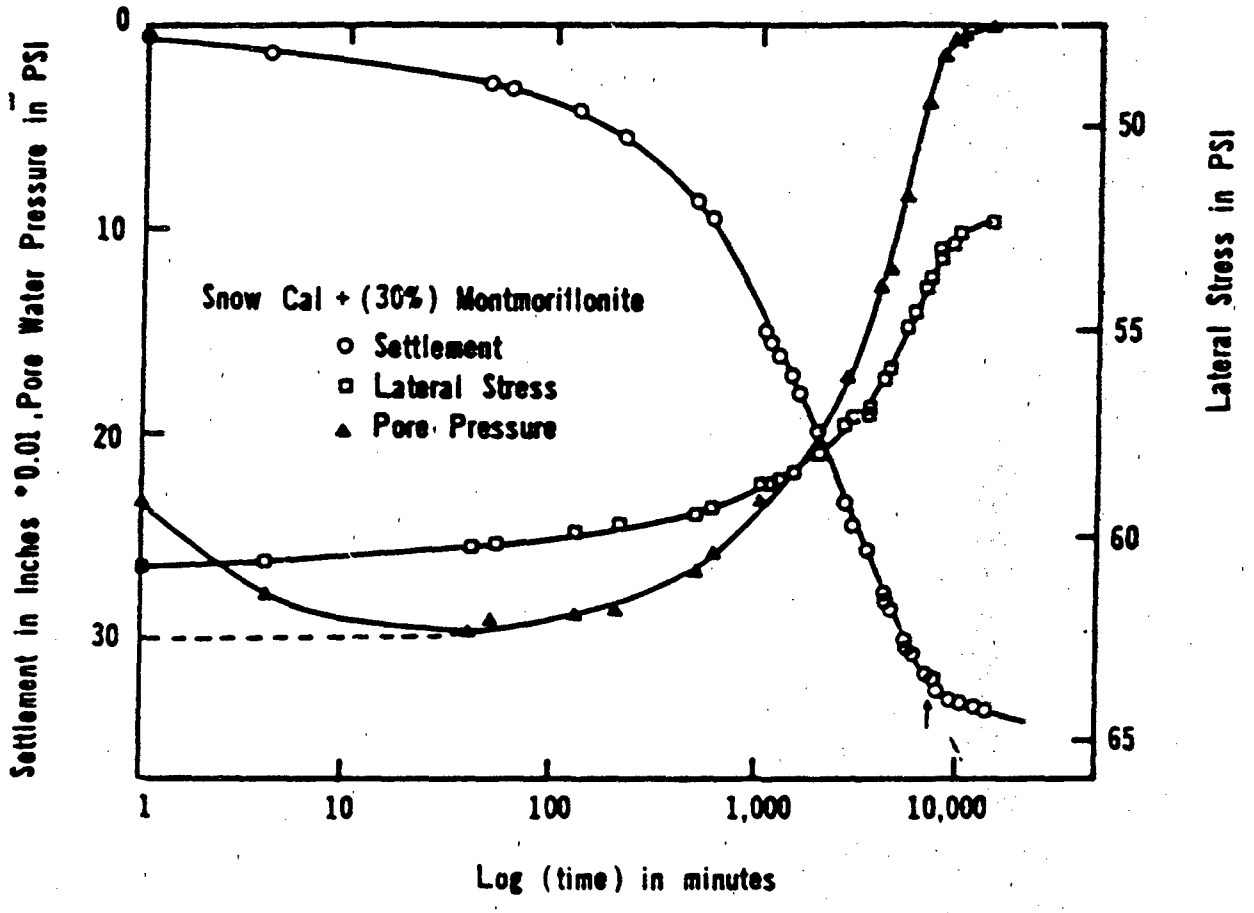

Figure 50 - Variation of settlement, lateral stress and pore pressure with logarithmic time for Snow Cal + 30% Montmorillonite 39.64 - 39.44 psi

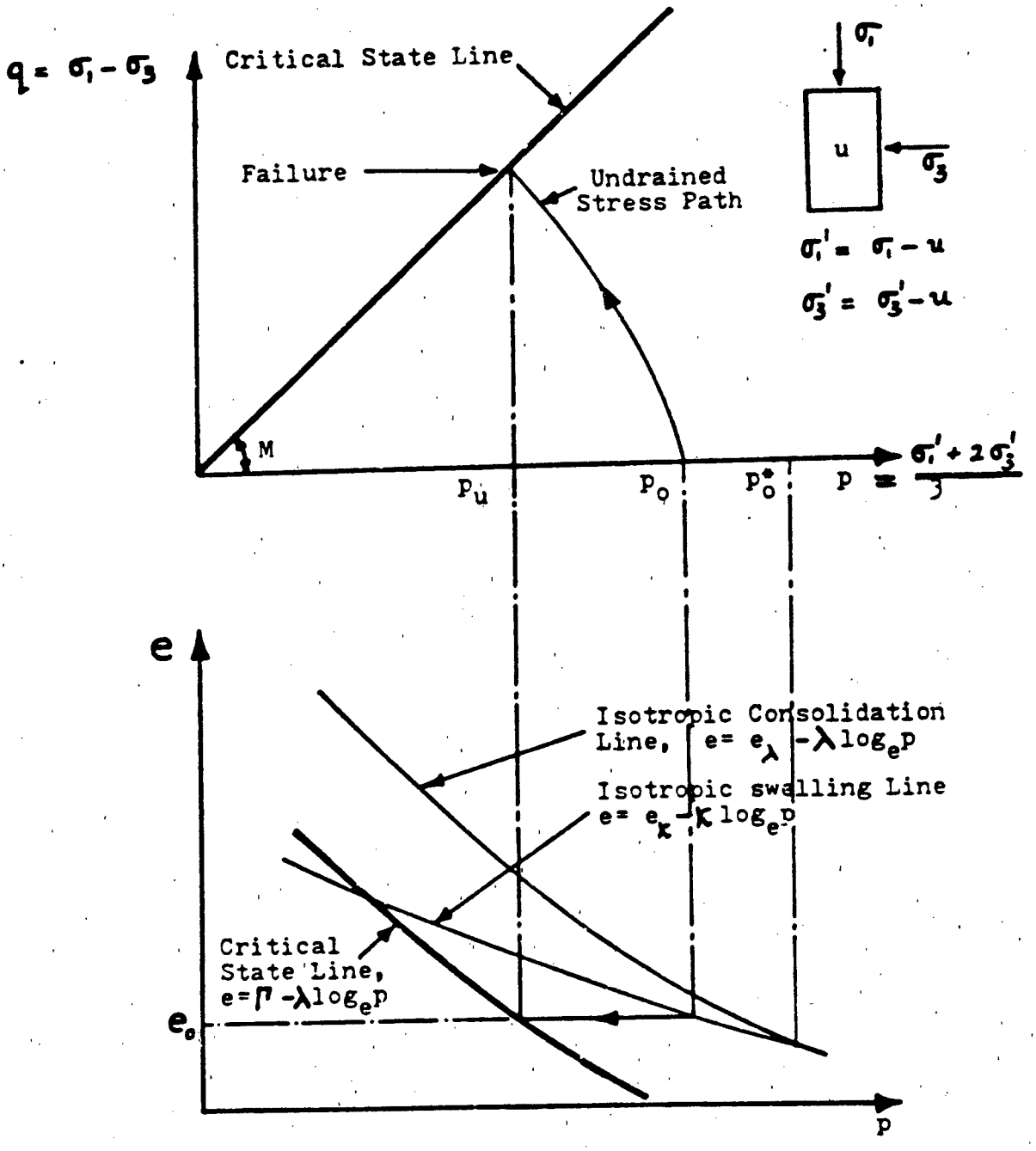

p_o^* = Pre-cosolidation pressure

OCR = p_o^*/p_o

Fig. 51 Schematic Illustration of the definition of λ, κ, M, e_o and OCR

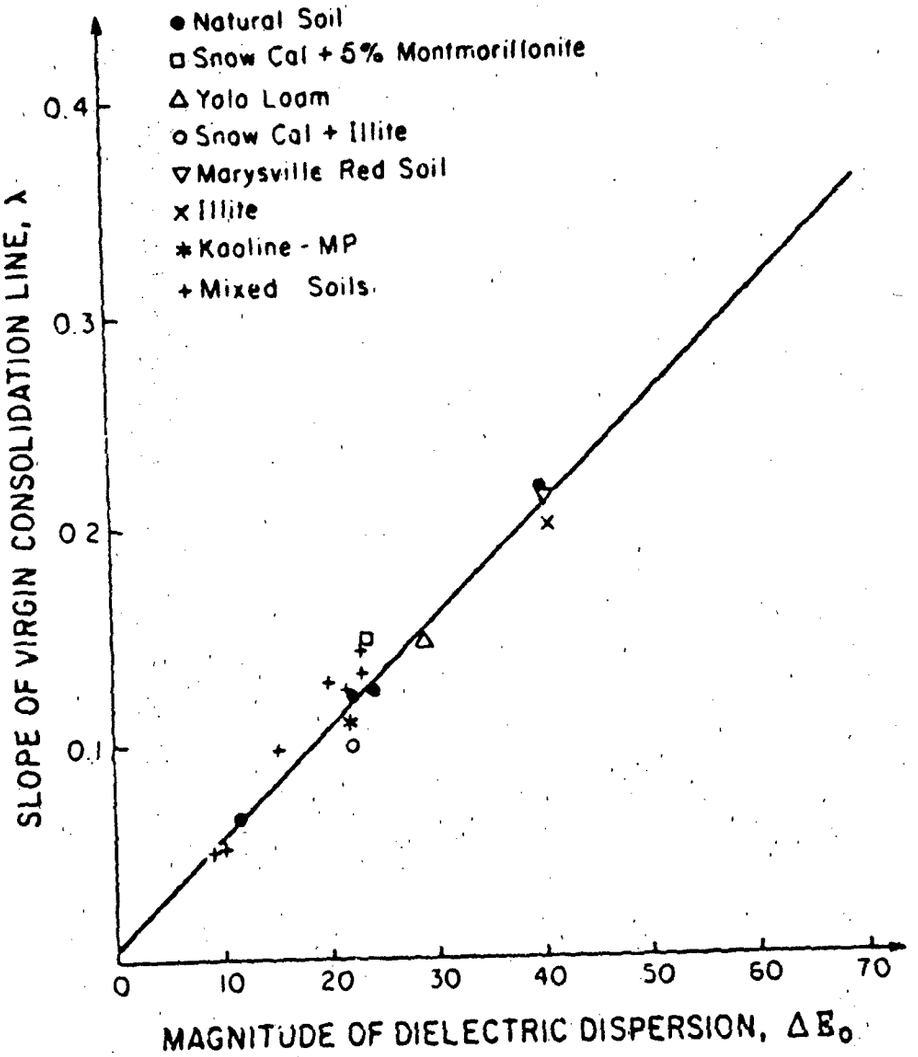

Figure 52 - Correlation Between Compression Index (λ) and the Magnitude of Dielectric ($\Delta\epsilon_o$)

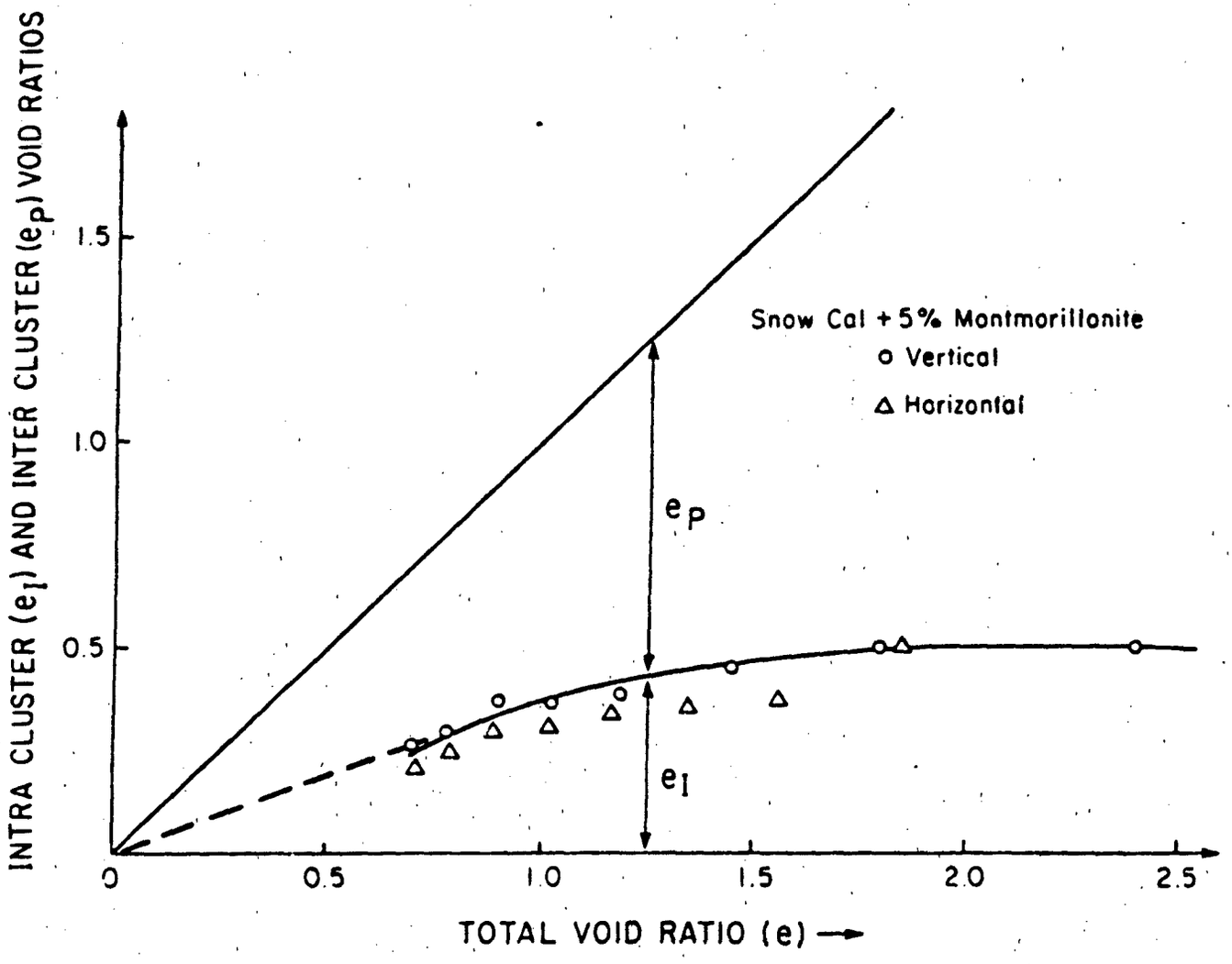

Figure 53 - Variation of Inter and Intra Cluster Void Ratios with Total Void Ratio

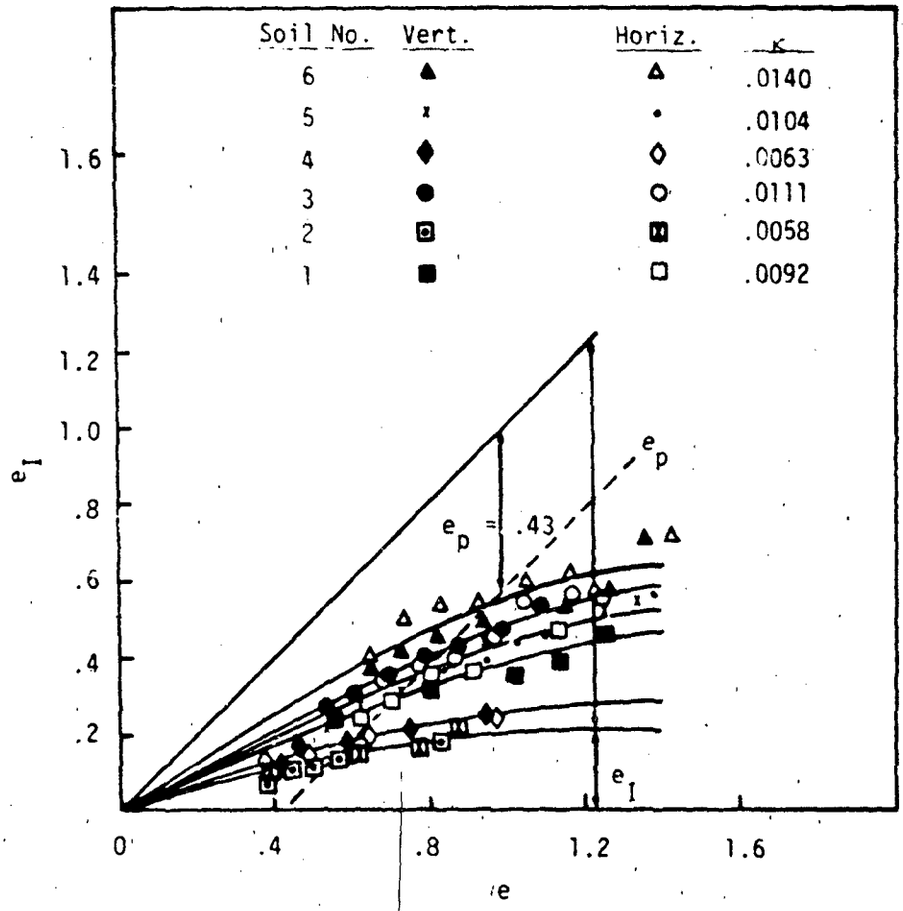

Fig. 54 : Relationship Between Intra Cluster Void Ratio and Total Void Ratio for Soils of Different Gradient Swell Line

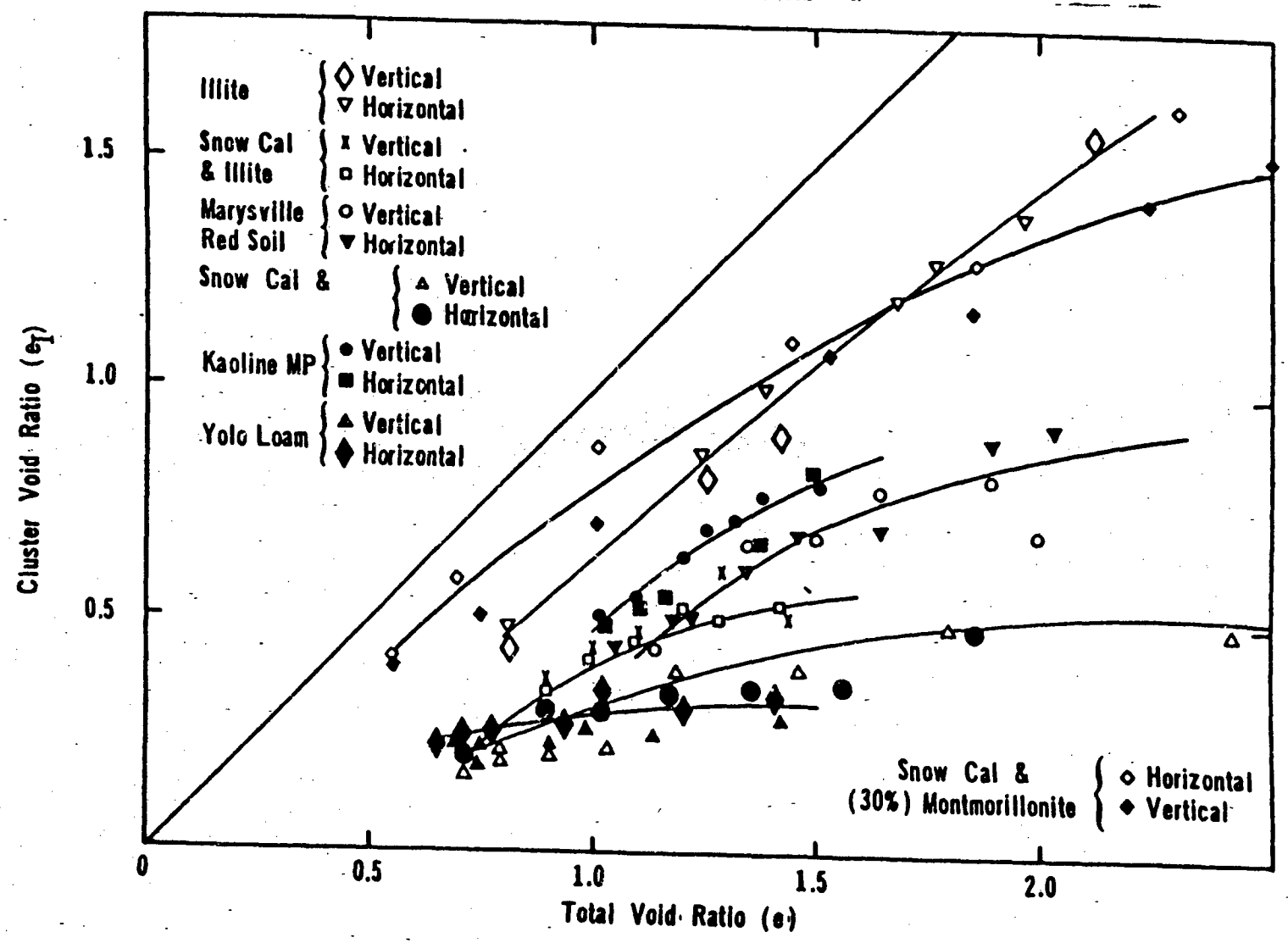

Note: For Snow Cal + (30%) Montmorillonite Scale = 2

Figure 55 - The relationship between Intra (e_I) and Inter (e_p) Cluster voids and total void ratio (e)

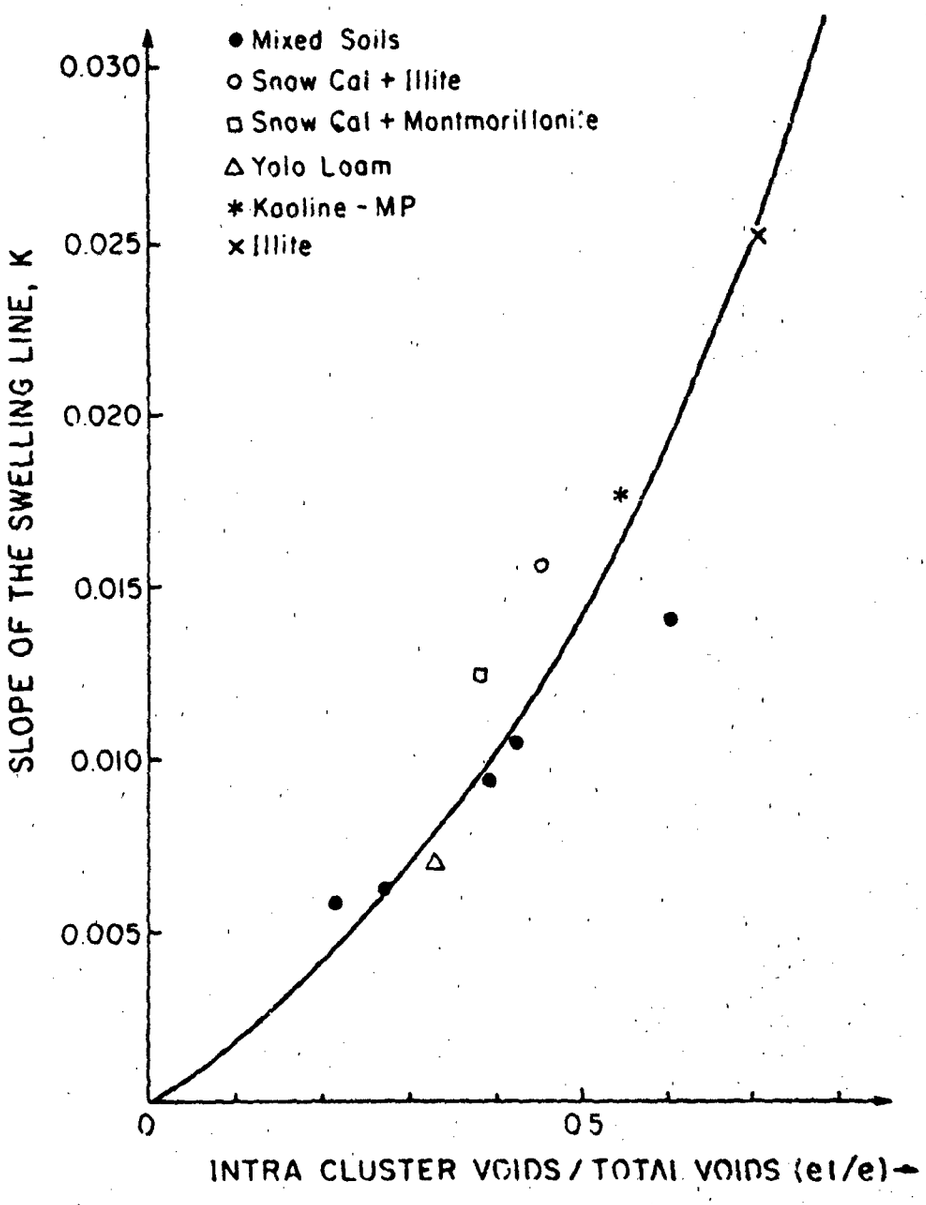

Figure 56 - Correlation Between Swelling Index (K) and the Ratio of Intra Cluster Void Ratio to Total Void Ratio

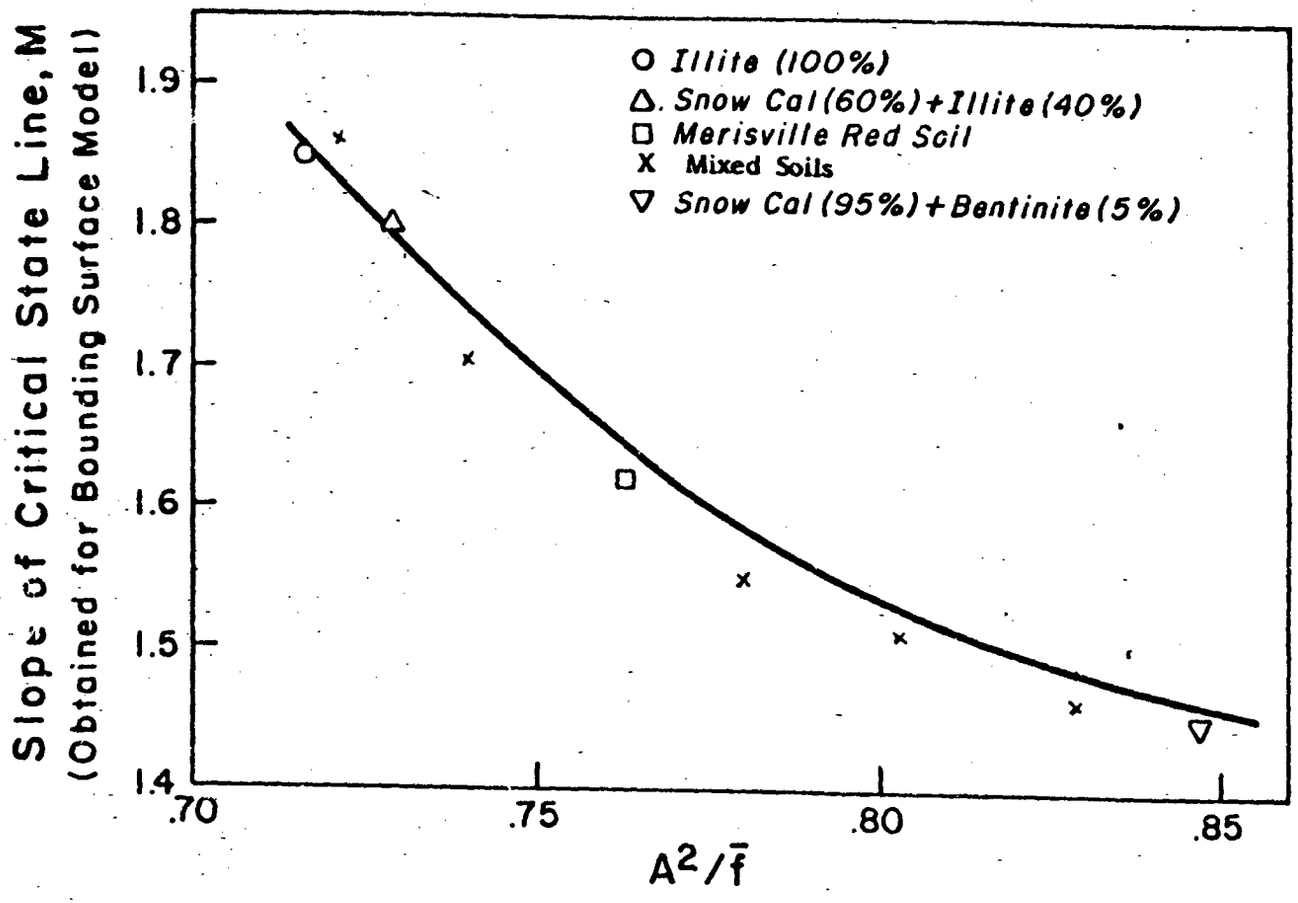

Fig. 57 The relationship between the slope of the critical state line, M, and the electrical index, $A^2/\bar{f}$

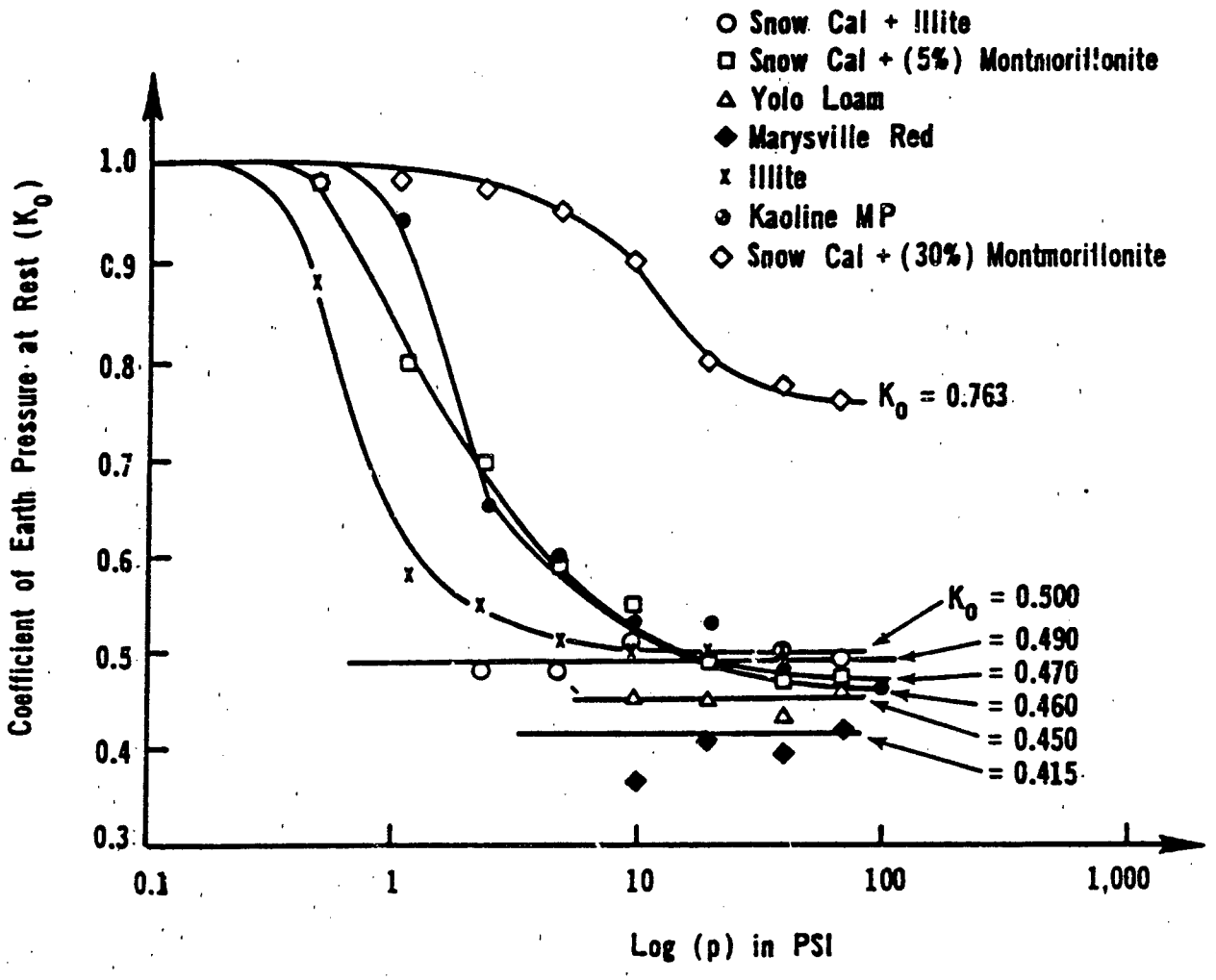

Figure 58 - The variation of coefficient of earth pressure at rest with consolidation pressure

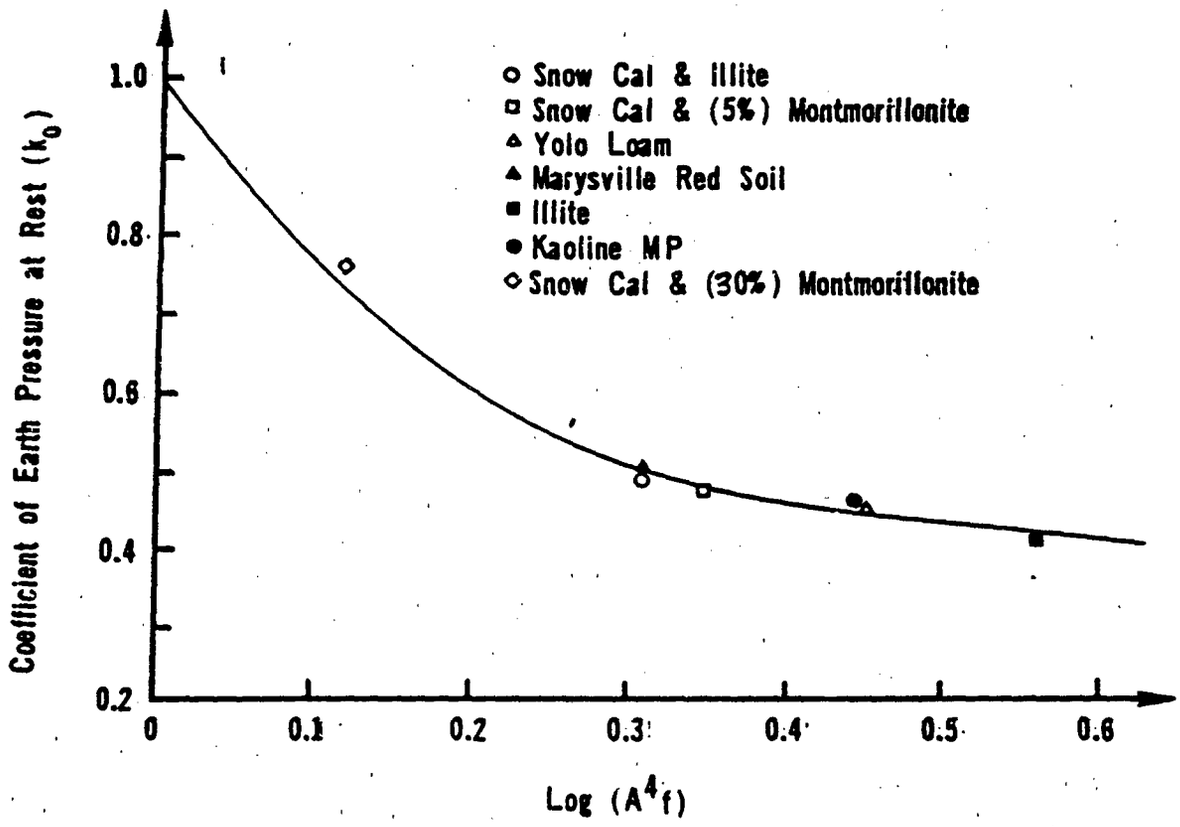

Figure 59 - The relationship between the coefficient of earth pressure at rest and electrical index A^4f

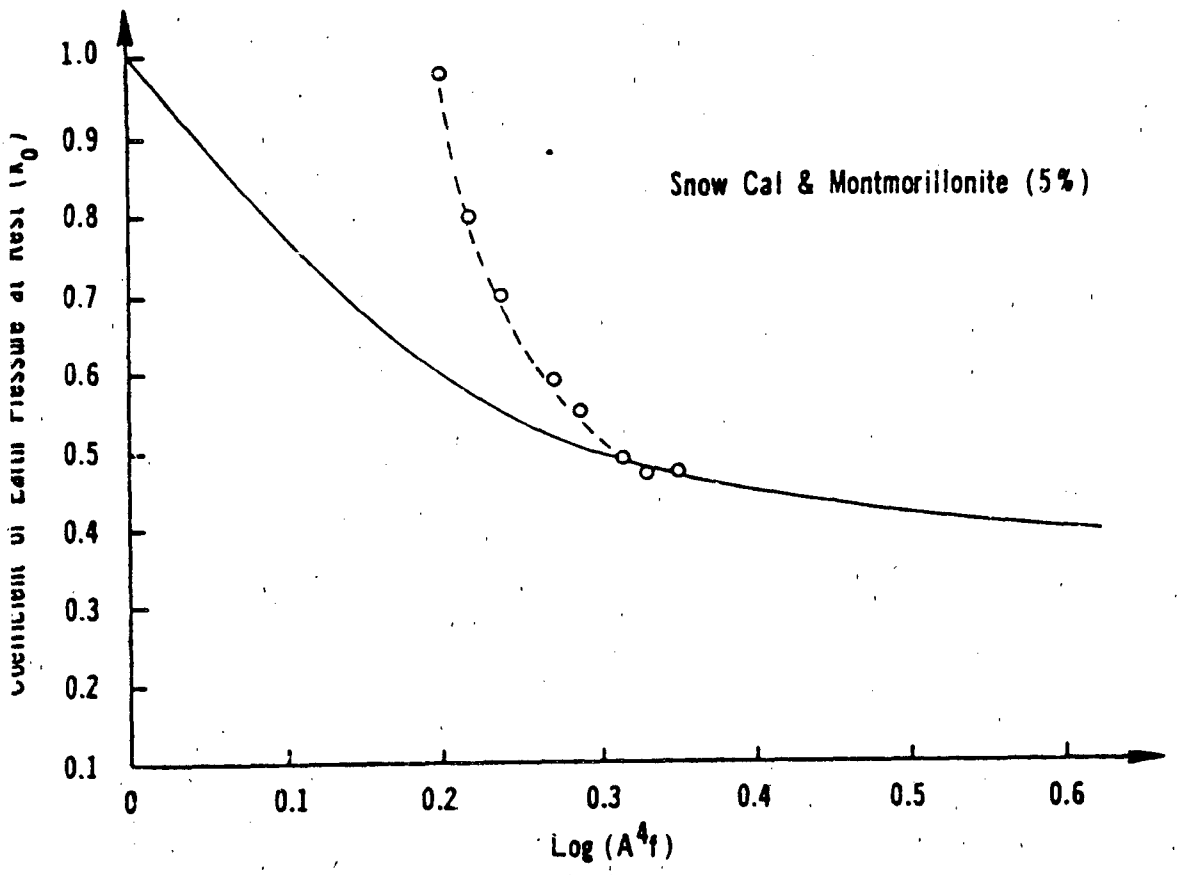

Figure 60- The Variation of Electrical Index A^4f and Coefficient of Earth Pressure at Rest with Loading for Snow Cal + (5%) Montmorillonite

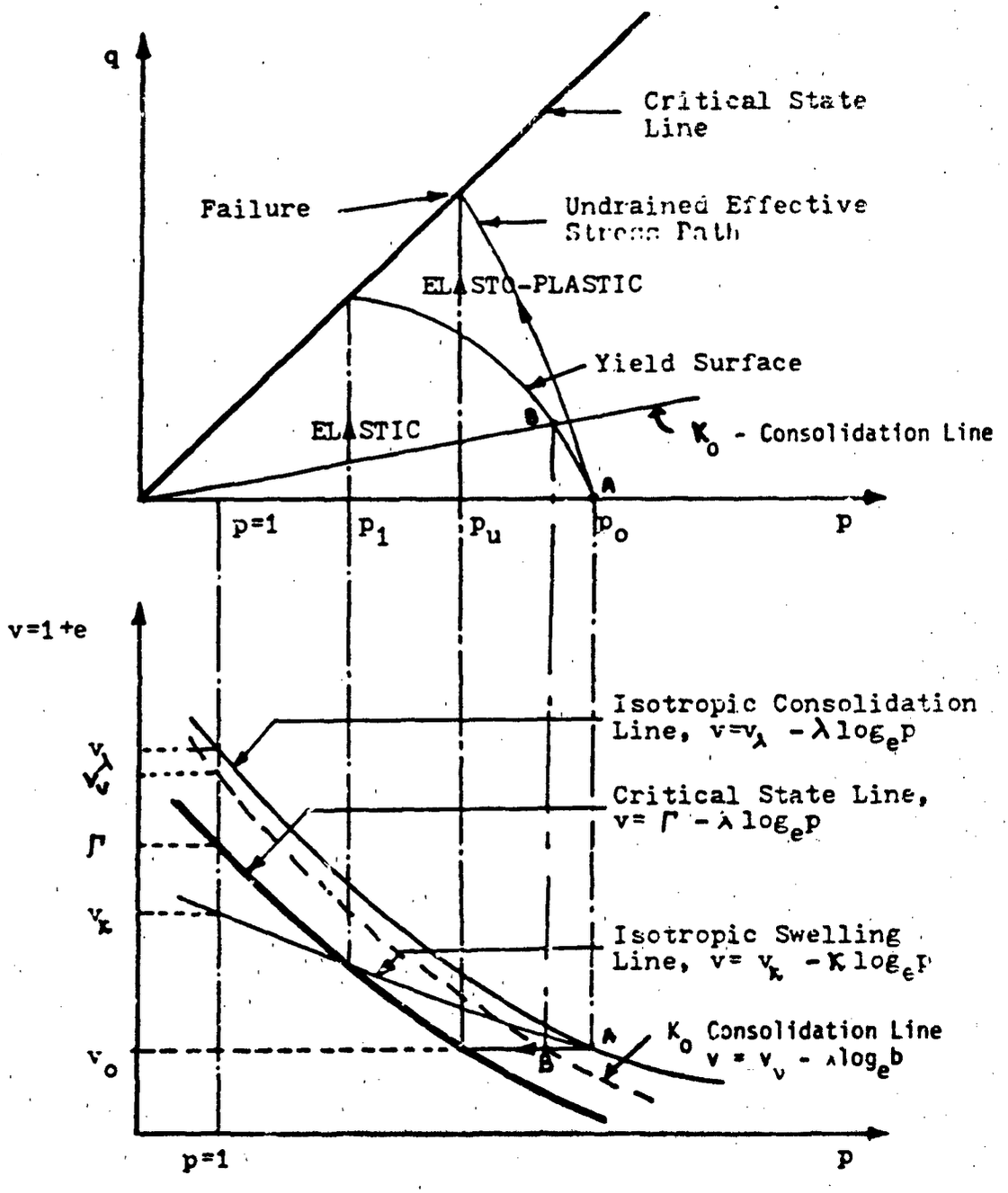

Fig. 61 The relationship between q, p and v for undrained conditions.

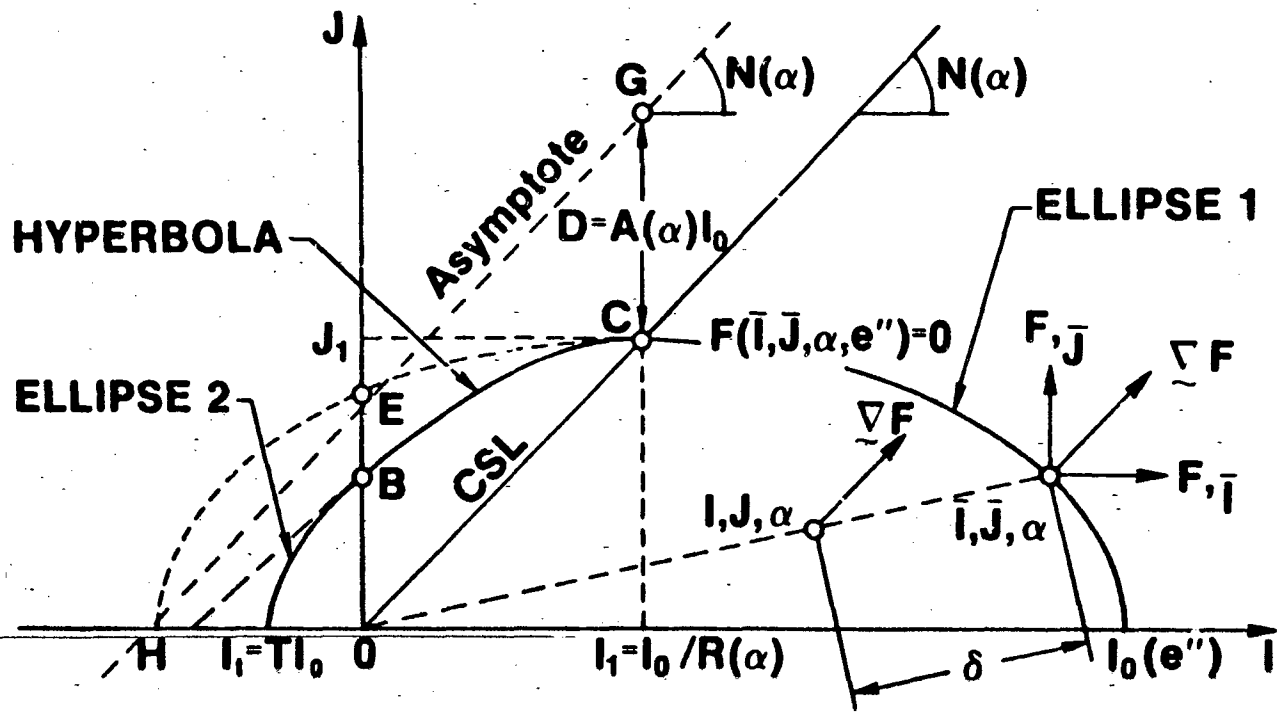

Fig. 62 Bounding Surface Model

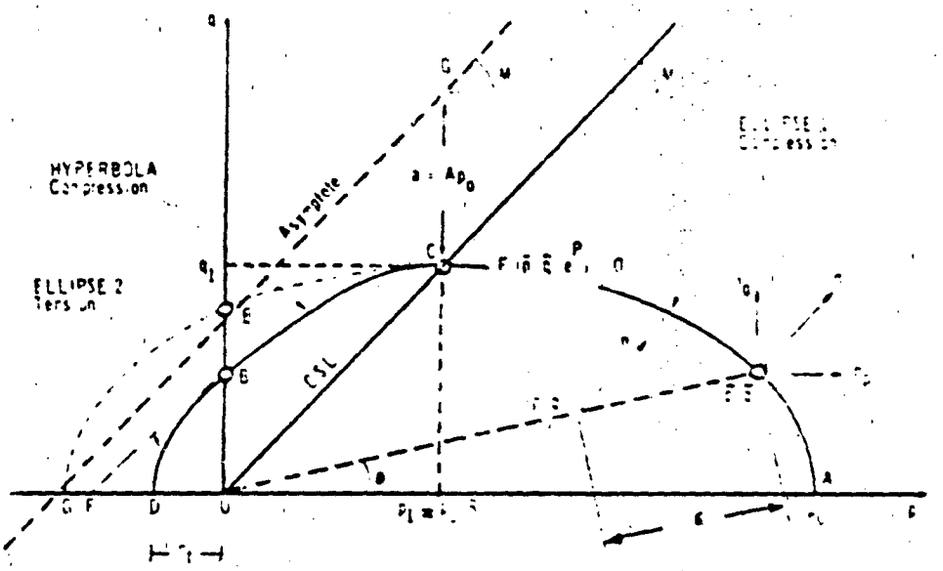

Fig. 63 :Bounding surface in the triaxial space.

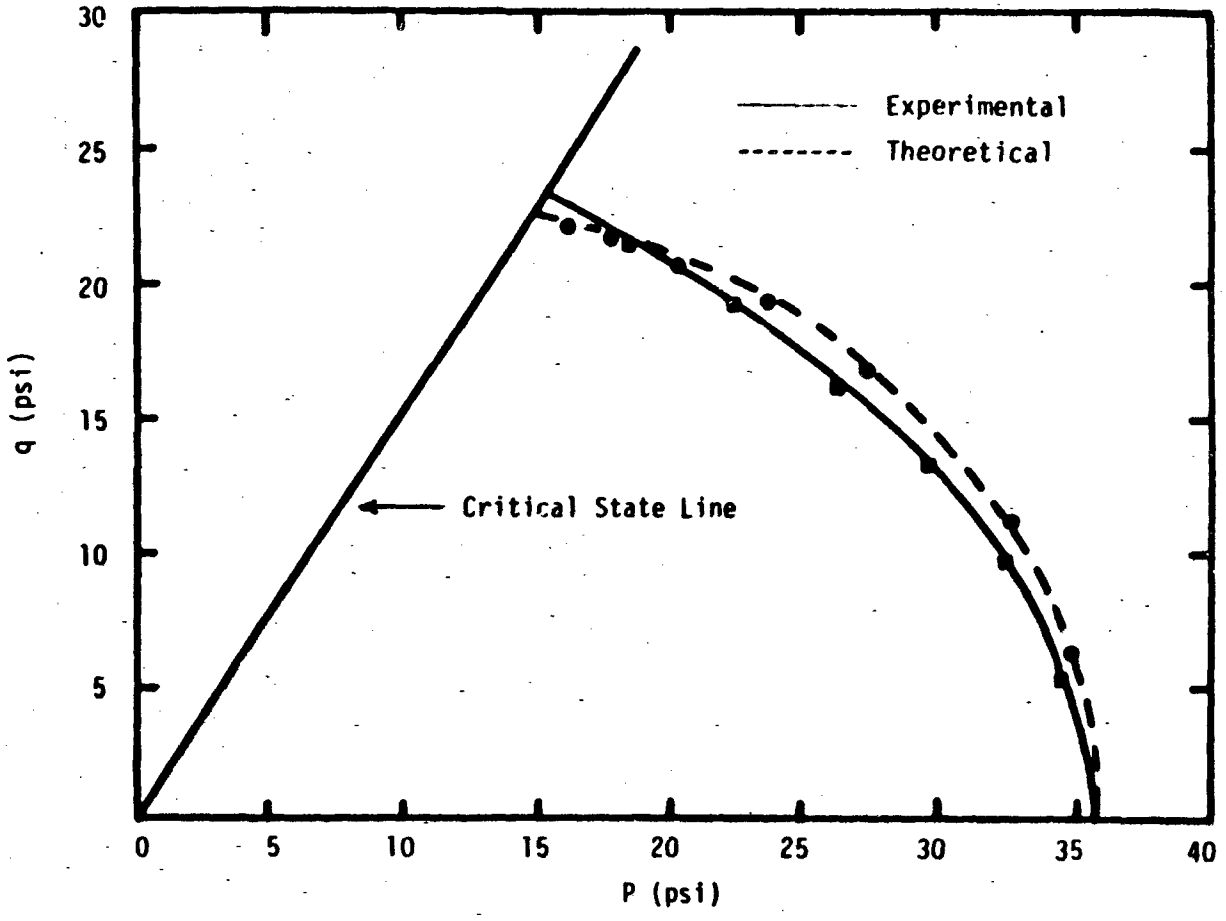

Fig. 64 : Experimental And Theoretical q vs p Relationship (Soil #1)

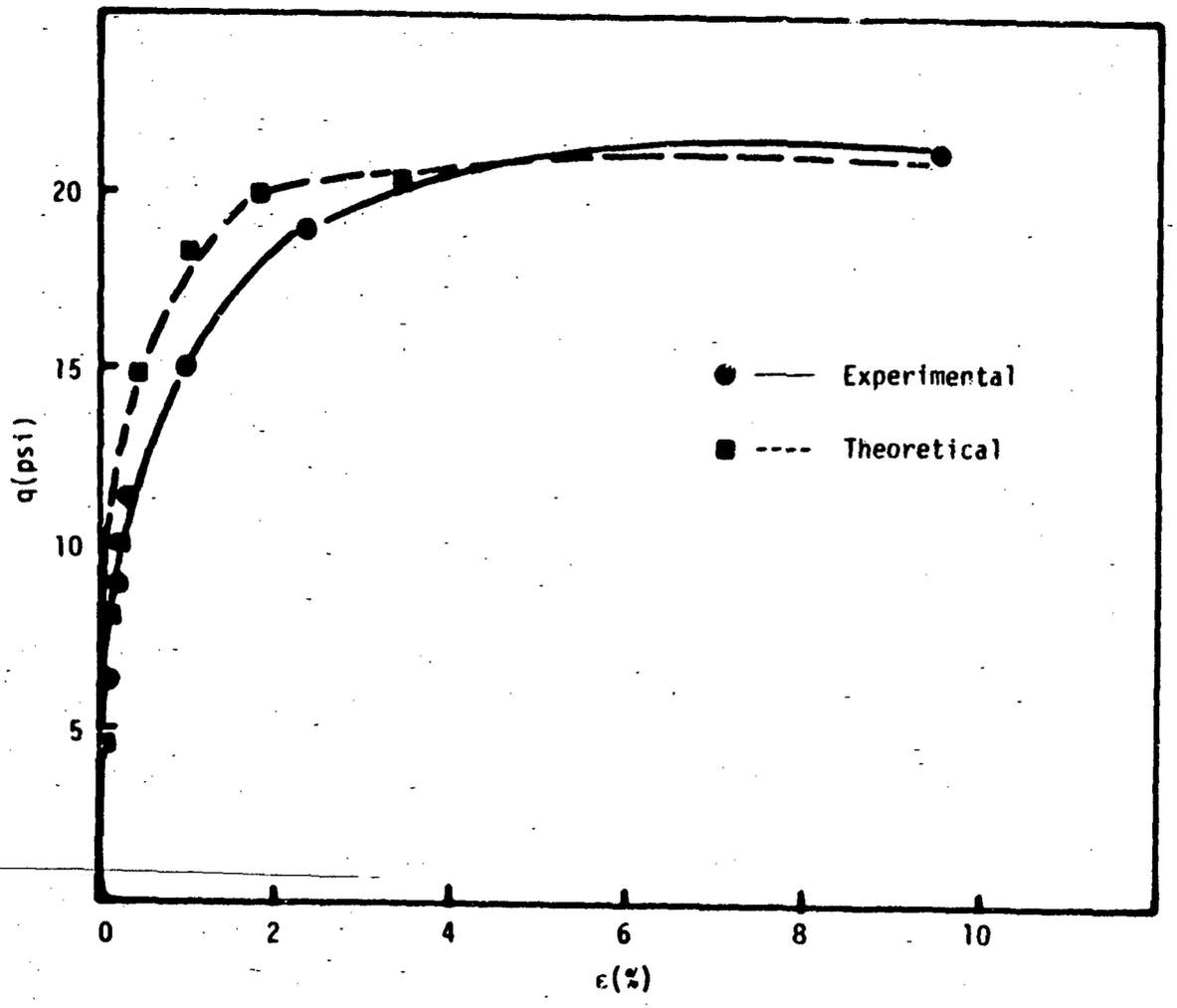

Fig. 65 Experimental and Theoretical Stress-Strain Relationship (Soil #1)

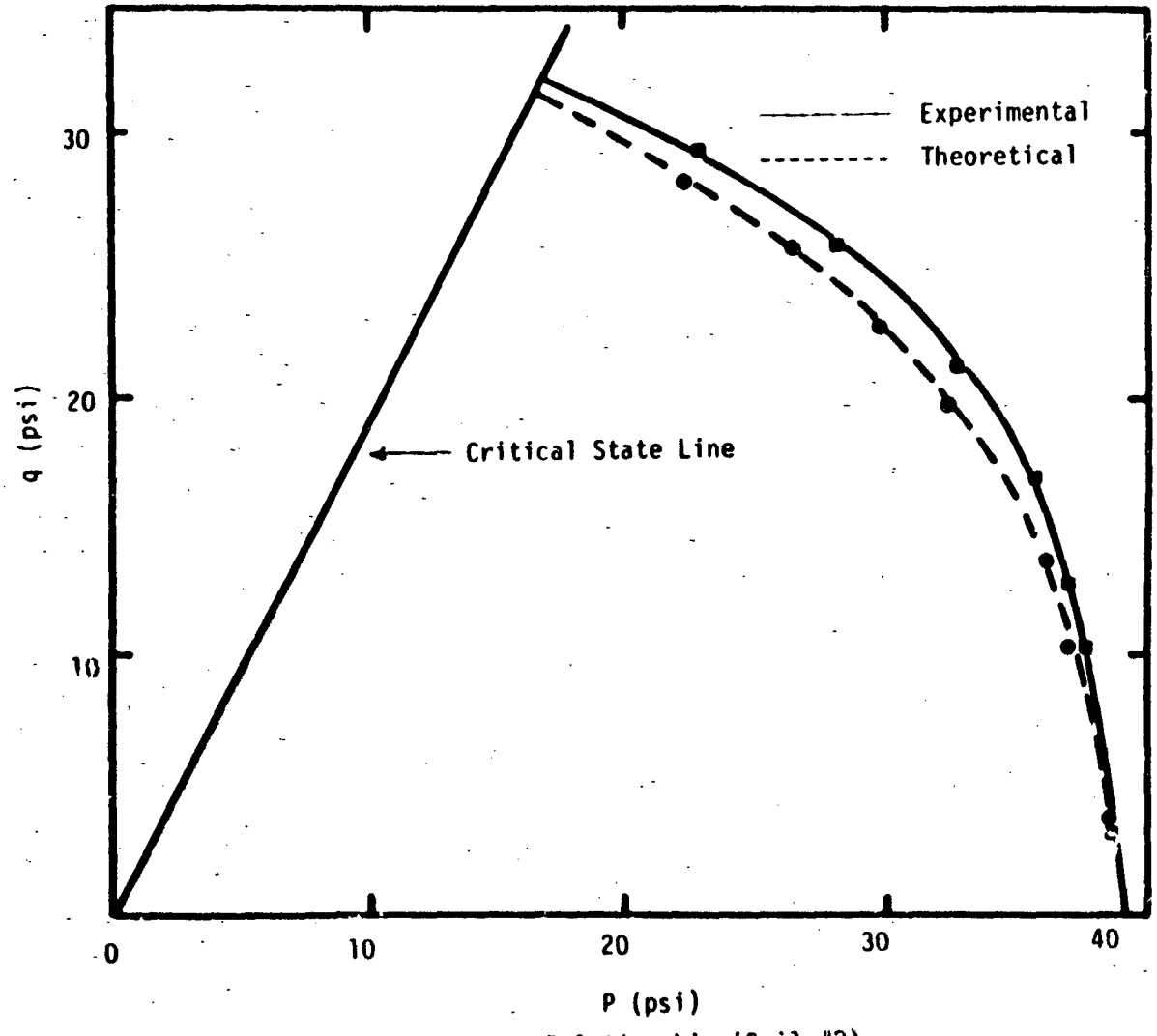

Fig. 66 Experimental And Theoretical q vs p Relationship (Soil #2)

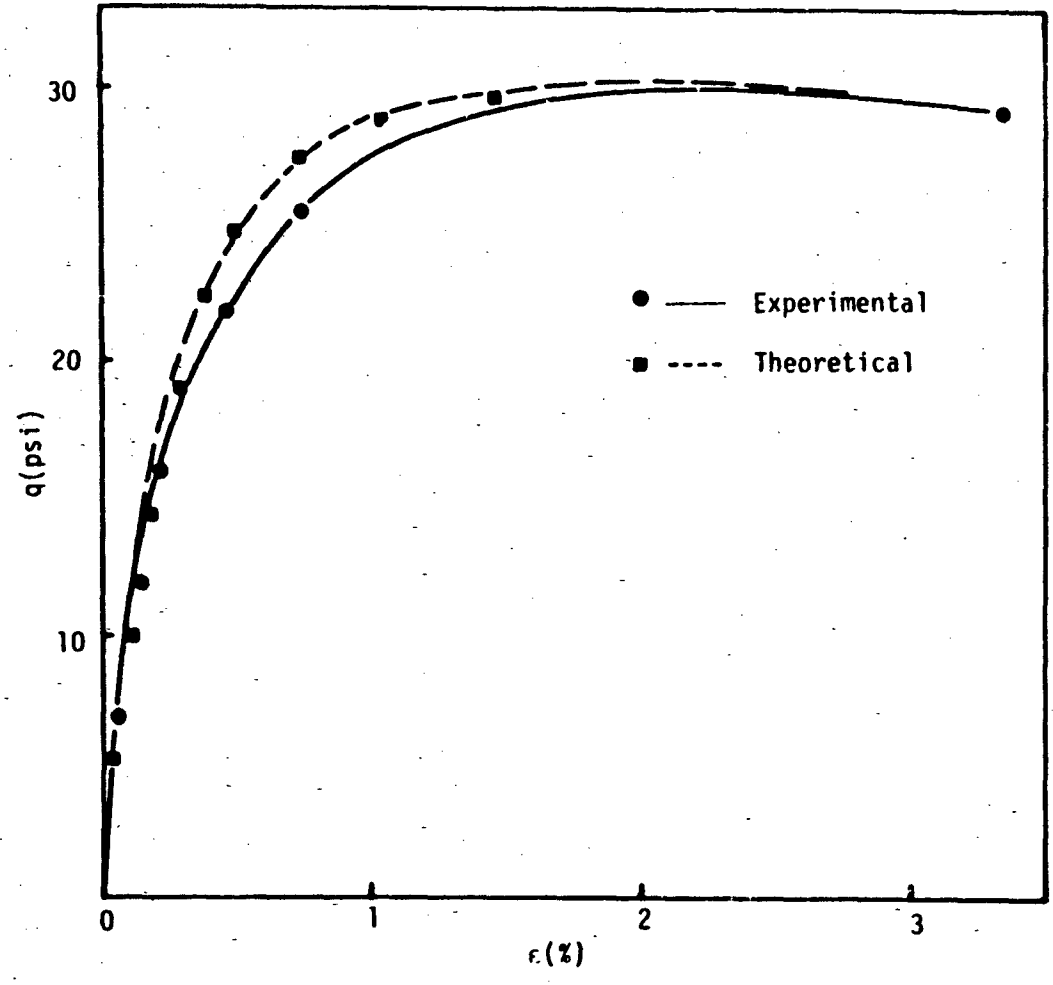

Fig. 67 : Experimental and Theoretical Stress-Strain Relationship (Soil #2)

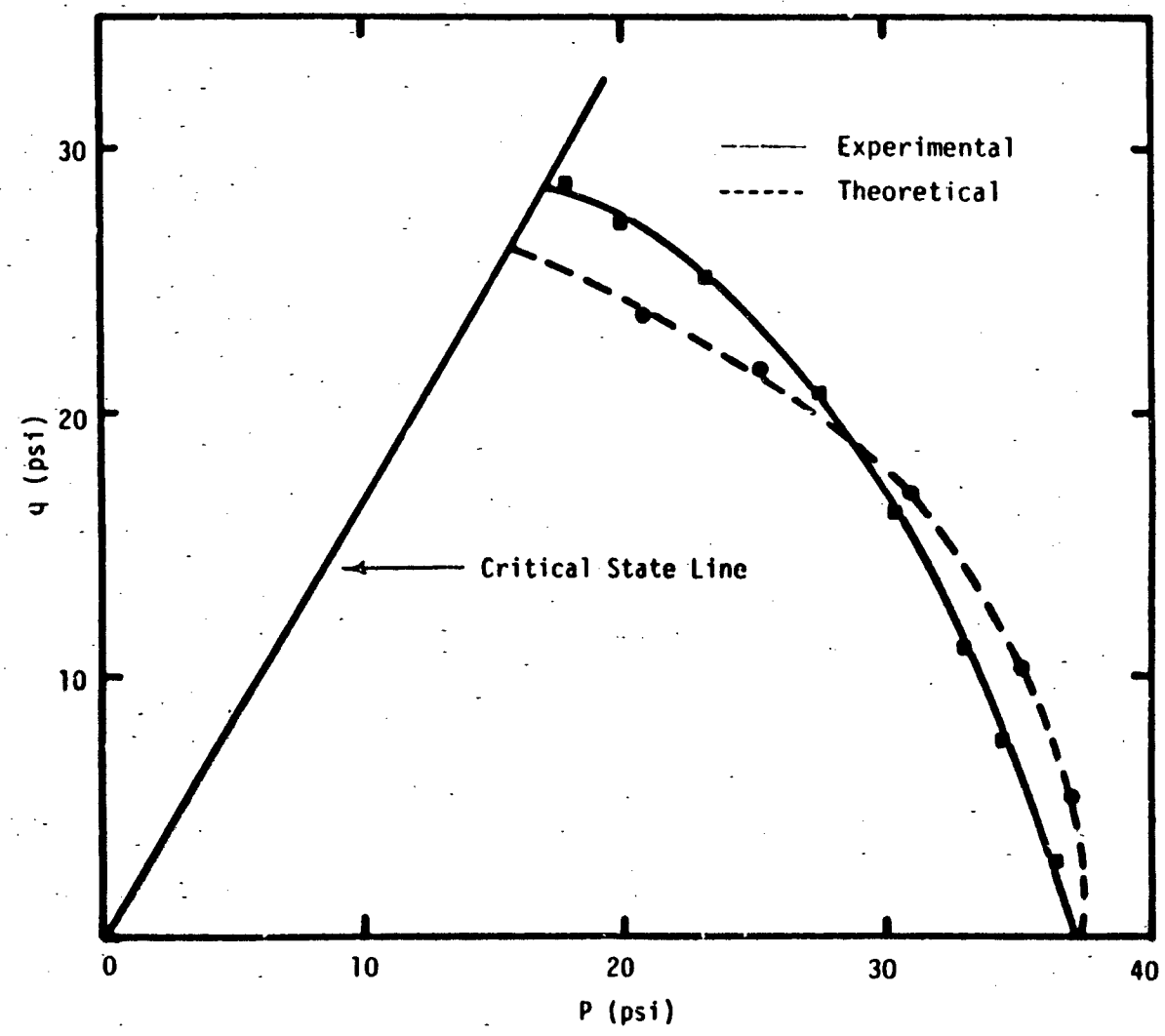

Fig. 68 : Experimental And Theoretical q vs p Relationship (Soil #3)

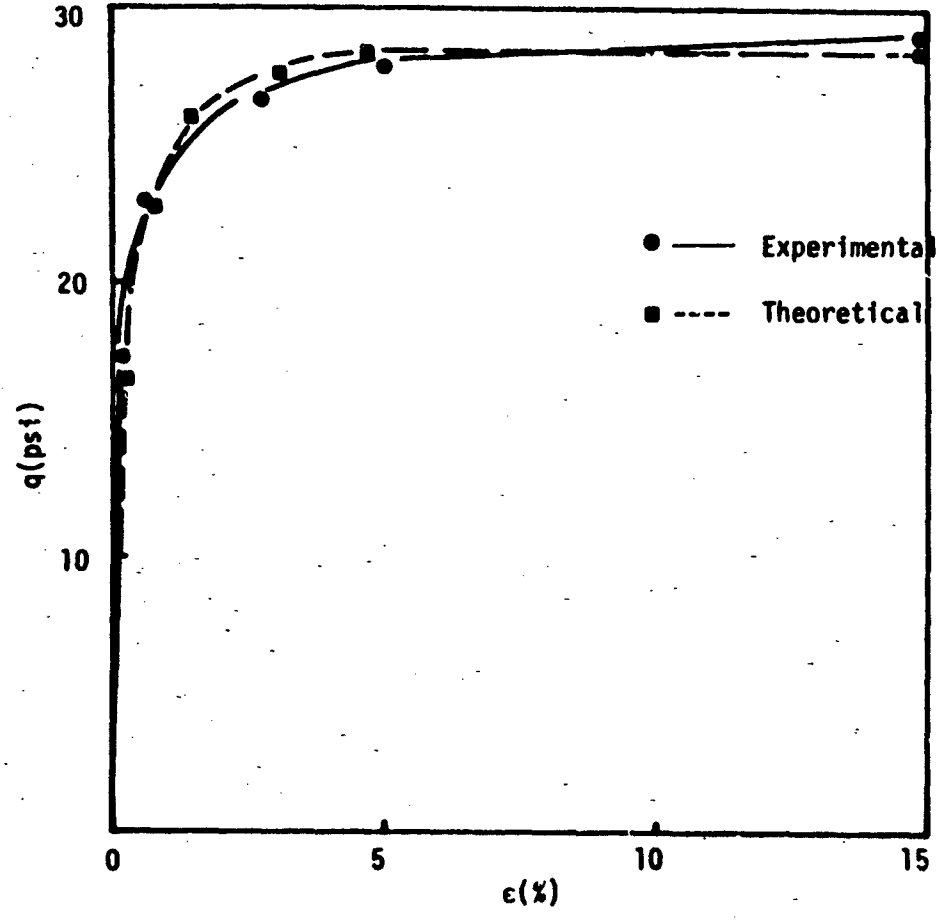

Fig 69 : Experimental and Theoretical Stress-Strain Relationship (Soil #3)

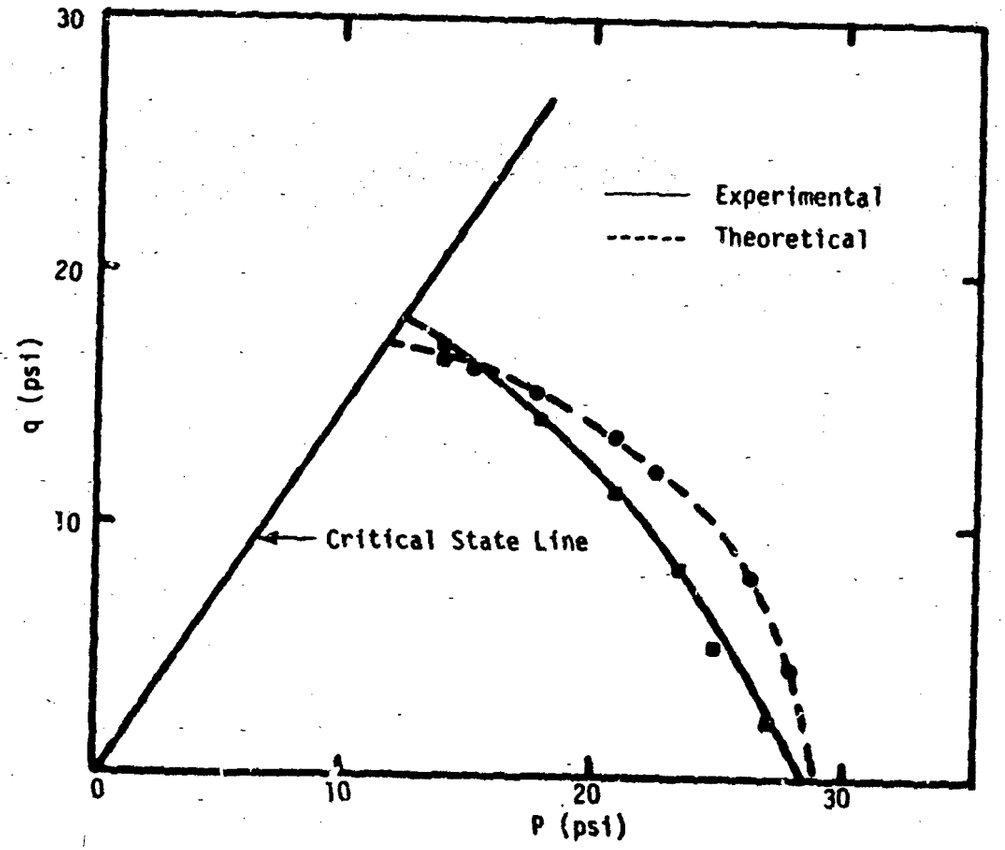

Fig. 70 : Experimental And Theoretical q vs p Relationships (Soil #5)

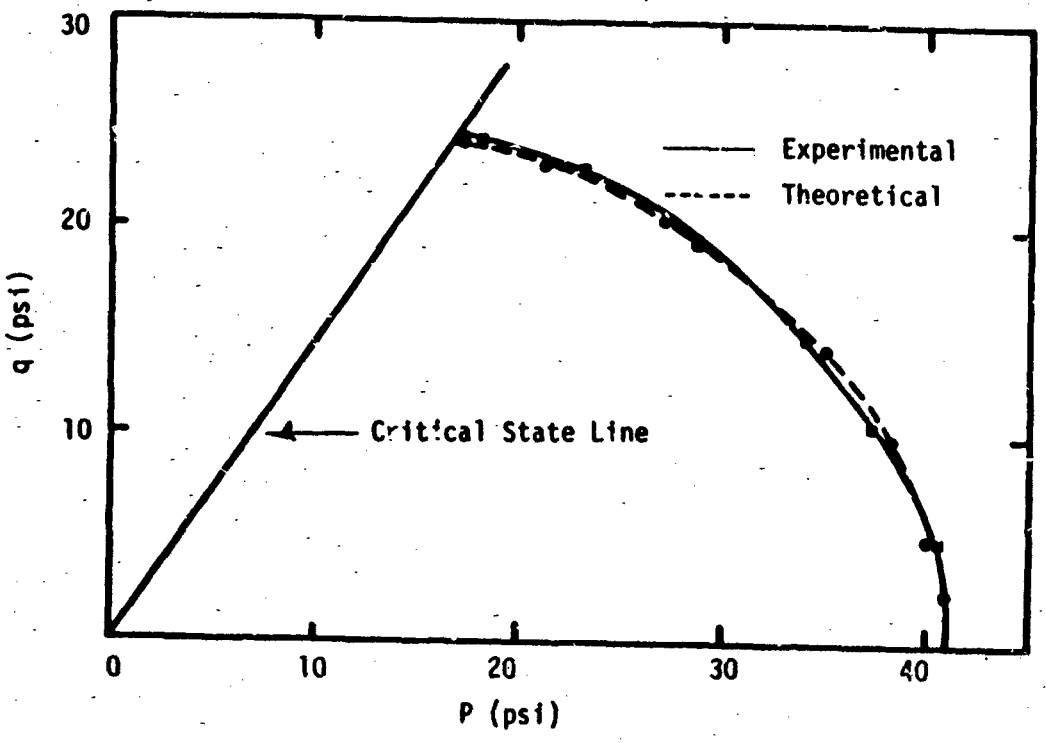

Fig. 71 : Experimental And Theoretical q vs p Relationships (Soil #4)

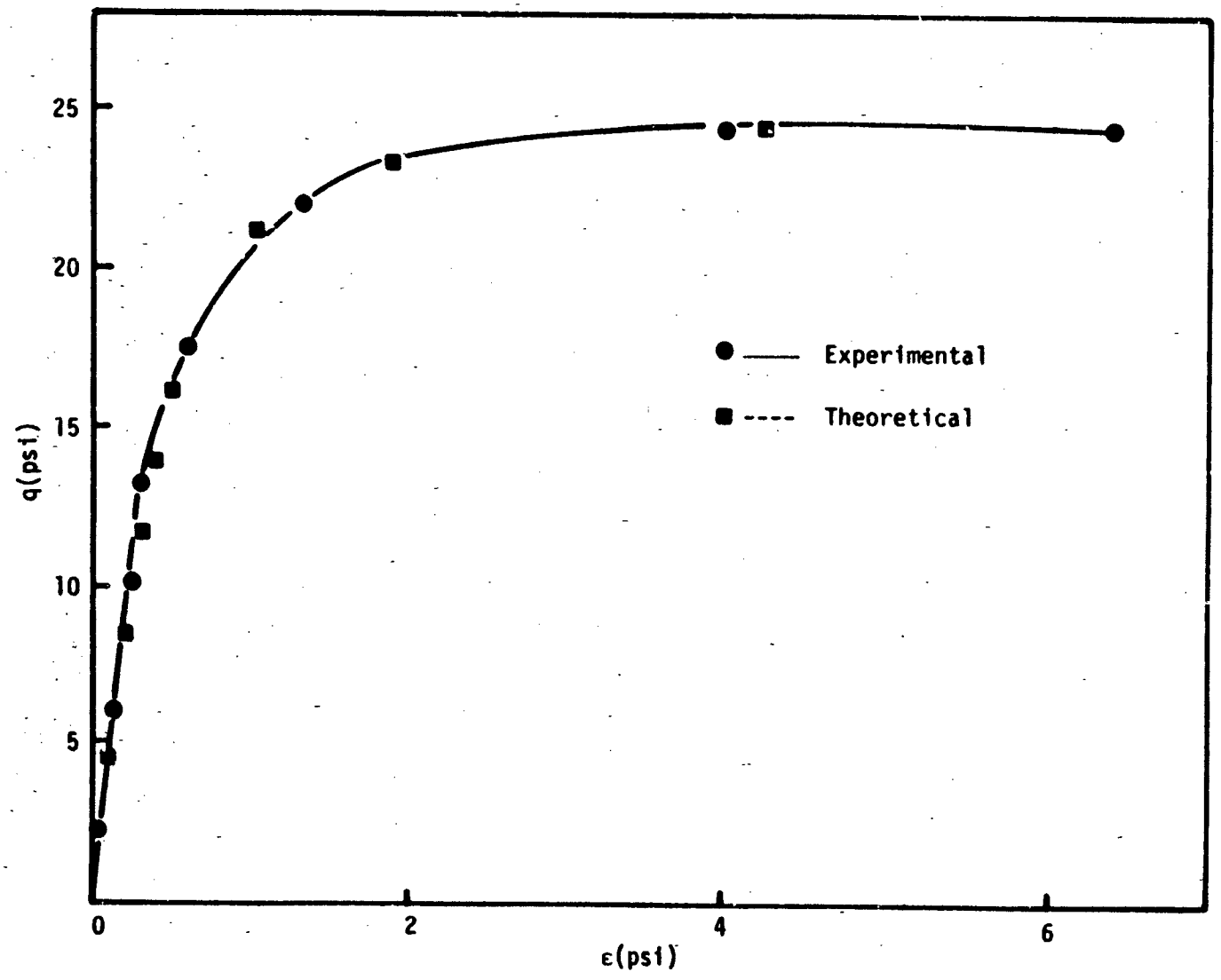

Fig. 72 : Experimental and Theoretical Stress-Strain Relationship (Soil #4)

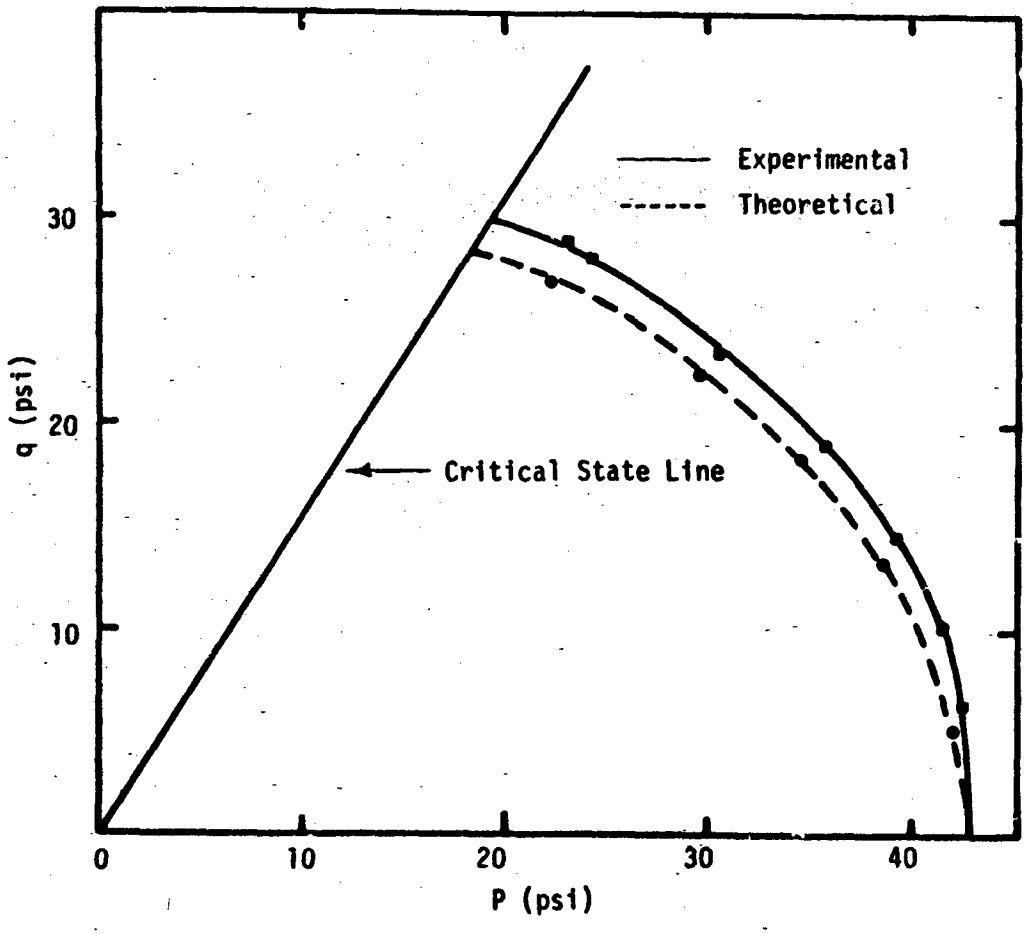

Fig. 73 : Experimental And Theoretical q vs p Relationships (Soil #6)

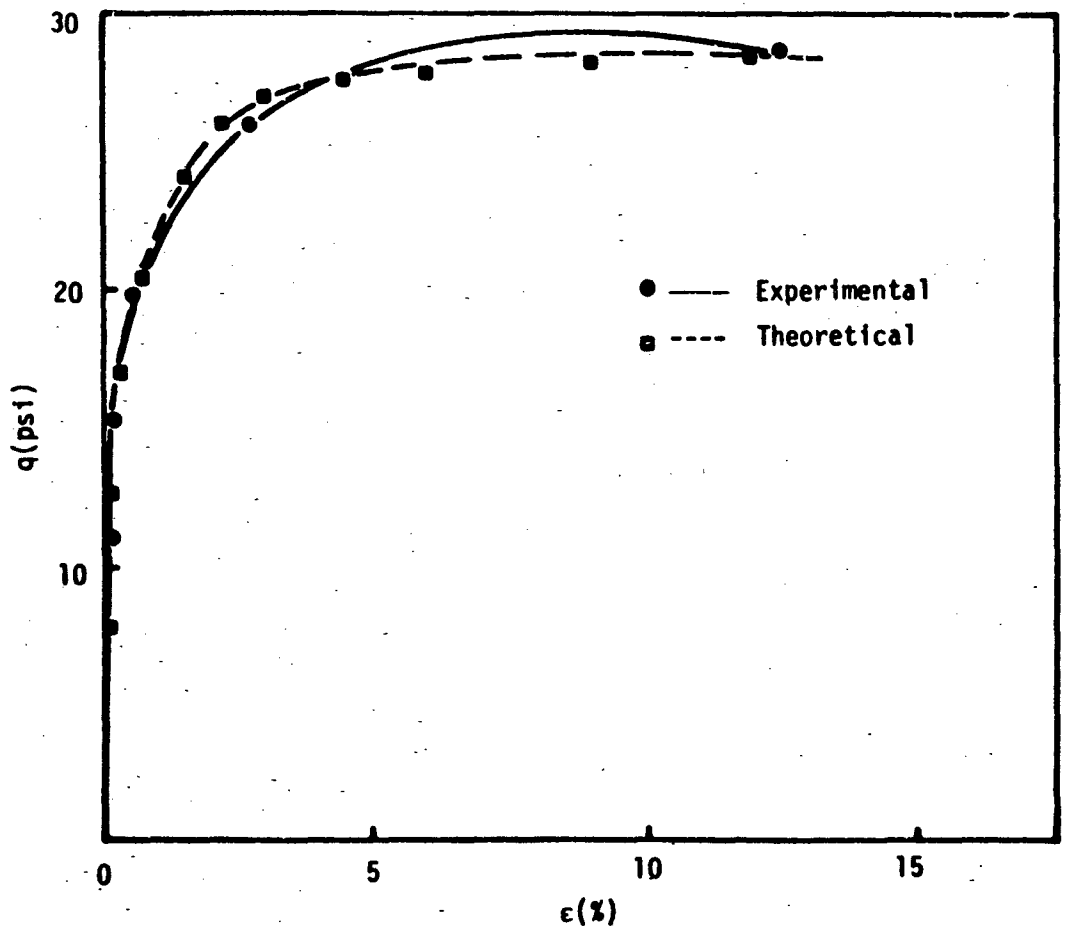

Fig. 74 : Experimental and Theoretical Stress-Strain Relationship (Soil #6)

Table 1

Proportions of Soil Mixtures

Soil No.	% of Sand	% of Silt	% Natural clay	% Kaolinite	% Mont.
1	20	74	6	-	-
2	17	74	6	3	-
3	17	74	6	-	3
4	47	44	6	3	-
5	47	44	6	-	3
6	-	94	6	-	-

Table ? : Optimized Electrical Model Parameters For Soil #1
(Vertical Measurement)

#	1	2	3	4	5	6	7	8	9	10	11
pressure (psi)	1.119	2.36	9.814	39.63	69.44	39.63	19.75	9.814	4.845	2.36	1.119
water con. measu. (%)	42.05	37.56	29.49	22.89	20.35	20.49	20.69	21.01	21.28	21.56	21.74
water con. calcu. (%)	42.04	37.56	29.50	22.27	20.34	20.49	20.69	21.00	21.28	21.54	21.74
e_l	.405	.343	.314	.299	.249	.268	.278	.289	.293	.318	.327
e_p	.735	.675	.486	.305	.302	.287	.283	.280	.284	.266	.262
$\Delta\epsilon$	30.19	30.25	30.30	29.83	30.44	28.89	28.89	28.78	28.78	28.80	28.78
ϵ_{min}	20.95	20.97	21.12	21.30	21.39	20.99	20.99	20.86	20.94	20.86	20.88
a	.271	.289	.400	.578	.635	.683	.589	.682	.574	.571	.610
b	.0033	.0082	.0022	.0045	.0035	.0017	.0019	.0019	.0019	.0022	.0023
c	.174	.172	.141	.101	.108	.098	.085	.092	.084	.075	.074
d	.980	.978	.966	.935	.923	.906	.936	.906	.938	.941	.927
ϵ_r	25.95	23.5	22.30	21.64	19.36	20.26	20.71	21.20	21.37	22.48	22.86
K_r	.012	.010	.0059	.0032	.0036	.0034	.0032	.0036	.0034	.0035	.0034
K_s	.00075	.00074	.00071	.00068	.00066	.00070	.00069	.00071	.00070	.00071	.00071

Table 3 : Optimized Electrical Model Parameters For Soil #1
(Horizontal Measurement)

#	1	2	3	4	5	6	7	8	9	10	11	12
pressure (psi)	1.119	4.845	9.814	19.75	39.63	69.44	39.63	19.75	9.814	4.845	2.36	1.119
water con. measu. (%)	41.56	33.60	29.46	26.07	22.77	20.29	20.39	20.65	20.97	21.29	21.58	21.69
water con. calcu. (%)	40.23	33.64	29.66	26.00	21.88	21.74	21.43	21.84	21.64	21.77	21.74	21.87
e_l	.477	.377	.359	.292	.241	.210	.232	.245	.255	.313	.355	.364
e_p	.614	.535	.336	.414	.352	.379	.349	.347	.331	.277	.234	.228
$\Delta\varepsilon$	24.91	26.49	26.97	27.61	28.16	28.65	27.72	28.20	27.97	27.92	27.94	27.94
ε_{min}	36.83	34.06	34.95	33.05	31.58	31.42	31.20	31.58	31.49	31.55	31.63	31.65
a	.558	.614	.824	.738	.818	.783	.819	.818	.828	.864	.893	.900
b	.033	.0051	.0020	.0020	.0024	.017	.0016	.0017	.0014	.0039	.0016	.0018
c	.263	.230	.174	.203	.179	.199	.179	.180	.171	.132	.105	.098
d	.982	.972	.971	.961	.949	.950	.949	.953	.954	.951	.953	.950
ε_r	26.54	24.89	24.19	21.33	18.99	17.44	18.55	19.15	19.64	22.25	24.02	24.40
K_r	.0054	.0044	.0030	.0032	.0028	.0028	.0028	.0028	.0028	.0027	.0027	.0026
K_s	.0069	.00068	.00060	.00065	.00069	.00066	.00070	.00066	.00068	.00067	.00067	.00066

Table 4 : Optimized Electrical Model Parameters For Soil #2
(Vertical Measurement)

#	1	2	3	4	5	6	7	8	9	10	11	12
pressure (psi)	1.119	2.36	9.814	19.75	39.63	69.44	39.63	19.75	9.814	4.845	2.36	1.119
water con. measu. (%)	28.63	25.58	20.73	18.62	16.32	14.68	14.87	14.93	15.12	15.28	15.42	15.56
water con. calcu. (%)	28.64	25.57	19.66	18.60	16.32	15.42	14.87	15.54	15.09	15.28	15.52	15.59
e_l	.238	.201	.136	.118	.106	.053	.105	.102	.112	.119	.115	.121
e_p	.529	.484	.391	.380	.331	.360	.294	.315	.293	.291	.301	.292
$\Delta\epsilon$	17.11	17.04	17.31	17.33	17.22	17.70	19.09	19.09	19.04	19.09	19.08	19.08
ϵ_{min}	22.76	22.52	22.22	21.61	21.33	20.92	18.34	18.44	18.26	18.34	18.24	18.27
a	.380	.475	.582	.620	.733	.733	.799	.736	.786	.745	.715	.716
b	.0013	.0001	.0000	.0011	.0010	.0039	.0001	.0001	.00009	.0001	.0001	.0001
c	.215	.170	.183	.177	.158	.177	.095	.108	.093	.093	.104	.096
d	.960	.968	.948	.926	.917	.917	.881	.889	.881	.892	.897	.895
ϵ_r	18.82	16.99	13.41	12.38	11.66	8.25	11.56	11.37	11.99	12.36	12.20	12.67
K_r	.0070	.0037	.0028	.0024	.0019	.0016	.0016	.0016	.0016	.0017	.0019	.0018
K_s	.00072	.00070	.00061	.00061	.00059	.00056	.00065	.00062	.00066	.00065	.00066	.00066

Table 5 Optimized Electrical Model Parameters For Soil #2
(Horizontal Measurement)

#	1	2	3	4	5	6	7	8	9	10	11	12	13
pressure (psi)	.508	1.119	4.845	9.814	19.75	39.63	69.04	39.63	19.75	9.814	4.845	2.36	1.119
water con. measu. (%)	32.41	28.93	22.93	20.58	18.47	16.43	14.88	15.01	15.06	15.22	15.35	15.50	15.60
water con. calcu. (%)	32.20	28.93	22.91	19.68	19.06	18.19	17.58	16.78	16.99	16.77	16.84	16.68	16.80
e_l	.226	.156	.159	.128	.123	.116	.099	.140	.150	.147	.176	.172	.172
e_p	.637	.619	.459	.399	.388	.372	.372	.309	.306	.302	.275	.275	.278
Δc	14.94	15.51	15.54	15.50	21.03	16.69	17.74	16.91	16.82	16.60	16.77	16.45	16.64
c_{min}	31.05	30.46	29.20	28.64	28.65	27.21	26.71	25.80	25.74	25.72	25.77	25.74	25.77
a	.525	.534	.675	.761	.758	.785	.781	.829	.839	.837	.858	.855	.855
b	.0067	.00086	.00079	.00131	.0009	.0003	.0022	.00009	.0001	.00009	.0001	.0002	.00008
c	.259	.282	.233	.227	.234	.212	.217	.170	.161	.163	.142	.145	.144
d	.97	.975	.963	.956	.972	.952	.954	.948	.941	.946	.944	.947	.945
c_f	18.25	14.57	14.49	12.98	12.64	12.22	11.23	13.67	14.20	14.07	13.64	13.41	13.65
K_f	.0041	.0038	.0025	.0021	.0020	.0018	.0017	.0017	.0016	.0017	.0017	.0018	.0017
K_s	.00072	.00067	.00063	.00062	.00042	.00056	.00050	.00056	.00056	.00057	.00056	.00058	.00057

Table 6 : Optimized Electrical Model Parameters For Soil #3
(Vertical Measurement)

#	1	2	3	4	5	6	7	8	9	10	11	12	13	14
pressure (psi)	.508	1.119	2.36	4.84	9.814	19.75	39.63	69.68	39.63	19.75	9.814	4.845	2.36	1.119
water con. measu. (%)	40.50	39.69	35.62	31.86	28.50	25.18	22.12	19.59	19.96	20.18	20.47	20.77	21.06	21.28
water con. calcu. (%)	40.48	39.69	35.69	31.87	28.48	25.16	23.89	19.58	19.95	20.19	20.51	20.77	21.04	21.27
e_l	.552	.536	.475	.411	.384	.346	.289	.252	.260	.280	.294	.299	.363	.423
e_p	.667	.546	.463	.463	.397	.344	.366	.284	.287	.273	.268	.270	.214	.159
$\Delta\epsilon$	29.38	29.34	29.46	29.41	29.39	29.47	29.86	29.38	28.95	28.95	30.77	28.93	28.86	28.87
ϵ_{min}	22.48	22.50	22.56	22.73	22.87	22.95	22.87	23.14	22.28	22.25	22.57	22.24	22.22	22 21
a	.328	.372	.406	.440	.497	.557	.617	.795	.641	.664	.647	.692	.659	.670
b	.011	.0013	.0026	.0016	.0019	.0015	.0032	.0027	.001	.0018	.0017	.0016	.0011	.0018
c	.134	.166	.131	.125	.115	.109	.135	.093	.099	.094	.092	.099	.056	.032
d	.982	.970	.971	.969	.958	.953	.920	.902	.941	.933	.946	.926	.937	.942
ϵ_r	30.03	29.90	27.88	25.67	24.67	23.16	20.77	19.11	19.87	20.79	21.49	21.64	24.34	26.66
K_r	.008	.010	.006	.0054	.0043	.0037	.0035	.0024	.0027	.0027	.0026	.0030	.0026	.0027
K_s	.00079	.00075	.00073	.00071	.00068	.00067	.00069	.00063	.00060	.00060	.00055	.00060	.00060	.00061

Table 7 Optimized Electrical Model Parameters For Soil #3
(Horizontal Measurement)

#	1	2	3	4	5	6	7	8	9	10	11	12	13	14
pressure (psi)	.508	1.119	2.36	4.845	9.814	19.75	39.63	69.44	39.63	19.75	9.814	4.845	2.36	1.119
water con. measu. (%)	42.19	38.03	35.00	31.31	27.92	24.96	22.15	20.07	20.22	20.44	20.69	20.95	21.20	20.39
water con. calcu (%)	42.05	37.18	35.00	32.65	28.23	26.93	22.39	21.79	21.80	21.70	21.79	21.66	21.89	21.79
e_i	.558	.546	.448	.398	.377	.327	.273	.271	.266	.279	.308	.353	.378	.394
e_o	.561	.439	.479	.467	.371	.387	.320	.307	.331	.316	.290	.240	.222	.203
Δe	19.53	28.12	25.88	30.69	28.19	27.86	28.25	30.49	28.86	28.63	28.60	28.38	28.70	28.98
e_{min}	32.99	35.97	33.22	33.15	32.14	30.86	31.24	30.58	31.23	31.34	31.60	31.60	31.72	31.82
a	.550	.693	.630	.641	.744	.710	.848	.847	.821	.839	.857	.889	.903	.910
b	.00004	.000	.0012	.0021	.0001	.0011	.0023	.0000	.0013	.0012	.0017	.0011	.0011	.0015
c	.193	.207	.196	.196	.176	1.69	.149	.145	.168	.159	.141	.110	.096	.089
d	.941	.983	.967	.978	.958	.950	.939	.943	.952	.954	.953	.954	.952	.958
e_r	31.195	30.824	27.55	25.41	24.899	22.866	20.48	20.38	20.15	20.75	22.02	23.95	24.93	25.55
K_r	.0069	.0048	.0045	.0041	.0035	.0035	.0025	.0025	.0026	.0025	.0024	.0025	.0024	.0025
K_s	.0012	.00056	.00074	.00059	.00066	.00073	.00067	.00063	.00062	.00059	.00059	.00060	.00058	.00058

Table 8 : Optimized Electrical Model Parameters For Soil #9
(Vertical Measurement)

#	1	2	3	4	5	6	7	8	9	10	11	12	13	a
pressure (psi)	.508	2.36	4.845	9.814	19.75	39.63	69.44	39.63	19.75	9.814	4.845	2.36	1.119	.508
water con. measu. (%)	35.14	27.97	25.01	22.07	19.50	16.92	15.05	15.16	15.35	15.67	15.68	15.83	16.00	16.50
water con. calcu. (%)	32.06	27.99	25.03	21.67	16.27	16.94	14.91	15.16	15.36	15.44	15.69	15.83	16.04	16.91
e_i	.296	.227	.227	.180	.165	.178	.129	.151	.179	.194	.176	.195	.195	.203
e_p	.627	.526	.446	.408	.273	.278	.272	.257	.234	.221	.247	.231	.247	.252
$\Delta\epsilon$	30.79	22.37	22.26	22.08	21.53	22.44	21.77	22.27	22.23	22.20	22.21	22.22	22.38	22.44
ϵ_{min}	23.25	21.69	21.37	21.05	21.03	20.54	20.29	18.68	18.65	18.64	18.64	18.64	18.53	18.55
a	.391	.411	.437	.487	.763	.731	.818	.733	.837	.787	.757	.766	.762	.736
b	.000	.0039	.0010	.0033	.0037	.0012	.0013	.0001	.00009	.00011	.00008	.00013	.00011	.00009
c	.181	.165	.181	.177	.112	.107	.110	.079	.059	.052	.072	.055	.071	.075
d	.973	.961	.943	.934	.916	.915	.905	.906	.884	.902	.899	.895	.897	.904
ϵ_f	19.21	18.26	18.28	15.87	15.04	15.74	13.01	14.29	15.81	16.63	15.64	16.67	16.65	17.05
K_f	.0036	.0030	.0039	.0048	.0026	.0023	.0019	.0020	.0020	.0020	.0021	.0020	.0023	.0026
K_s	.00081	.00076	.00076	.00072	.00069	.00064	.00063	.00067	.00067	.00067	.00068	.00067	.00069	.00068

Table 9 : Optimized Electrical Model Parameters For Soil #4
(Horizontal Measurement)

#	1	2	3	4	5	6	7	8	9	10	11	12	13
pressure (psi)	.508	2.36	4.845	9.814	39.63	69.44	39.63	19.75	9.814	4.845	2.36	1.119	.508
water con. measu. (%)	36.15	28.00	25.10	22.10	17.06	15.25	15.31	15.65	15.57	15.74	15.86	16.03	16.20
water con. calcu. (%)	36.14	28.01	20.65	19.11	17.48	16.70	16.77	16.64	16.78	16.62	16.77	16.52	16.57
e_l	.238	.219	.200	.156	.141	.132	.155	.167	.195	.191	.209	.201	.228
e_p	.736	.535	.350	.358	.329	.317	.297	.281	.257	.257	.242	.243	.218
Δc	16.56	17.07	17.03	18.92	19.52	20.33	21.06	21.28	21.33	21.28	21.92	21.14	21.11
c_{min}	31.23	29.60	29.54	28.43	26.17	25.33	25.80	25.86	25.88	25.90	26.01	25.86	25.89
a	.672	.580	.801	.805	.834	.838	.843	.853	.874	.870	.882	.879	.898
b	.0075	.0059	.0028	.0018	.0001	.0011	.00014	.00012	.00001	.00002	.00009	.00002	.0002
c	.264	.225	.183	.193	.166	.160	.155	.107	.126	.130	.118	.121	.101
d	.973	.961	.950	.945	.930	.931	.942	.946	.942	.946	.945	.946	.945
c_r	18.84	17.88	16.92	14.54	13.68	13.20	14.48	15.16	16.63	16.42	17.41	16.97	18.31
K_r	.0049	.0035	.0025	.0026	.0021	.0019	.0019	.0020	.0019	.0020	.0019	.0020	.0020
K_s	.00085	.00079	.00075	.00073	.00071	.00067	.00060	.00059	.00059	.00059	.00057	.00060	.00060

Table 10 Optimized Electrical Model Parameters For Soil #5
(Vertical Measurement)

#	1	2	3	4	5	6	7	8	9	10	11	12
pressure (psi)	.508	1.119	4.845	19.75	39.63	69.44	39.63	19.75	9.814	4.845	2.36	1.119
water con. measu. (%)	48.89	46.06	34.53	26.80	23.26	20.61	20.72	21.09	21.35	21.75	21.97	22.19
water con. calcu. (%)	48.90	46.09	34.52	26.83	23.26	20.03	20.76	20.99	21.34	21.77	21.95	22.21
e_l	.554	.528	.449	.300	.265	.211	.250	.271	.250	.347	.222	.288
e_p	.776	.726	.490	.429	.368	.334	.315	.299	.331	.246	.375	.316
$\Delta\epsilon$	26.59	26.58	26.60	26.85	26.99	26.11	28.82	28.74	28.68	28.63	28.66	28.66
ϵ_{min}	25.08	25.03	25.08	25.41	25.59	25.44	23.79	23.75	23.68	23.65	23.70	23.69
a	.326	.335	.355	.503	.629	.737	.670	.651	.622	.646	.595	.650
b	.008	.000	.033	.014	.0017	.0002	.0008	.0003	.0014	.0045	.0009	.0082
c	.190	.206	.220	.207	.146	.156	.135	.119	.128	.085	.163	.143
d	.981	.979	.951	.946	.952	.928	.941	.952	.953	.9555	.947	.936
ϵ_r	31.05	30.23	27.58	21.71	20.09	17.78	19.39	20.40	19.39	23.68	18.02	21.18
K_r	.0096	.011	.011	.0059	.0031	.0029	.0031	.0031	.0031	.0032	.0035	.0037
K_s	.00074	.00075	.00070	.00067	.00065	.00068	.00061	.00062	.00062	.00063	.00062	.00062

Table 11 Optimized Electrical Model Parameters For Soil #5
(Horizontal Measurement)

#	1	2	3	4	5	6	7	8	9	10	11
pressure (psi)	.508	2.36	4.845	9.814	19.75	39.63	19.75	9.814	4.845	2.36	1.119
water con. measu. (%)	50.91	40.48	34.77	30.84	27.16	20.80	21.16	21.48	21.91	22.16	22.41
water con. calcu. (%)	51.18	40.43	43.72	30.81	27.21	20.06	21.15	20.23	20.02	20.24	20.21
e_l	.568	.456	.395	.365	.290	.237	.294	.270	.358	.292	.285
e_p	.824	.644	.549	.473	.450	.308	.281	.281	.186	.258	.264
Δc	29.73	25.72	25.67	25.71	25.85	34.25	34.51	34.43	34.44	34.34	34.28
ϵ_{min}	36.27	35.28	35.30	35.28	35.31	30.14	29.98	30.25	30.49	30.44	30.49
a	.492	.559	.625	.694	.746	.845	.815	.856	.921	.878	.871
b	.0024	.0022	.0023	.0047	.0024	.000	.0045	.0008	.0012	.0009	.0010
c	.251	.233	.228	.211	.226	.154	.131	.137	.077	.121	.127
d	.989	.978	.974	.966	.964	.946	.953	.949	.953	.948	.951
ϵ_r	31.50	27.82	25.60	24.43	21.24	18.78	21.45	20.32	24.15	21.34	21.04
K_r	.0061	.0052	.0046	.0038	.0035	.0029	.0032	.0029	.0029	.0029	.0029
K_s	.00058	.00074	.00074	.00073	.00073	.00068	.00069	.00067	.00067	.00067	.00068

Table 12 : Optimized Electrical Model Parameters For Soil #6
(Vertical Measurement)

#	1	2	3	4	5	6	7	8	9	10	11	12	13
pressure (psi)	.508	1.119	2.36	4.845	9.814	19.75	39.63	69.44	39.63	19.75	9.814	4.845	1.119
water con. measu. (%)	49.28	45.81	41.75	37.64	33.71	29.86	26.18	23.45	23.62	24.05	24.52	24.95	25.59
water con. calcu. (%)	49.31	45.7	41.69	37.66	33.72	24.02	23.32	22.73	23.62	24.04	24.39	24.94	26.08
e_i	.724	.569	.521	.442	.487	.444	.420	.368	.446	.466	.456	.503	.575
e_p	.637	.695	.630	.597	.444	.207	.212	.248	.205	.197	.217	.186	.145
Δc	33.59	33.63	33.65	33.69	33.53	28.66	28.68	28.68	32.02	31.98	31.65	31.95	34.38
c_{min}	21.96	21.95	26.67	22.20	22.36	33.67	32.84	32.17	21.99	21.83	21.89	21.83	22.16
a	.263	.248	.296	.256	.233	.903	.908	.891	.582	.703	.561	.707	.574
b	.0087	.0049	.000	.0074	.099	.0011	.0031	.0030	.0024	.0005	.0023	.0005	.0024
c	.179	.187	.283	.204	.160	.096	.089	.106	.049	.046	.052	.036	.026
d	.961	.966	.986	.952	.890	.967	.955	.948	.948	.927	.950	.926	.957
c_r	35.78	31.5	30.00	27.33	28.89	27.40	26.53	24.55	27.49	28.19	27.84	29.42	31.69
K_r	.023	.022	.023	.022	.011	.0027	.0025	.0024	.0038	.0041	.0040	.0041	.0039
K_s	.00090	.00090	.00038	.00086	.00068	.00057	.00060	.00062	.00070	.00072	.00071	.00072	.00065

Table 13 : Optimized Electrical Model Parameters For Soil #6
(Horizontal Measurement)

#	1	2	3	4	5	6	7	8	9	10	11	12	13	14	15
pressure (psi)	.508	1.119	2.36	4.845	9.814	19.75	39.63	69.84	39.63	19.75	9.814	4.845	2.36	1.119	.508
water con. measu. (%)	51.33	44.45	42.32	37.89	33.79	30.04	26.50	23.87	24.01	24.36	24.75	25.20	25.55	25.83	26.08
water con. calcu. (%)	51.34	44.72	42.31	38.47	26.31	24.67	27.69	23.83	24.01	24.36	24.77	25.16	25.53	25.82	25.88
e_i	.721	.568	.629	.600	.546	.546	.511	.408	.411	.496	.502	.531	.556	.561	.575
e_p	.696	.666	.538	.462	.180	.135	.253	.250	.251	.177	.181	.164	.149	.152	.139
$\Delta\epsilon$	29.64	30.48	29.64	39.17	29.79	21.08	45.13	29.66	32.22	32.32	32.25	32.23	32.19	32.23	32.21
ϵ_{min}	32.99	32.73	32.54	35.12	36.07	32.96	35.49	32.66	31.40	31.46	31.42	31.46	31.38	31.39	31.49
a	.410	.422	.533	.634	.900	.964	.834	.839	.808	.853	.878	.849	.857	.884	.868
b	.016	.016	.014	.000	.017	.003	.0001	.023	.0007	.0027	.0008	.0026	.0025	.0009	.0012
c	.271	.282	.189	.175	.082	.0002	.126	.108	.104	.064	.063	.054	.041	.044	.038
d	.975	.976	.973	.990	.976	.920	.986	.951	.958	.959	.952	.959	.955	.953	.957
ϵ_f	35.70	31.49	33.27	32.44	30.82	30.81	29.69	26.10	26.21	29.19	29.41	30.32	31.12	31.26	31.71
K_f	.013	.012	.0069	.0052	.0033	.0034	.0034	.0034	.0035	.0035	.0034	.0036	.0035	.0036	.0036
K_s	.00080	.00077	.00079	.00047	.00060	.0011	.00039	.00077	.00072	.00072	.00071	.00072	.00072	.00072	.00072

END

FILMED

3-85

DTIC